2009

ENHANCED ENVIRONMENTAL DETECTION OF URANYL COMPOUNDS BASED ON LUMINESCENCE CHARACTERIZATION

Jean Nelson
Virginia Commonwealth University

ENHANCED ENVIRONMENTAL DETECTION OF URANYL COMPOUNDS BASED ON LUMINESCENCE CHARACTERIZATION

A dissertation submitted in partial fulfillment of the requirements for the degree of Doctor of Philosophy at Virginia Commonwealth University.

by

Jean Dennis Nelson
Master of Science, Virginia Commonwealth University, 2001
Bachelor of Science, Radford University, 1999

Director: John E. Anderson
Associate Professor, Department of Biology

Virginia Commonwealth University
Richmond, Virginia
December, 2009

ACKNOWLEDGMENT

First and foremost, I would like to thank the members of my dissertation committee: Dr. John Anderson, Dr. Gary Tepper, Dr. Charles (Mike) Reynolds, Dr. Lemont Kier and Dr. David Edwards. They were each an endless source of support, patience and guidance.

There are several of my teammates I would like to thank. Specifically, I am grateful to Jarrod Edwards for all his assistance in collection of the soil samples. Further, I am grateful to Ricky Massaro for his assistance with generating the spectral scores using MATLAB software. In general, I am thankful to all my co-workers for being so supportive and understanding throughout the years.

In addition, I would like to thank Dr. Dmitry Pestov and Ken Chen of VCU Engineering for their assistance during all the preliminary studies and guidance with regards to selection of the distributable enhancing material.

I extend my gratitude to A&L Eastern Laboratories, Inc. for conducting several of the soil analyses, and specifically to Dr. Paul Chu for taking the time to discuss the analytical procedures with me. I am also appreciative to the ERDC Environmental Lab (EL), specifically to members of the Environmental Chemistry Branch for further analysis of my soil samples, in addition to Dr. Vic Medina and Dr. Afrachanna Butler for supplying the YPG soil and discussing soil preparation procedures.

I am grateful to my employer, the Engineer Research and Development Center (ERDC), and further to the DoD, for supporting me financially and morally throughout my research and for providing me with the long-term training opportunity. This research project was supported in part by a DOE NA22 grant (DE-FG52-06NA27491). Also, I am very grateful to VCU Life Sciences, for creating the Integrative Life Sciences program, enabling Ph.D. students to partake in such an interdisciplinary approach to coursework and research, and also for being supportive of me over the last six years.

Finally, I extend my deepest gratitude and appreciation to my family, especially to my husband Dan, my daughters Kayleigh and Allison, and to my mother; for their endless source of love and support. Last, but most importantly, I thank God for providing me with the strength, patience and perseverance I needed.

TABLE OF CONTENTS

List of Tables.....v

List of Figures.....viii

List of Abbreviations.....xiii

Abstract.....xv

CHAPTER 1: INTRODUCTION – REVIEW.....1

1.1 Introduction to Uranium and the Uranyl Ion (UO_2^{2+}).....1

1.2 Uranium Contamination in the Environment.....9

1.3 Luminescence Detection and Characterization of Uranyl.....19

1.4 Uranium Extraction and Fluorescence Enhancement.....23

1.5 Remote Sensing of Uranium.....28

1.6 Comprehensive Mission Statement.....29

1.7 Key Features of Environmental Samples.....33

1.7.1 Introduction.....33

1.7.2 Soil Texture.....35

1.7.3 Moisture Content and Water Potential.....39

1.7.4 pH Related Effects.....44

1.7.5 Soil Organic Matter (SOM).....54

1.7.6 Iron Content.....61

1.7.7 Summary and Hypothesis Statements.....68

CHAPTER 2: EMPIRICAL INVESTIGATIONS.....73

2.1 Preliminary Studies.....73

2.1.1 Introduction.....73

2.1.2 Steady-state Fluorescence Spectroscopy.....76

2.1.3 Data Related to Key Features of Environmental Samples.....77

2.2 Research Design.....91

2.2.1 Introduction.....91

2.2.2 Luminescence Detection and Spectral Scoring – Test Dataset.....92

2.2.3 Experiments for Testing Hypotheses.....102

2.3 Comprehensive Experimental Matrix and Data Analysis.....106

2.3.1 Introduction.....106

2.3.2 Statistical Variables.....109

2.3.3 Response (Y) Variables…….....113

2.3.4 Populations of Spectra – Achieving Desired Detection Thresholds…...117

2.3.5 Predictor (X) Variables – Relationships…….....125

2.3.6 Predictor (X) and Response (Y) Variables – Bivariate Relationships….127

2.3.7 Development of Predictive Models for the Comprehensive Dataset…...145

2.3.8 Multivariate Regression……..……154

2.3.9 Final Discussion……...……156

Literature Cited.....160

Vita…….....171

LIST OF TABLES

Page

Table 1. General background information for Uranium.....2

Table 2. Key molecular processes pertinent to the fluorescence spectroscopy of U(VI). Refer also to Figure 4. Adapted from (Meinrath 1997).....7

Table 3. Names and chemical formulas for commonly studied Uranium (VI) minerals. Adapted from (Morris, Allen et al. 1996).....12

Table 4. Reference information for estimates of uranium concentrations (ppm) in environmental soil samples.....16

Table 5. Key mechanisms by which U mobility can be retarded in the surface and subsurface geologic environment. Adapted from (Duff, Coughlin et al. 2002).....34

Table 6. Standard soil pH classifications. Adapted from USDA NRCS public information.....45

Table 7. Reference information for pH levels in environmental soil samples used in U studies.....46

Table 8. Chemical formulas for commonly encountered hydroxyl and carbonate forms of U(VI) in aqueous phases and corresponding optimal pH values.....48

Table 9. Summary of U sorption, dissolution and diffusion studies and their findings associated with pH changes.....50

Table 10. Descriptions for the room temperature fluorescence emission spectra of various uranyl silicates. Adapted from (Wang, Zachara et al. 2005).....53

Table 11. Summary of U sorption and mobility studies and their findings associated with the presence of humic acid (HA).....60

Table 12. Summary of studies describing the strong association between U and Fe – phases resulting in enhanced sorption and reduced mobility.....65

Table 13. Key influential features of environmental samples selected for further investigation.....69

Table 14. A proposed best-case scenario for uranyl fluoresce detection at soil surfaces with a silica gel – based distributed sensor, and detailed explanations related to environmental factors.....72

Table 15. Chemical composition (wt. %, dry) of KGa-1b clay (kaolinite) standard sample, obtained from the Clay Minerals Society, Source Clays Repository in Columbia, USA. Adapted from (Payne, Davis et al. 2004) 74

Table 16. List of soil samples utilized for discussed studies.....75

Table 17. Approximate intensity counts for U or OM fluorescence peaks in filtered (0.22 μm) soil supernatants.....89

Table 18. Attempted procedures for scoring steady-state uranyl fluorescence band structure.....98

Table 19. Uranyl peaks successfully identified by the 'Peak Analyzer' function in OriginPro v8 (Guassian based calculations) for sample emission spectra (490 – 555 nm range, normalized for intensity and center peak position, smoothed using weighted averages) 102

Table 20. Soil sample analyses performed by A&L Eastern Laboratories Inc., Richmond, VA.....104

Table 21. Variables utilized for statistical analyses.....109

Table 22. Low and high initial percent moisture contents (% MC) selected for soil samples.....111

Table 23. Results of soil sample analyses, relevant to key soil parameters.....111

Table 24. Summary of procedure for generating response variables from collected sample fluorescence emission spectra.....112

Table 25. Distribution details for the generated response variables, Intensity score and Structure score, for the comprehensive dataset (n = 3360).....116

Table 26. Correlation values generated by the multivariate routine (JMP v8) for pairs of continuous predictor variables.....126

Table 27. Results of the principal components analysis routine (PCA, JMP v8), displaying the continuous predictor variables examined, the arbitrary extracted factors, their corresponding eigenvalues and the estimated percent of total variation and cumulative variation they represent.....127

Table 28. Means comparison results (JMP v8) showing the means of different levels of X variables that are significantly different from each other, relative to the response variables.....140

Table 29. Results of the least squares fitting routine (JMP v8) in testing for the significance of single continuous X variable models (linear fits), in predicting each of the response variables…….....141

Table 30. Results of the least squares fitting routine (JMP v8) in testing for the significance of single categorical X variable models, in predicting the response variables individually.....145

Table 31. Selected multiple linear regression model: Results of the least squares fitting routine (JMP v8) in testing for the significance of the whole model, parameter estimates and individual effects in predicting the response variable – *Intensity* Score.....150

Table 32. Selected multiple linear regression model: Results of the least squares fitting routine (JMP v8) in testing for the significance of the whole model, parameter estimates and individual effects in predicting the response variable – *Structure* Score.....151

Table 33. Parameter estimates generated by the MANOVA routine (JMP v8) in developing a multivariate regression model for predicting both response variables: Structure and Intensity.....155

Table 34. Results of the MANOVA routine (JMP v8) in testing for the significance of the whole multivariate regression model and individual effects in predicting both response variables: Structure and Intensity.....155

LIST OF FIGURES

Page

Figure 1. Structural representation of the uranyl ion: U atom (blue), axial oxygen atoms (red), and coordinating atoms (4-6) in equatorial plane (green). Adapted from (Morris, Conradson et al. 1992).....3

Figure 2. Proposed ground state (f^0) structures for common *trans*-uranyl (VI) systems, based on density functional calculations. Adapted from (Schreckenbach, Hay et al. 1999).....3

Figure 3. Steady-state excitation (blue) and fluorescence emission (red) scans demonstrating the vibrational spectral structure of a uranyl aqueous solution at room temperature (arbitrary intensity units).....6

Figure 4. Jablonski diagram of an absorption and emission process (right, adapted from Meinrath, 1997) 6

Figure 5. Sand standard contaminated with 100 ppm U, with silica gel on the surface and lacking silica gel, under UV (254 nm) irradiation.....31

Figure 6. Enhancement effect on uranyl fluorescence using silica gel and sapphire beads (individually and combined) on the surface of sand contaminated with 100 ppm U.....32

Figure 7. Comparison between sand and clay related to their soil texture and interaction with water. Classification of soil types based on particle sizes, and the soil texture triangle showing the classification of the mixtures of the different soil types.....36

Figure 8. Generic soil water release curves demonstrating the relationship between available water as % MC and soil water potential, with consideration for soil texture.....44

Figure 9. Generalized diagram showing the predominant trends of U(VI) aqueous speciation (%) as a function of pH.....47

Figure 10. Diagram showing the general trend of U sorption (%) on solid materials as a function of pH.....49

Figure 11. Soil organic matter (SOM) fractionation diagram. Adapted from the Soil Science Society of America's (SSSA) book series No. 5, Methods of Soil Analysis, Part 3, Chemical Methods (Organic matter characterization), p. 1025 (Swift 1996) 55

Figure 12. Diagram showing the general trend of U sorption (%) on natural solid materials as a function of pH, in comparison to the pH dependent trend of uranyl – silica gel solution fluorescence intensity, in the absence of carbonates.....70

Figure 13. Steady-state fluorescence emission scans demonstrating the effect of variation in humidity on uranyl detection when enhanced by NaF powder on sand samples contaminated with 120 ppm U.....78

Figure 14. Single-point fluorescence intensity counts demonstrating the rapid migration of U with water through sand (λ_{Ex} = 300 nm, λ_{Em} = 519 nm, 3 nm bp). Water was added (10 mL at ~0.1 mL/sec) to dry sand (30 g) previously contaminated with 100 ppm U, with silica gel on the surface.....79

Figure 15. Steady-state fluorescence emission scans demonstrating the time dependence of uranyl detection when enhanced by silica gel on sand samples contaminated with 12 ppm U.....80

Figure 16. Effect of moisture content and time on detected uranyl fluorescence enhanced by silica gel for varying soil samples.....82

Figure 17. Water potential readings related to % MC for varying soil samples.....83

Figure 18. Steady-state fluorescence emission scans for filtered soil supernatants demonstrating the variation in uranyl detection in the aqueous phase, aside from U – soil particle interactions.....85

Figure 19. Steady-state fluorescence emission scans demonstrating both the spectral overlap and static quenching of humic acid and uranyl (λ_{Ex} = 420 nm) 86

Figure 20. Steady-state fluorescence emission scans for a filtered James River soil supernatant demonstrating the effect of acidification on uranyl detection.....87

Figure 21. Steady-state fluorescence emission scans demonstrating the effect of acidification on uranyl detection in aqueous solution.....88

Figure 22. Steady-state fluorescence emission scans demonstrating the loss of band structure in the uranyl spectra in the presence of concrete.....91

Figure 23. Emission spectra for aqueous environmental samples containing comparable levels of U, demonstrating the importance of uranyl detection based on band structure.....93

Figure 24. A sample set of uranyl emission spectra representing the diversity of possible and typically observed responses, used here as a dataset for testing a new scoring procedure.....95

Figure 25. A sample set of steady-state fluorescence emission spectra for uranyl samples (490 – 555 nm range, normalized for intensity and center peak position, smoothed using weighted averages).....97

Figure 26. A sample set of steady-state fluorescence emission spectra for uranyl samples (490 – 555 nm range, normalized for intensity and center peak position, smoothed using weighted averages, with the lowest normalized intensity values at 555 nm adjusted to zero).....99

Figure 27. Scores for uranyl emission band structure based on the sum of the square of the differences between the reference spectrum and sample spectra, for the adjusted uranyl spectral test dataset.....100

Figure 28. Comparison of fluorescence intensity and band structure scores for the adjusted uranyl spectral test dataset.....101

Figure 29. Digital photograph of soil samples utilized for discussed studies, previously air-dried, mixed, and sieved (2 mm).....103

Figure 30. Steady-state fluorescence emission scans for soil sample KGa-1b, displaying the relationship between U soil concentrations and detection.....107

Figure 31. Steady-state fluorescence emission scans for soil sample SDc, demonstrating the importance of adequate initial moisture content levels, necessary for silica gel – based enhancement (top: 10% initial MC, bottom: 2.5% initial MC)…….....108

Figure 32. A promising sample spectrum (green) centralized for band structure variation within the reference spectrum (blue). See Table 24, step 6.....113

Figure 33. Comparison of fluorescence intensity and band structure scores for the control samples, [U] = 0 ppm (n = 840).....115

Figure 34. Comparison of fluorescence intensity and band structure scores for the comprehensive dataset (n = 3360).....115

Figure 35. Distribution plots for the generated response variables, Intensity score and Structure score, for the comprehensive dataset (n = 3360).....116

Figure 36. Number of spectra achieving selected detection thresholds (structure scores < 3.23, intensity scores > 10.43, *n* = 169), based on uranium concentration and whether readings were collected over silica gel versus bare soil.....119

Figure 37. Number of spectra achieving selected detection thresholds (structure scores < 3.23, intensity scores > 10.43, *n* = 169), based on initial percent moisture content and further categorized as the low or high level selected for soils (see Table 22)…....120

Figure 38. Number of spectra achieving selected detection thresholds (structure scores < 3.23, intensity scores > 10.43, *n* = 169), based on time of analysis and further distinguishing between readings collected over silica gel versus bare soil.....121

Figure 39. Number of spectra achieving selected detection thresholds (structure scores < 3.23, intensity scores > 10.43, *n* = 169), based on soil features: Soil texture, % Sand and % Clay.....122

Figure 40. Number of spectra achieving selected detection thresholds (structure scores < 3.23, intensity scores > 10.43, *n* = 169), based on soil features: % Silt, % OM and Total CEC.....123

Figure 41. Number of spectra achieving selected detection thresholds (structure scores < 3.23, intensity scores > 10.43, *n* = 169), based on soil features: Soil pH, Iron content and Total Iron.....124

Figure 42. Least squares means plots relating intensity scores (left) or structure scores (right) to uranium concentration, whether readings were collected over silica gel versus bare soil, initial percent moisture content and further categorized as the low or high level selected for soils.....130

Figure 43. Least squares means plots relating intensity scores (left) or structure scores (right) to initial percent moisture content for soil texture groups: Sand, Loamy Sand and Sandy Loam.....131

Figure 44. Least squares means plots relating intensity scores (left) or structure scores (right) to initial percent moisture content for soil texture groups: Sandy Clay Loam, Loam and Clay.....132

Figure 45. Least squares means plots relating intensity scores (left) or structure scores (right) to time of analysis and further distinguishing between readings collected over silica gel versus bare soil.....133

Figure 46. Least squares means plots relating intensity scores (top) or structure scores (bottom) to soil sample identity.....134

Figure 47. Least squares means plots relating intensity scores (top) or structure scores (bottom) to soil texture classification.....135

Figure 48. Least squares means plots relating intensity scores (left) or structure scores (right) to % Sand (top) and % Clay (bottom).....136

Figure 49. Least squares means plots relating intensity scores (left) or structure scores (right) to % Silt (top) and % OM (bottom)……...137

Figure 50. Least squares means plots relating intensity scores (left) or structure scores (right) to Total CEC (top) and Soil pH (bottom)……..138

Figure 51. Least squares means plots relating intensity scores (left) or structure scores (right) to Iron content by Mehlich III (top) and Total Iron (bottom)……....139

Figure 52. Scatter plot of the residuals by the predicted values (top), and distribution plot of the residuals (bottom) for the selected multiple linear regression model – *Intensity* Score.....152

Figure 53. Scatter plot of the residuals by the predicted values (top), and distribution plot of the residuals (bottom) for the selected multiple linear regression model – *Structure* Score…….....153

LIST OF ABBREVIATIONS

Bq kg^{-1}……..becquerel per kilogram, radioactivity measurement
bp……...bandpass, parameter for spectral data
CEC……cation exchange capacity
cm……centimeters, 10^{-2} meters
cps……...…counts per second, units for intensity measurements
CRREL……..Cold Regions Research and Environmental Lab (of USACE ERDC)
DOC……...dissolved organic carbon
DoD……US Department of Defense
DOE…….US Department of Energy
DU…….depleted uranium, ^{238}U
EM……...emission
EPA……...US Environmental Protection Agency
ERDC…….US Army Engineer Research and Development Center
EX……..excitation
EXAFS……extended X-ray absorption fine structure analysis
FA…….fulvic acid(s)
Fe…….iron
Fe(II), Fe^{2+}.....ferrous ions, reduced form
Fe(III), Fe^{3+}……...……ferric ions, oxidized form
FL……...fluorescence
FSI……..…fluorescence spectral imaging
g……grams
HA……humic acid(s)
HS……..humic substances
IT……..integration time, parameter for spectral data
K……...…Kelvin, temperature unit (298 K is room temperature)
kg……kilograms, 10^{3} grams
L……...……..liters
LANL……Los Alamos National Laboratory
LIFI……...laser-induced fluorescence imaging
% MC…….percent moisture content
mg…….milligrams, 10^{-3} grams
mL……..milliliter, 10^{-3} liters
mm……...millimeters, 10^{-3} meters
MPa……milli Pascals, 10^{-3} Pascals, pressure unit for WP measurements
ms……...…….milliseconds, 10^{-3} seconds, unit for fluorescence lifetime
n……..vibrational energy states within each of the electronic states
NATO……North Atlantic Treaty Organization

nm……..……..nanometers, 10^{-9} meters, energy wavelength unit
NOM……...natural organic matter
NRCS……USDA Natural Resources Conservation Service
ns……nanoseconds, 10^{-9} seconds, unit for fluorescence lifetime
OC…….organic content
OM…….organic materials or organic matter
ORNL……..Oak Ridge National Laboratory
pH……..measure of the acidity or alkalinity of a solution
ppb……parts per billion
ppm……..parts per million
QY……...quantum yield, ratio of # of photons emitted to # of photons absorbed
s…….seconds
SOM…….soil organic matter
SSSA……..Soil Science Society of America
TOC……total organic carbon
TRES……...time-resolved emission spectroscopy
TRLFS……time-resolved laser-induced fluorescence spectroscopy
U……...uranium
[U]……..uranium concentration
^{238}U……..U isotope with atomic mass ~ 238 u, most common form in nature
^{235}U……U isotope with atomic mass ~ 235 u, used for nuclear reactions
^{233}U……U isotope with atomic mass ~ 233 u, used for nuclear reactions
^{tot}U……total uranium, all isotopes
U(IV), U^{4+}……tetravalent oxidation state of uranium, existing under reducing conditions
U(VI), U^{6+}……...hexavalent oxidation state of uranium, existing under oxic conditions
UCC……...uranyl complex compounds
UNEP……...United Nations Environment Programme
UO_2……uranium dioxide (tetravalent, reduced form), in uraninite mineral
UO_2^{2+}.....uranyl ion (hexavalent, oxidized form)
$UO_2^{2+}{}_{(aq)}$.....aqueous uranyl ion
USDA……United States Department of Agriculture
UV……..ultraviolet radiation
UV-Vis……ultraviolet through the visible spectrum
VCU……...Virginia Commonwealth University, Richmond, VA
WP……..water potential
WP4…….water potential (dewpoint) meter by Decagon Devices, Inc.
λ_{Ex}……excitation wavelength in nanometers
λ_{Em}……emission wavelength in nanometers
µL…….microliter, 10^{-6} liters
µm……micrometers, micron, 10^{-6} meters
µs……...microseconds, 10^{-6} seconds, unit for fluorescence lifetime
ν…….electronic energy states, $^0\nu$ is ground state, $^1\nu$ and $^2\nu$ are excited states
Ψ……..……symbol for water potential
Ψ_m…….symbol for water potential matrix effects

ABSTRACT

ENHANCED ENVIRONMENTAL DETECTION OF URANYL COMPOUNDS BASED ON LUMINESCENCE CHARACTERIZATION

By Jean Dennis Nelson, Ph.D.

A dissertation submitted in partial fulfillment of the requirements for the degree of Doctor of Philosophy at Virginia Commonwealth University.

Virginia Commonwealth University, 2009.

Director: John E. Anderson
Associate Professor, Department of Biology

Uranium (U) contamination can be introduced to the environment as a result of mining and manufacturing activities related to nuclear power, detonation of U-containing munitions (DoD), or nuclear weapons production/processing (DOE facilities). In oxidizing environments such as surface soils, U predominantly exists as U(VI), which is highly water soluble and very mobile in soils. U(VI) compounds typically contain the UO_2^{2+} group (uranyl compounds). The uniquely structured and long-lived green luminescence (fluorescence) of the uranyl ion (under UV radiation) has been studied and remained a strong topic of interest for two centuries.

The presented research is distinct in its objective of improving capabilities for remotely sensing U contamination by understanding what environmental conditions are ideal for detection and need to be taken into consideration. Specific focuses include: 1) the accumulation and fluorescence enhancement of uranyl compounds at soil surfaces using distributed silica gel, and 2) environmental factors capable of influencing the luminescence response, directly or indirectly.

In a complex environmental system, matrix effects co-exist from key soil parameters including moisture content (affected by evaporation, temperature and humidity), soil texture, pH, CEC, organic matter and iron content. Chapter 1 is a review of pertinent background information and provides justification for the selected key environmental parameters. Chapter 2 presents empirical investigations related to the fluorescence detection and characterization of uranyl compounds in soil and aqueous samples.

An integrative experimental design was employed, testing different soils, generating steady-state fluorescence spectra, and building a comprehensive dataset which was then utilized to simultaneously test three hypotheses: The fluorescence detection of uranyl compounds is dependent upon 1) the key soil parameters, 2) the concentration of U contamination, and 3) time of analysis, specifically following the application of silica gel enhancing material. A variety of statistical approaches were employed, including the development of multiple regression models for predicting both intensity and band structure responses. These statistical models validated the first two listed hypotheses, while the third hypothesis was not supported by this dataset. The combination of inadequate moisture levels and reaction times ($\leq$ 24 hrs) greatly limited the detection of varying levels of U, depending on the soil.

CHAPTER 1: INTRODUCTION – REVIEW

1.1 Introduction to Uranium and the Uranyl Ion (UO_2^{2+})

Following the discovery of nuclear fission in 1939, an enormous amount of scientific work was directed to Uranium (U) due to its nuclear applications (Meinrath 1997). Presently, U contamination can be and has been introduced to the environment as a result of mining and manufacturing activities related to nuclear power, detonation of U-containing munitions (DoD), or nuclear weapons production and processing (at DOE facilities for example). In many locations around the world, U is considered to be a significant contaminant of both soil and water systems (both surface and deep below ground). Spent nuclear fuel, for example, contains > 95% UO_2 (Greathouse, O'Brien et al. 2002; Kim, Wronkiewicz et al. 2006), and U is considered a common and heavily studied soil and aquifer contaminant of concern at nuclear waste management facilities (Morris, Allen et al. 1996). Depleted uranium (DU, primarily ^{238}U) is considered an ideal munition for defeating protective armor due to its high density, self-sharpening and pyrophoric properties (tendency of fine particles to ignite). Several studies have focused on monitoring U contamination at sites (both test facilities and battlespace environments) where DU munitions have been fired (Sansone, Danesi et al. 2001; Johnson, Buck et al. 2004; Sztajnkrycer and Edward 2004; Di Lella, Nannoni et al. 2005; Radenkovic, Cupac et al. 2008). Table 1 summarizes general background information for Uranium.

Table 1. General background information for Uranium.

▪ Symbol: U Atomic number: 92 ▪ White/black metallic chemical element, in the actinide series of the periodic table ▪ 92 protons and electrons, 6 of which are valence electrons ▪ 141 to 146 neutrons
▪ Weakly radioactive ▪ Occurs naturally in low concentrations (a few ppm) in soil, rock and water, and is commonly extracted from uranium-bearing minerals such as uraninite ▪ In nature, exists as ^{238}U (~99.27%), ^{235}U (~0.72%) and ^{234}U (~0.0054%) ▪ ^{238}U half-life is ~ 4.5 billion yrs
▪ U is one of 3 fissile elements (can easily break apart into lighter daughter elements) ▪ High probability of ^{235}U (to a lesser degree ^{233}U) to fission when bombarded with slow neutrons generates the heat in nuclear reactors used as a source of power, and provides the fissile material for nuclear weapons (based on a sustained nuclear chain reaction) ▪ ^{238}U (depleted uranium, DU) used in kinetic energy penetrators and armor plating

Adapted from an online Encyclopedia of Chemistry.

The oxidation state of uranium is a fundamental property that can greatly influence its solubility and mobility. From an environmental perspective, the U^{6+} and U^{4+} oxidations states of U are the most important, and correspond to the hexavalent, U(VI) and the tetravalent U(IV) forms respectively. Most U(VI) compounds contain the O=U=O group and are referred to as uranyl compounds, which result from U compounds being exposed to air (Cotton 2006). The uranyl ion (UO_2^{2+}) is a highly reactive dipositive cation in which U exists as U(VI), and is the most common form encountered in the aqueous chemistry of U. While tetravalent U(IV) forms highly insoluble phases, hexavalent U(VI) forms, including the uranyl ion, are potentially much more mobile. It is well known that U predominantly exists as the hexavalent 'uranyl moiety' under many environmentally relevant redox conditions (Murakami, Ohnuki et al. 1997; Hunter and Bertsch 1998).

The uranyl ion readily forms coordination compounds, and the resulting 'uranyl species' are derived from hydrolysis (reactions with water) and complexation with carbonate, fluoride, sulfate and phosphate ligands (to name a few) (Meinrath 1997; Hunter and Bertsch 1998). These

uranyl complexes (or uranyl complex compounds, UCC) can be cationic, neutral, or anionic, but all feature a *trans*-UO_2 group (Cotton 2006). The uranyl complexes are characterized by a linear (or near-linear) O=U=O group bounded to 3 – 6 ligands in the equatorial plane (see Figure 1 and Figure 2) (Morris, Conradson et al. 1992; Meinrath 1997; Formosinho Sebastiao, Burrows Hugh et al. 2003). The hydrated uranyl ion, for example, is pentagonally coordinated by five water ligands in the equatorial sphere. The linear UO_2^{2+} group is thermodynamically and kinetically stable, and its characteristic short U – O bonds indicate a strong covalent interaction between the central U atom and the two axial oxygen atoms. On the contrary, the equatorial ligands are highly subject to change, and are characterized by significantly longer U – ligand bond lengths (Meinrath 1997).

Figure 1. Structural representation of the uranyl ion: U atom (blue), axial oxygen atoms (red), and coordinating atoms (3 – 6) in equatorial plane (green). Adapted from (Morris, Conradson et al. 1992).

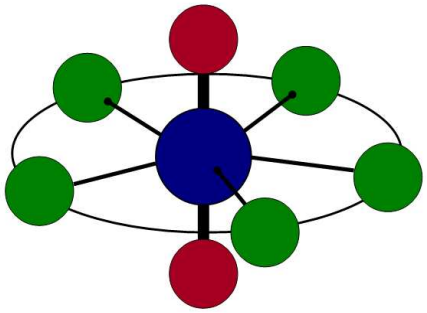

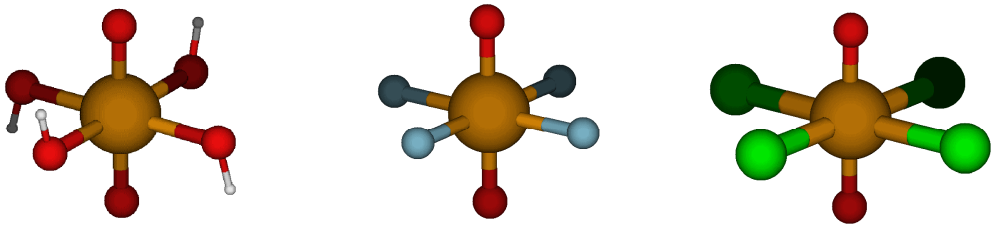

$[UO_2(OH)_4]^{2-}$ $[UO_2F_4]^{2-}$ $[UO_2Cl_4]^{2-}$

Figure 2. Proposed ground state (f^0) structures for common *trans*-uranyl (VI) systems, based on density functional calculations. Adapted from (Schreckenbach, Hay et al. 1999).

Simply stated, uranyl compounds tend to emit a bright green fluorescence when exposed to ultraviolet and visible (UV-Vis) irradiation (light) (Cotton 2006). While the uranyl ion (consisting of U(VI)) exhibits this natural (intrinsic) and long-lived fluorescence (referred to by some as phosphorescence), other oxidative states of U (such as U(IV)) are generally non-luminescent (Sowder, Clark et al. 1998). The uranyl ion's very unique green emission (fluorescence) spectral signature consists of several approximately equally spaced bands or peaks (see Figure 3). This diagnostic 'vibronic structure' seen in the emission spectrum is principally due to the symmetric stretching vibrations of the UO_2^{2+} molecule in the *ground* electronic state. Note the emission spectrum occurs at the long-wavelength (lower energy) side of the absorption spectrum. The excitation or absorption spectrum can also display this unique fine structure (depending on the conditions, such as extremely low temperature or cryogenic spectra) due to the symmetric O=U=O vibrations occurring in the *excited* electronic states (refer to Figure 4) (Clark, Conradson et al. 1999). Table 2 describes the key molecular processes pertinent to the fluorescence spectroscopy of U(VI). Excitation in the UV range (~ 250 – 300 nm) is often preferred due to the intense absorption at these shorter (higher energy) wavelengths, whereas the direct excitation of the fluorescence state by absorption of light in the 370 – 460 nm range (415 – 420 nm peak) is a much weaker process (Meinrath 1997). This is clearly depicted by the excitation spectrum shown in Figure 3.

The intense luminescence and corresponding spectroscopic properties of uranyl compounds have been studied for over 200 years (Syt'ko and Umreiko 1998). A comprehensive monograph, published by E. Rabinowitch and R. Belford in 1964, provided an overview of spectroscopic studies performed during the Manhattan Project. These works, while generally focusing on the luminescence and photochemistry of uranyl compounds, specifically addressed:

the luminescence intensities and decays, temperature effects on spectra, vibrational frequencies (band locations), lifetimes of the excited states, and interactions resulting in enhancement and quenching by inorganic ions and organic materials (Rabinowitch and Belford 1964). It is well known that, in addition to their 'steady-state' emission properties, uranyl compounds are also characterized by relatively long fluorescence lifetimes (decays), both of which can be altered based on U speciation, complexation, and quenching.

The spectroscopic properties of a uranyl compound is very sensitive to the nature of the complex (U and atoms in its first coordination sphere) (Syt'ko and Umreiko 1998). The intensity of the absorption bands in the excitation spectra of uranyl compounds significantly depends on the symmetry of the complexes (Formosinho Sebastiao, Burrows Hugh et al. 2003). Similarly, the detailed characteristics of the vibrationally-structured luminescence spectra of uranyl compounds varies in a sensitive way to changes in the coordination environment in the equatorial plane of the ion (Duff, Morris et al. 2000). Detailed information encoded in the spectral data is often used for uranyl species identification (Duff, Morris et al. 2000). Speciation, in this context, refers to the specific form of the uranyl complex, and the local environment of the uranyl ion (Meinrath 1997). Looking at the vibrationally structured emission spectrum (refer to Figure 3), the four main diagnostic features that have been used for characterizing uranyl speciation are: 1) electronic energy (appearance of emission peaks), 2) vibronic spacing (spaces between peaks), 3) vibronic linewidth (peak widths), and 4) intensity pattern (peak heights) (Morris, Conradson et al. 1992).

As previously stated, the ligand surrounding the UO_2^{2+} molecule is one of the most important factors determining the optical properties of uranyl complex compounds (UCC). A comprehensive review regarding the spectroscopic properties and electronic structure of UCC

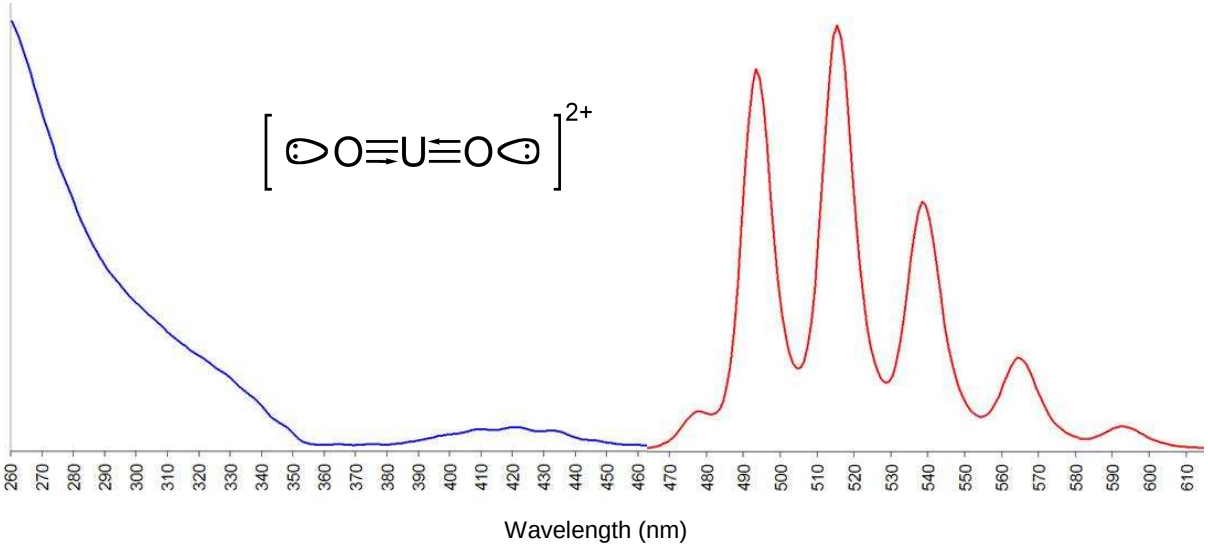

Figure 3. Steady-state excitation (blue) and fluorescence emission (red) scans demonstrating the vibrational spectral structure of a uranyl aqueous solution at room temperature (arbitrary intensity units).

Figure 4. Jablonski diagram of an absorption and emission process (right, adapted from Meinrath, 1997). Refer also to Table 2.

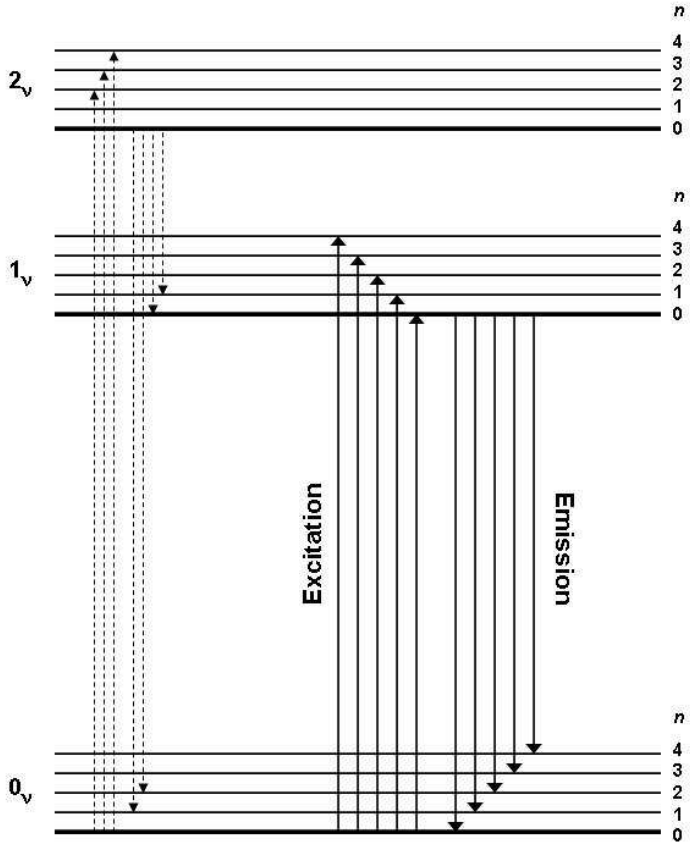

Table 2. Key molecular processes pertinent to the fluorescence spectroscopy of U(VI). Refer also to Figure 4. Adapted from (Meinrath 1997).

1. Upon light absorption, an electron is excited from the ground state to excited states. Energy is transferred from an electronic ground state ($^0\nu_n$) to different excited states ($^1\nu_n$ and $^2\nu_n$), each electronic state having *n* vibrational energy levels. At room temperature (298 K), only vibrational ground levels ($n = 0$) are typically occupied.
2. With excitation from the ground state to one of the excited states (governed by the Franck-Condon principle), molecules are excited to higher vibrational levels ($n > 0$) within the excited electronic states (the excited molecule strongly vibrates).
3. The vibrational energy quickly dissipates due to collisions with neighboring molecules. Equilibrated excited states are then formed with excited electrons now occupying the vibrational ground states of the excited electronic states ($^1\nu_0$ and $^2\nu_0$).
4. The electronic relaxation of the $^2\nu_0$ excited state can occur either by direct relaxation to the electronic ground state ($^0\nu$) or to the first excited state ($^1\nu$). Studies have shown that when U(VI) is excited to states higher than $^1\nu$ (such as $^2\nu$, etc), relaxation occurs to the first excited state ($^1\nu$).
5. Occupation of the fluorescence first excited state ($^1\nu$) via excitation first to higher excited states followed by relaxation to the first excited state is preferred and more efficient compared to direct excitation from the ground state to the first excited state. In the case of $UO_2^{2+}{}_{(aq)}$, the direct excitation of the fluorescence state by absorption of visible light (370 – 500 nm) is a weak process compared to the intense absorption of UV light, and therefore excitation in the UV range is often preferred. For UO_2^{2+}, while the intense UV light absorption results in the occupation of the $^2\nu$ state, the absorption of visible light results in the occupation of the $^1\nu$ state.
6. The fluorescence emission process (also governed by the Franck-Condon principle) results from the relaxation processes of $^1\nu_0 \rightarrow {}^0\nu_n$ states. The approximately equally spaced emission bands (see Figure 3) correspond to the different energies emitted as the electrons return to the varying vibrational energy levels of the electronic ground state.

was provided by Syt'ko and Umreiko in 1998. The authors describe in more detail how, as an individual class of compounds, UCC possess electronic spectra similar to each other in the UV region (i.e., display the same number of bands of electronic transitions), while the nature and symmetry of the coordinated ligands predominantly influences the vibrational spectra seen in the

visible range (Syt'ko and Umreiko 1998). The most detailed and reliable depiction of the uranyl excited states (electronic structure) and resulting spectroscopic vibrational structure is provided by the Denning group (Denning, Snellgrove et al. 1979; Denning 1992).

The optical properties of uranyl compounds result from electronic transitions from three occupied molecular orbitals (displaying a specific *f*-electronic structure). The highest occupied orbital of the uranyl complex is predominantly ligand in nature (i.e., associated with the transfer of electrons from the equatorial ligands to uranium). The lower-lying occupied orbitals, however, are primarily associated with the 'self-isolated' uranyl group, which is known for maintaining its individuality in the majority of chemical reactions (Syt'ko and Umreiko 1998). The excited uranyl's reactions can include hydrogen atom abstraction, electron transfer, and energy transfer (Formosinho Sebastiao, Burrows Hugh et al. 2003).

The fluorescence quantum yield (QY) is defined as the number of photons emitted to the number of photons absorbed, and is reflected in the intensity (height) of the emission spectra. While the QY of luminescence for UCC is dependent upon the excitation radiation frequency (or excitation wavelength, λ_{Ex}), the luminescence spectra (band structure) for UCC are independent of the excitation frequency. Higher-energy excitations act upon the uranyl complex as a whole, potentially resulting in: 1) the 'interior filter' effect due to the absorption of energy by the ligands themselves, 2) the transfer of electronic excitation energy from UO_2^{2+} to ligands, followed by nonradiative decays, or 3) intrinsic dissipation of electronic excitation energy due to the simultaneous excitation of both uranyl and ligand electrons. On the contrary, lower energy excitations (λ_{Ex} longer than ~ 330 nm) result in a constancy of QY of UCC luminescence due to localization of electronic excitation in the UO_2^{2+} group (Syt'ko and Umreiko 1998). The effect

of using higher versus lower energy excitation frequencies or wavelengths is further discussed in Table 2, block 5.

1.2 Uranium Contamination in the Environment

Uranium (U) occurs naturally in low concentrations (a few ppm) in soil and water systems, as well as in U-bearing minerals (uranium ores such as uraninite). However, U is also a contaminant of concern introduced into the environment as a result of: mining, milling and other processes related to the nuclear power industry, nuclear weapons production and processing, and detonation of U-containing munitions (Hunter and Bertsch 1998; Greathouse, O'Brien et al. 2002). An immense body of literature exists related to U surface and subsurface contamination at DOE sites, for example. The geochemical behavior of U, including its transport and potential remediation, has been a strong area of concern and intensive research (Liu, Zachara et al. 2004). The environmental behavior of uranium itself is the same whether naturally occurring or anthropogenically introduced; however it is the chemical and physical form of the U-containing molecule or compound that determines its fate (Sansone, Danesi et al. 2001).

In the environment, U typically exists in either the hexavalent [U^{6+}, U(VI), oxidized] or tetravalent [U^{4+}, U(IV), reduced] state (Bostick, Fendorf et al. 2002; Stork, Smartt et al. 2006). The oxidation state of U in sediments is very important since the solubility of U(VI) species (including uranyl) is much greater than that of U(IV) species (Bostick, Fendorf et al. 2002; Tokunaga, Wan et al. 2008). Under naturally occurring oxidizing conditions (such as aqueous systems and surface soils), U predominantly exists as the hexavalent U(VI)- uranyl form, potentially very mobile in the environment but readily forming stable complexes with solids and a range of anions (Reeder, Nugent et al. 2000; Bostick, Fendorf et al. 2002; Greathouse, O'Brien

et al. 2002). Several studies of uranyl sorbed on a variety of mineral types (such as silica, kaolinite, etc.) (Greathouse, O'Brien et al. 2002) as well as studies of contaminated soils from specific DOE sites (such as the Fernald, OH and Savannah River, SC sites) have all confirmed that the majority of U (75 – 95%) exists as the hexavalent, U(VI) form (Morris, Conradson et al. 1992; Morris, Allen et al. 1996; Hunter and Bertsch 1998). This further confirms the appropriateness of uranyl-based detection schemes. From a remediation perspective, however, the dominance of hexavalent U is seen as a drawback since its greater solubility and mobility increases the likelihood of ground water contamination and resulting need for timelier remediation (Morris, Conradson et al. 1992). In fact, the microbial reduction of U(VI) to U(IV) has been investigated as a promising remediation strategy below ground to help keep the U immobilized (Hunter and Bertsch 1998; Tokunaga, Wan et al. 2008).

The transport of U in the environment is not only a function of this metals' oxidation state, but also the aqueous and solid phase chemistry of its surroundings (Duff, Morris et al. 2000). In natural aqueous systems, the uranyl ion forms complexes with various ligands (Liu, Zachara et al. 2004), but the most fundamental reaction it undergoes is hydrolysis. The fluorescent properties of the various hydrolyzed species of U(VI) have been studied by many (Eliet, Bidoglio et al. 1995; Billard, Ansoborlo et al. 2003; Formosinho Sebastiao, Burrows Hugh et al. 2003), predominantly as a function of pH (discussed in more detail below). The hydroxide-U complexes can be presented as: $(UO_2)_m(OH)_n^{(2m-n)}$ where (m, n) typically are (1, 0), (1, 1), (1, 3), (2, 2), (3, 5) and (4, 7) corresponding to: UO_2^{2+}, UO_2OH^+, $UO_2(OH)_3^-$, $(UO_2)_2(OH)_2^{2+}$, $(UO_2)_3(OH)_5^+$, and $(UO_2)_4(OH)_7^+$ respectively (Eliet, Bidoglio et al. 1995; Kirishima, Kimura et al. 2004; Mibus, Sachs et al. 2007). These different aqueous species of uranyl hydroxides can display some variations in their spectral properties. For example, one study indicated that as you

progress from $UO_2^{2+} \rightarrow (UO_2)_2(OH)_2^{2+} \rightarrow (UO_2)_3(OH)_5^{+}$ with pH increasing from highly acidic to neutral, a strong increase in molar absorption as well as a 'red - shift' (peak shift to longer wavelengths) is seen in the absorption spectrum (Meinrath 1997). Another study indicated that the $(UO_2)_2(OH)_2^{2+}$and $(UO_2)_3(OH)_5^{+}$ forms tend to be more fluorescent (in pure aqueous solutions) than UO_2^{2+} (Eliet, Bidoglio et al. 1995).

As previously stated, UO_2^{2+} displays a strong tendency to form complexes with other ligands in addition to hydroxides, such as carbonates, silicates and phosphates. Table 3 lists the names and chemical formulas for several commonly studied U(VI) minerals. In both aqueous and soil/sediment systems (typically neutral or higher pH), complexation with carbonate (CO_3^{2-}) is a dominant geochemical reaction (Meinrath 1997; Reeder, Nugent et al. 2000). Uranyl's complexation with carbonates, in addition to other dissolved ligands such as sulfates, phosphates, and organic matter (OM) can significantly limit sorption to soil particles, thereby enhancing the transport of U (Meinrath 1997; Bostick, Fendorf et al. 2002). While adsorption appears to be the primary means of uptake of uranyl by fine-grained mineral phases (such as hydroxides, oxides, and clays), co-precipitation is believed to dominate uranyl's uptake by carbonates (Reeder, Nugent et al. 2000).

The uptake of U by soil and sediment components has been extensively studied (Moyes, Parkman et al. 2000; Reeder, Nugent et al. 2000; Giammar and Hering 2001; Bostick, Fendorf et al. 2002; Chisholm-Brause, Berg et al. 2004; Johnson, Buck et al. 2004; Payne, Davis et al. 2004; Catalano and Brown 2005; Arai, McBeath et al. 2006). Investigations of uranyl sorption reactions in heterogeneous soils are complicated in that they depend strongly on the pore-water geochemical conditions (such as pH, ionic strength, and total U concentration) (Um, Serne et al. 2007), as well as the presence of variable mineral types, biological (reducing) activity, and

Table 3. Names and chemical formulas for commonly studied Uranium (VI) minerals. Adapted from (Morris, Allen et al. 1996).

Mineral Name	Chemical Formula
Hydroxides and Oxyhydroxides	
bedquerelite	$Ca[(UO_2)_6O_4(OH)_6] \cdot 8H_2O$
billietite	$Ba[(UO_2)_6O_4(OH)_6] \cdot 4H_2O$
curite	$Pb_2U_5O_{17} \cdot 4H_2O$
schoepite	$(UO_2)(OH)_2 \cdot H_2O$
Carbonates	
kamotoite	$Y_2U_4(CO_3)_3O_{12} \cdot 14.5H_2O$
liebigite	$Ca_2UO_2(CO_3)_3 \cdot 11H_2O$
rutherfordine	UO_2CO_3
Silicates	
beta-uranophane	$Ca(UO_2)SiO_3(OH)_2 \cdot 5H_2O$
boltwoodite	$(H_2O)K(UO_2)(SiO_4)$
cuprosklodowskite	$(H_3O)_2Cu(UO_2)_2(SiO_4)_2 \cdot 2H_2O$
kasolite	$Pb(UO_2)SiO_4 \cdot H_2O$
sklodowskite	$(H_3O)_2Mg(UO_2)_2(SiO_4)_2 \cdot 2H_2O$
soddyite	$(UO_2)_2SiO_4 \cdot 2H_2O$
Phosphates	
meta-ankoleite	$K_2(UO_2)_2(PO_4)_2 \cdot 6H_2O$
meta-autunite	$Ca(UO_2)_2(PO_4)_2 \cdot 2\text{-}6H_2O$
meta-torbernite	$Cu(UO_2)_2(PO_4)_2 \cdot 8H_2O$
phosphuranylite	$Ca(UO_2)_3(PO_4)_2(OH)_2 \cdot 6H_2O$
saleeite	$Mg(UO_2)_2(PO_4)_2 \cdot 10H_2O$

organic matter (Bostick, Fendorf et al. 2002). Sorption specifically to clays, ferric (iron) oxides, and silicate minerals are known to strongly limit migration through increased retention of U(VI) (Payne, Davis et al. 1994; Johnson, Buck et al. 2004; Walter, Arnold et al. 2005; Radenkovic, Cupac et al. 2008). The sorptive interactions of U with metal oxides and clays can be quite strong (Morris, Conradson et al. 1992), and studies have shown that increased fractions of clay minerals as well as the formation of insoluble uranyl oxide-silicate aggregates can significantly retard U migration (Johnson, Buck et al. 2004). Computer simulation models of DU transport in natural subsurface systems have further verified that redox conditions, precipitation and sorption processes result in the significant immobilization of DU (Chen and Yiacoumi 2002).

The mobility of U in soils is predominantly controlled by sorption to mineral surfaces and dissolution or precipitation of U solids (Liu, Zachara et al. 2004). The weathering of uranyl minerals due to episodic influx of rain results in the continued dissolution and reprecipitation of uranyl species (Morris, Conradson et al. 1992). These competing processes are strongly dependent upon the concentration of the contamination (Tokunaga, Wan et al. 2004; Krepelova, Brendler et al. 2007). As would be expected, the sorption of U by soils is strongest when U concentrations are low, whereas the diffusion of U through soils is greater when U concentrations are high. In highly contaminated areas, U is weakly bound and easily exchangeable (Radenkovic, Cupac et al. 2008). Hydrodynamic experiments have demonstrated the labile nature of uranyl contamination, and the reversibility of its sorption (Bostick, Fendorf et al. 2002). Aged soil samples from contaminated DOE sites as well as arid soils contaminated by DU penetrators both indicated that the majority of the precipitated or sorbed U was easily removed (labile) and diffused into the aqueous phase, while only a small percentage was so strongly bound or imbedded within the particle interiors that it could not be removed without strong leaching agents (Johnson, Buck et al. 2004; Liu, Zachara et al. 2004). Kinetic simulation models of DU transport in natural systems have indicated that while the sorption of DU appears to be a rapid process, the subsequent mobilization of DU is a relatively slow process (Chen and Yiacoumi 2002). Empirical studies of U(VI) adsorption and transport in natural heterogeneous subsurface media showed that the rate of U(VI) adsorption is nonlinear in that it is more rapid at first, but then slows after 24 – 48 hours, suggesting a decreased adsorption of U on soil particle surfaces with increasing surface loading (Barnett, Jardine et al. 2000).

The US DOE is responsible for a large number of sites that are known to have U contaminated soils resulting from over 50 years of nuclear weapons and energy production. A

vast number of large area subsurface waste sites exist, in addition to U mill tailing sites (Kelsh and Parsons 1997). Natural, heterogeneous soil samples used for adsorption and U transport studies have typically been obtained from contaminated DOE sites including: Oak Ridge (OR) Reservation in East Tennessee, the Savannah River (SR) site on the Georgia – South Carolina border, and the Hanford (HF) Reservation in southeastern Washington. All three of these sites are known for having subsurface contamination due to their history of U waste disposal (Barnett, Jardine et al. 2000; Bostick, Fendorf et al. 2002). Studies of soil-core samples from the Hanford Reservation indicated that the U contamination was most abundant between 20 – 50 meters below ground, for sites contaminated 50 years prior (Liu, Zachara et al. 2004; Wang, Zachara et al. 2005). The Fernald Environmental Management Site in Ohio has been a heavily studied location due to its history of uranium processing and weapons production during the Cold War years (Buck, Brown et al. 1996). However, the migration of U at this site has not be nearly as extensive, with the shallow subsurface primarily requiring significant remediation in order to meet EPA standards (Morris, Conradson et al. 1992; Morris, Allen et al. 1996). DOE reports generated by Oak Ridge National Laboratory (ORNL) and Los Alamos National Laboratory (LANL) provided detailed characterization of U contaminated soils at Fernald, focusing on: 1) U distribution with soil depth, 2) soil particle size distributions and their U contribution, and 3) soil chemical and physical properties (Lee and Marsh 1992; Morris, Conradson et al. 1992). These reports focused on specific locations at Fernald representing a broad range of U source terms, such as drum storage areas contaminated by U product spills and incinerator areas contaminated by airborne U material. These studies confirmed that, for the most part, the high U concentrations were fairly shallow (< 10 cm depth), with undisturbed sites typically displaying a

clear distinction between the 0 – 5 cm and 5 – 10 cm ranges in depth. Reference information for estimates of U contamination (in parts-per-million, ppm) is listed in Table 4.

Certain circumstances can result in significantly high U levels in areas where U exists naturally. In the San Joaquin Valley (SJV) in California, evaporation ponds are used for containment of irrigation drainage waters of local agricultural soils that contain low levels of naturally occurring U (Duff, Morris et al. 2000). While the surface sediments (0 – 5 cm) of these evaporation ponds contained one-third U(IV), the data suggested that there was little variation in the mobility of U(VI) species as well, with the total U concentration and percent U(VI) being greatest in the surface sediments (see Table 4).

Table 4. Reference information for estimates of uranium concentrations (ppm) in environmental soil samples.

Site / Details	**Approx. [U] (ppm)** [*]
World average [U] for surface soils. [a,b] Absolute [U] for worldwide reported natural range in soil. [c]	*2 – 3* *0.8 – 11*
Fernald Environmental Management Site, Ohio (DOE) *Reference Sites* [d] U contamination was shallow (< 10 cm). [d] *Reference Sites* [e] U contamination was fairly shallow (< 30 cm). [e]	 *2 – 8* 30 – 8,500 *3 – 5* 10 – 8,000 (avg. ~ 500)
Hanford Reservation, Washington (DOE) Contaminated 50 yrs prior to studies. Borehole samples revealed U was most abundant 20 – 50 m below ground. [f,g]	 100 – 400
Oak Ridge Field Research Center, Tennessee (DOE) Area 2, [U] in soil-saprolite core. Highest [U] found 6 m below ground. [h]	300
Southern Serbia / Kosovo (following 1999 conflict) Several studies examining soil samples in the close vicinity of DU penetrators and impact zones, associated with the use of DU ammunitions. Study 1: Large-scale, multi-organizational study (coordinated by UNEP). [i] [U] dropped to background levels below 18 cm depth. *Reference Sites* [i] Site 1: Site 3: Site 5: Site 6: Note: Site 2 and 4 had background levels. Study 2: [U] in topsoils (0 – 20 cm), several sampling sites. [c] Majority of sites showed below background levels (< 6 ppm). *Reference Sites* [c] Highest levels of U (> 6 ppm) seen for sites inside or close to clusters of DU penetrator holes.	 *1 – 4* 8 – 18,000 35 – 250 100 – 4500 200 – 700 *1 – 2* 6 – 32

Table 4. (Continued).

Site / Details	**Approx. [U] (ppm)** *
Study 3: DU concentrations fall down to 1% of the initial values ~15 cm from the source point. [j]	
Reference Sites [j]	*4 – 6*
Ground-level entrance site	6 – 8.5
Projectile path	6 – 7
Soil layer adjacent to penetrator	20 – 24
DU penetrator test range (Upper Mojave Desert) [k]	
Undisturbed penetrators fired in early 1980's, samples tested ~ 20 yrs later (DU in arid soils under penetrators, with depth).	
Reference Sites [k]	*4 – 5*
Site 1: 0 – 5 cm	10,000 – 1000
5 – 20 cm	500 – 50
Site 2: 5 – 20 cm	150 – 15
Evaporation pond sediments, SJV, CA [l]	
Used for the containment of irrigation drainage waters. Contain elevated [U] due to leaching via carbonate-rich irrigation waters of local agricultural soils containing low levels of naturally-occurring U.	
0 – 5 cm	180 – 280
5 – 10 cm	avg. 70
10 – 40 cm	< 50

* All reported U levels were converted to ppm estimates based on the assumptions: ^{238}U: 1 ppm ≈ 12.3 Bq kg^{-1}, ^{tot}U: 1 ppm ≈ 12.8 Bq kg^{-1}.

[a] (Bourabee, Bakir et al. 1995), [b] (Sztajnkrycer and Edward 2004),
[c] (Di Lella, Nannoni et al. 2005)
[d] (Lee and Marsh 1992), [e] (Morris, Allen et al. 1996)
[f] (Liu, Zachara et al. 2004), [g] (Wang, Zachara et al. 2005)
[h] (Moon, Roh et al. 2006)
[i] (Sansone, Danesi et al. 2001)
[j] (Radenkovic, Cupac et al. 2008)
[k] (Johnson, Buck et al. 2004)
[l] (Duff, Morris et al. 2000)

As previously stated, U can be introduced into the environment where DU ammunitions have been utilized. Following military activities, the kinetic DU penetrators or fragments remain buried in the ground where they undergo rapid corrosion. As water evaporates following seasonal rainfalls, aqueous U concentrations can become high enough to result in the precipitation of secondary U phases (Johnson, Buck et al. 2004). When the penetrators hit hard objects, DU dust is formed and dispersed in the environment, potentially contaminating the air, water and ground, with the rainfall and hydrology along with the chemistry and structure of the surrounding soil affecting its subsequent mobility (Sansone, Danesi et al. 2001). Several studies, have focused on examining soil and water samples in close vicinity to DU penetrators and impact zones (refer to Table 4) (Sansone, Danesi et al. 2001; Johnson, Buck et al. 2004; Di Lella, Nannoni et al. 2005; Radenkovic, Cupac et al. 2008). Some common observations supported by these particular studies are that the U contamination tends to be fairly shallow, and is highly variable, usually characterized by isolated 'hot spots' in close vicinity to the penetrator holes.

A large-scale, multi-organizational field study was conducted in 2000, coordinated by UNEP, to evaluate the level of DU released in the environment in specific areas where NATO had used DU ammunitions during the Kosovo conflict of 1999 (Sansone, Danesi et al. 2001). Natural versus anthropogenic U were distinguished based on ^{234}U / ^{238}U and ^{235}U / ^{238}U activity concentration ratios. All the water samples collected had very low (natural background) levels of U, with only two questionable groundwater samples. Soil samples were collected at sites where DU ammunition had been fired and where penetrator fragments or jackets were found on the soil surface. Surface soil samples showed large variability, indicating the impact of DU ammunitions can be very site-specific, depending on the physical and chemical conditions at the

time of impact and following. In general, the total concentration of U dropped to background natural levels after approximately 18 cm in depth.

Other studies confirmed elevated levels of U tend to exist within close vicinity to munition impact sites, with detectable levels of DU typically limited to the impact hole (Sztajnkrycer and Edward 2004). Studies conducted by others in southern Serbia/Kosovo more recently, though not indicating levels as high as seen in the previous study, still reported U contamination significantly higher than background levels in soils directly adjacent to DU penetrators and inside their impact holes (Di Lella, Nannoni et al. 2005; Radenkovic, Cupac et al. 2008). However, DU concentrations fell down to 1% of their initial values at only 15 cm from the source point (Radenkovic, Cupac et al. 2008). A study conducted at a DU penetrator test range in the Upper Mojave Desert, where soils are arid and alkaline, indicated that DU kinetic penetrators exposed on the desert surface for 22 years can still result in significantly high U contamination levels in soils (Johnson, Buck et al. 2004). However, the concentration of U steadily dropped with depth for the 0 – 20 cm range.

1.3 Luminescence Detection and Characterization of Uranyl

The luminescence detection and characterization of U contamination has been undertaken for soil and water samples from sites described above and elsewhere. The application of phosphorimetry for detecting U in real world samples is complicated, however, by sample matrix interferences. Such matrix effects could include the influence of cations, anions and other ligands common in natural systems that are known to quench uranyl fluorescence (Sowder, Clark et al. 1998). Most halides for example (such as chloride, but with fluoride being an exception) (Yokoyama, Moriyasu et al. 1976; Moriyasu, Yokoyama et al. 1977) as well as oxidizable metals

such as lead, iron (II), and manganese (II) are strong quenching agents for uranyl luminescence (Brina and Miller 1993). Inorganic ions like iron and chloride (depending on their charge) are of concern because they are commonly abundant in environmental systems, and are capable of either extracting excited electrons from uranyl entities or transferring electrons to electronically excited U-containing molecules, thereby reducing the emission of the excited uranyl species (Meinrath 1997). The abundance of carbonate in environmental systems is also of concern since high concentrations of free carbonate (radicals) has been associated with the quenching and therefore decreased fluorescence yields of uranyl luminescence (Meinrath 1997).

Despite these potential interferences, spectroscopic characterization of uranyl compounds has extensively been used for studying U-containing minerals and aqueous phases, often times in an attempt to understand these complex matrix effects more fully. On one hand, optical luminescence spectroscopy is referred to as a powerful tool for characterizing U(VI) species in a variety of matrices, while on the other hand the in-situ spectroscopic characterization of U speciation and oxidative state in soils and sediments is described as being limited due to the interferences inherent in heterogeneous natural materials and limited analytical detection (Duff, Morris et al. 2000). Advanced spectroscopic techniques, such as time-resolved laser-induced fluorescence spectroscopy (TRLFS), are routinely utilized for collecting the emission spectra and determining the associated lifetimes for uranyl compounds, including the main environmental species: pure uranyl, hydrolyzed forms, and carbonate forms (Meinrath 1997). Some examples of detailed studies reporting fluorescence emission band locations (energy wavelengths) as well as associated lifetimes (decays) using TRLRS include: 1) a study of uranyl carbonate species adsorbed on mineral surfaces (Amayri, Reich et al. 2005), 2) a study of U sorbed to albite (silica-based) minerals for pH 5 – 6.5 (Walter, Arnold et al. 2005), and 3) a study of U(VI) surface

complexes on kaolinite (clay) for pH 5 – 8, in the presence and absence of humic acid (HA) (Krepelova, Brendler et al. 2007). Walter *et al.* (2005) also presented a summary table of fluorescence data (emission bands and lifetime values) reported for aqueous, sorbed and solid U reference species (Eliet, Bidoglio et al. 1995; Moll, Geipel et al. 1998; Moulin, Laszak et al. 1998; Chisholm-Brause, Berg et al. 2001; Gabriel, Charlet et al. 2001; Walter, Arnold et al. 2005). Other studies have focused on the application of time-resolved emission spectroscopy (TRES) in general to U(VI) characterization in aqueous media. A comprehensive multi-lab study discussed U speciation and lifetime changes for uranyl in aqueous solutions of varying pH (Billard, Ansoborlo et al. 2003). This study describes how the spectroscopic signature of a given $U(VI)_{(aq)}$ species is made through the emission spectrum rather than through its lifetime value, and that a complete understanding of the aqueous medium (chemical composition and ionic strength) is needed to allow for comparison of lifetime values. Some studies go as far as to claim that the fluorescence emission spectra can be used to identify specific U species in environmental sediment samples based on a library of luminescence spectral data for U(VI) mineral phases and inorganic salts (Duff, Morris et al. 2000).

When analyzing U-contaminated soil samples with varying physical and chemical features, spectroscopic techniques are typically applied as a means of bulk-scale analysis, determining the major chemical phases and average speciation for a given sample (Hunter and Bertsch 1998). A clear distinction was seen in the spectral emission patterns for sediment samples collected at the Fernald and Savannah River DOE sites, indicating that the primary U chemistry and speciation (on average) differs substantially between these two sites (Hunter and Bertsch 1998). Other studies examining soils from a variety of sampling locations at the Fernald site indicated clear spectroscopic distinctions: 1) location to location, 2) with depth and 3) within

different soil fractions, further demonstrating the potential heterogeneity of uranyl forms (Morris, Conradson et al. 1992). However, the luminescence from these U(VI) species at this site indicates the dominance of three major uranyl phases: a uranyl phosphate form (autunite), a uranyl hydroxide form (most likely schoepite), and a weakly-defined uranyl organic phase (Morris, Allen et al. 1996).

In examining complex environmental samples, it is not uncommon to observe weak, broad and featureless fluorescence spectra for samples analyzed at room temperature (Wang, Zachara et al. 2005). For this reason, many studies reported data collected at very low (cryogenic) temperatures utilizing liquid helium or nitrogen (Duff, Morris et al. 2000; Wang, Zachara John et al. 2005; Chang, Korshin Gregory et al. 2006). An in-depth comparison between uranyl silicate minerals and U(VI)-contaminated vadose zone sediments from the Hanford site, analyzed at both room temperature and under cryogenic conditions, indicated extreme low temperature fluorescence measurements can significantly improve both emission intensity and spectral resolution (peak definition) (Wang, Zachara et al. 2005). Another study examining real-world U-containing samples, utilizing cryogenic conditions for analysis, was that of evaporation pond sediments from the San Joaquin Valley, where clear distinctions were made between the luminescence spectra of surface sediments (0 – 5 cm) and deeper sediments (Duff, Morris et al. 2000).

Despite the advantages of using extremely low temperature conditions for study, spectroscopic analysis conducted under ambient conditions are more applicable and comparable to *in-situ* remote sensing techniques. As previously indicated, however, spectroscopic data of heterogeneous contaminated sediments can be difficult to interpret since samples can contain complex mixtures of chemical phases (Hunter and Bertsch 1998). Several studies used models

in conjugation with their data collection to help improve the detection and characterization of U by taking into account important features such as: absorption, quenching, and complexation (Moulin, Decambox et al. 1996). Spectral deconvolution techniques are also routinely utilized to improve determination of U speciation and concentration (Eliet, Bidoglio et al. 1995; Moulin, Decambox et al. 1996; Wang, Zachara John et al. 2005). In most cases, however, straight forward UV-Vis spectroscopy is typically thought of as not being sensitive enough to detect U(VI) concentrations even in contaminated areas (Meinrath 1997). Others have argued that there is a strong need for the development of reliable field-standard fluorescence values (emission peaks and lifetimes) for various uranyl species; otherwise the application of photophysics to uranyl might remain condemned as a 'black art' lacking quality assurance and control on levels of U under environmental conditions (Billard, Ansoborlo et al. 2003).

1.4 Uranium Extraction and Fluorescence Enhancement

Most efforts aimed at extending the detection limits for uranyl involve the enhancement of uranyl's fluorescence and phosphorescence, and utilize time-discrimination detection (Kaminski, Purcell et al. 1981). In other words: 1) improve its overall steady-state (average) fluorescence response (peak definition and intensity), 2) lengthen the lifetime decay and 3) use time-gated instrumentation. Both steady-state and time-resolved measurements have long been used to study the absorption and luminescent properties of uranyl (Lopez and Birch 1996). Time-resolved measurements, however, offer an advantage over steady-state measurements in that they can discriminate longer-lived luminescent responses, such as those of uranyl compounds with microsecond (μs) to millisecond (ms) decays, from shorter-lived luminescent

responses such as those of natural organic matter, NOM having nanosecond (ns) decays (described in more detail below) (Lopez and Birch 1996).

Outside the realm of remote sensing techniques, chemical and physical methods of enhancement have long been utilized for improvement of uranyl's fluorescence signal (Lopez and Birch 1996). For example, uranyl's interaction with fluoride ions (F^-) in solution can improve its analytical detection (Beitz and Williams 1997). Other studies describe enhancement by acids such as hydrofluoric, phosphoric and sulfuric acids, which in solution can shield the uranyl ion from nonradiative decays, thereby improving its overall fluorescence response (Kaminski, Purcell et al. 1981). Uranyl complexation with other ligands such as phosphates can also greatly reduce solution quenching effects (Brina and Miller 1993; Sowder, Clark et al. 1998). In fact, a very commonly used and excepted standard technique for determining trace U levels in water, urine, milk, and possibly soil extracts is referred to as the KPA method (Kinetic Phosphorescence Analyzer, Chemcheck Instruments, Inc.) (Brina and Miller 1992; Brina and Miller 1993; Sowder, Clark et al. 1998; Duff, Morris et al. 2000). This method involves the addition of the Uraplex^{TM} proprietary phosphate-based complexing solution to the samples prior to analysis, which enhances the uranyl's phosphorescence (Sowder, Clark et al. 1998) by protecting the uranyl ions from solvent quenching (Brina and Miller 1993).

The enhancement of uranyl's luminescence in aqueous solutions is also achieved via complexation with silica-based materials, such as silica gel and colloidal silica, which results in an increased: 1) molar absorption, 2) steady-state emission and 3) lifetime of the decay (Lopez and Birch 1996). Silica gel has been used extensively as a stable solid-matrix material for extracting uranyl from the solution phase, which can be subsequently filtered or dried out (Lopez and Birch 1996; Reich, Moll et al. 1998). Silica materials (SiO_2) act as strong extracting and

adsorbing materials due to their ion-exchange properties. They are typically characterized by a negative charge, which cations with stronger affinities for the oxygen atoms (such as uranyl) are strongly attracted to and bind to (Lopez and Birch 1996). Some studies have demonstrated that the charge on different silica surfaces can vary (from 0 to -100 mC/m^2) with pH, with the surface charge being close to zero for pH 2 – 5, but steadily becoming more negative from pH 5 – 10 (Gabriel, Charlet et al. 2001). Others claim, however, that certain colloidal silica exhibit a fixed negative charge independent of pH, with the colloids stabilized in the neutral pH range (Lopez and Birch 1996). Empirical investigations using EXAFS (extended X-ray absorption fine structure analysis) have indicated that the sorption between uranyl and silica gel surfaces is characterized by the formation of inner-sphere, mononuclear uranyl complexes, lacking U – U interactions, and similar to that seem for uranyl-ferrihydrite (natural iron oxide mineral coatings) surface complexes (Reich, Moll et al. 1998). Molecular dynamics models of aqueous uranyl in silica mesoporous confinement have further demonstrated how the uranyl ions are attracted and bind to the pore walls and exhibit a strong and stable association with the silica inner surfaces (Patsahan and Holovko 2007).

While the application of silica materials for uranyl adsorption and extraction in aqueous solutions has long been utilized, limited attention and discussion has been aimed at their advantageous effects on the spectroscopic properties of uranyl. Once the uranyl ions are adsorbed to silica surfaces as described above, they are in a sense isolated or protected from the surrounding aqueous medium, inaccessible to quenching water molecules. The negative surface charge of the silica also reduces the effects of other anionic quenchers (Lopez and Birch 1996). Compared to free uranyl ions in aqueous solution, uranyl on silica surfaces exhibit an overall increase in absorption, and the emission intensity is not only greatly enhanced but can also

exhibit a ‘red-shift’ up to 10 nm. The observed increase in the steady-state emission is directly attributed to the increase in the molar absorption and in the quantum yield (QY). The QY for uranyl on silica is approximately 25%, whereas the QY for uranyl in aqueous solutions can be less than 1%. Through the addition of silica to uranyl solutions, the steady-state emission intensity increases linearly with U-concentration over a large range, and detection limits can be improved by a factor of 100 (Lopez and Birch 1996). In addition to enhancing the absorption and emission, the interaction between uranyl and silica can also result in a significant increase in its fluorescence lifetime, by over two orders of magnitude (Lopez and Birch 1996). Many TRLFS studies have reported the longer lifetimes characteristic of U(VI) when sorbed to silica (Wheeler and Thomas 1984; Gabriel, Charlet et al. 2001; Walter, Arnold et al. 2005; Krepelova, Brendler et al. 2007). While one study noted that the lifetime values of uranyl adsorbed to silica gel and to colloidal silica were very similar (~ 240 μs), the lifetime properties observed are not necessarily stable with time, and may first exhibit a biexponential decay (such as 240 μs and 55 μs) followed by a monoexponential decay (~ 240 μs) after a couple hours of interaction (Lopez and Birch 1996).

Despite these advantages in using silica materials for improved uranyl detection, there are limitations to be considered in relation to pH. A general speciation diagram for uranyl in solution in the presence of silica indicates that the main uranyl-silica species ($UO_2H_3SiO_4^+$) exists primarily over the pH 3 – 7 range, peaking around pH 5. At lower pH values, the free uranyl ion (UO_2^{2+}) predominates, and at higher pH values various hydroxyl and carbonate uranyl species dominate (Gabriel, Charlet et al. 2001). A study of the adsorption of uranyl to amorphous silica as a function of pH indicated a general trend with adsorption climbing in the pH 3 – 5 range, peaking in the neutral range, and dropping rapidly in the pH 8.5 – 9 range. This

general uranyl-silica adsorption trend with pH is very similar to that seen when uranyl sorbs to natural mineral surfaces (described in more detail below). For uranyl adsorption to amorphous silica, three main surface species were identified: 1) $\equiv SiO_2UO_2^\circ$, at pH ~ 5, fluorescent; 2) $\equiv SiO_2UO_2OH^-$, at pH ~ 7.5, fluorescent; and 3) $\equiv SiO_2UO_2OHCO_3^{3-}$, at pH ~ 8.5, non-fluorescent (Gabriel, Charlet et al. 2001). Therefore, careful consideration needs to be given to pH when utilizing silica materials for improved uranyl detection; the stability of the uranyl-silica complexes as well as their fluorescence responses can be vulnerable.

While silica materials have been used extensively in the lab for extraction of uranyl from solution phases, other wet chemical techniques have been traditionally employed for the selective and sequential extraction of uranyl from soils and sediments (Lee and Marsh 1992; Duff, Morris et al. 2000). Due to soils' complex matrix containing a variety of metal ions and humic substances, sample pretreatment is typically required to allow for subsequent fluorescence analysis, and can include extracting the leachable U and decomposing the existing organics (Brina and Miller 1993). Studies have compared different leaching solutions, characterized by different pH values, for extracting U from sediments prior to fluorescence analysis (Duff, Morris et al. 2000). The uranium mining and milling industry has traditionally used both acid and alkaline leaching processes to transition uranium from the solid phase into solution. A comprehensive report by Sandia National Laboratory describes these processes in detail (Stork, Smartt et al. 2006). For acidic leaching, sulfuric acid is most frequently used which reacts with U(VI) to form the highly water soluble uranyl ion, subsequently forming a variety of uranyl sulfate forms. Though the intention of this process is simply to extract the U from the natural solid materials, coincidentally uranyl sulfate forms (such as UO_2SO_4) exhibit enhanced spectral properties. Alkaline leaching processes have also extensively been employed, not only for the

milling industry but also from a remediation perspective. Oxidized U minerals are readily soluble in carbonate (CO_3^{2-}) solutions (Stork, Smartt et al. 2006). Sodium (bi)carbonate solutions (pH 9.3) for example have been routinely employed to remove the labile U from soils and sediments prior to analysis (Mason, Turney et al. 1997; Stork, Smartt et al. 2006; Um, Serne et al. 2007). Ammonium carbonate [$(NH_4)_2CO_3$] is a strong U complexant and has also been used to expedite the rate and extent of U dissolution (Duff, Morris et al. 2000; Liu, Zachara et al. 2004). Studies have shown ammonium carbonate can accelerate U release rates from sediments by factors of 15 or more, and can liberate not only the labile U, but also the U from deeper intraparticle regions. Regarding carbonate leaching applied to Fernald contaminated soils, one study indicated that U was successfully and substantially (75 – 90%) removed (Mason, Turney et al. 1997), while another study indicated that some U(VI) phases, such as uranium metaphosphate common to the incinerator area, were not successfully removed by this technique (Buck, Brown et al. 1996).

1.5 Remote Sensing of Uranium

Research and publications related to the true remote sensing of U in the environment are limited. That is to say, techniques that utilize instrumentation to interrogate a target (uranyl) in the environment with a light source from reasonable stand-off distances above ground level, as well as positively detect its luminescent response. A few studies published in the early 1980's by a limited group of researchers focused on the remote sensing of U-containing materials, such as uranyl geologic targets, via laser-induced fluorescence (Chimenti 1981; deNeufville, Kasdan et al. 1981; Kasdan, Chimenti et al. 1981). In these studies, data is presented for the characterization of a wide variety of U-containing materials via a ground-based laser system, and

considerations for a conceptual airborne system designed specifically to detect uranyl signatures are discussed in detail. The system design and detection scheme takes into account the distinctive characteristics of uranyl's absorption and luminescence spectrum, as well as the need for time-delayed measurements of the intensity and decay. According to these studies, a preferred technique would utilize a laser illumination at ~ 425 nm, and detect luminescence in the 500 – 600 nm range.

In the mid to late 1990's, DiBenedetto (Special Technologies Laboratory) and collaborators (DOE) successfully developed and demonstrated a portable laser-induced fluorescence imaging (LIFI) system, designed for both ground-survey and airborne applications (DiBenedetto, Abbott et al. 1996; USDOE 1999). This system utilized a pulsed Nd:YAG laser (λ_{Ex} = 355 nm and 532 nm), and collected time-delayed measurements for improved uranyl detection on contaminated surfaces. More recently, researchers as Mississippi State University have also worked towards developing and characterizing an improved transportable fluorescence spectral imaging (FSI) system for detection U-surface contamination (Wang, Su et al. 2008; Monts, Wang et al. 2009). Their in-depth investigations have examined the effects of utilizing varying excitation wavelengths and laser powers.

1.6 Comprehensive Mission Statement

The ultimate objective of this dissertation research is to understand how to improve the level of detection of the uranium in the environment, while focusing on 1) the extraction and accumulation of the contamination from soil surfaces, and 2) the environmental factors that can influence the luminescence response. Following the completion of these studies, models will exist which help define what is and is not feasible, addressing how and when enhancing –

accumulating materials should it be applied and examined, and what ground-level environmental conditions are ideal for detection.

This dissertation work will fulfill part of the objectives and requirements outlined under the DOE grant entitled “Stand-off Fluorescence Detection of Uranium in Soil” (Proliferation Detection Program; DE-FG52-06NA27491; PI: Dr. Gary Tepper; Institution: Virginia Commonwealth University). Under this grant, two main focus areas emerged: 1) the design, development and study of a distributable sensor that exhibits the capability to absorb uranyl from the near-surface soil layer, and subsequently result in an improved stand-off detection based on enhanced fluorescence (emission intensity, structure and extended lifetime), and 2) determination and in-depth examination of ground-level key environmental factors most probable to influence (negatively or positively) the above described scenario, by affecting the fluorescence detection of uranyl either directly or indirectly.

Researchers within the Department of Engineering at VCU have focused primarily on the first main focus area described above. A variety of different accumulating and enhancing materials were investigated in aqueous solutions and on contaminated sand systems at the early stages of this grant work, however it was determined that silica gel (Acros Organics, particle size 40 – 60 μm, average pore size 4 nm) provided the optimal response and desired features. Figure 5 demonstrates the visual improvement in uranyl detection based on its green fluorescence observed under UV (254 nm) light. For this sample, 50 mg of the silica gel power was applied to the top of the moist sea sand sample, which was contaminated at 100 ppm U. Presently, a fairly sophisticated distributable sensor has been designed and is under continual improvement based on combining the advantageous properties of silica gel (described above) with the light enhancing properties of glass (sapphire) beads, which act as focusing lenses. The use of glass

beads results in a directed fluorescence response, enhancing detection of all the light generated by the sample, while the silica gel results in the extraction and specific enhancement of the uranyl fluorescence signal. Figure 6 demonstrates the enhancement effect on uranyl's steady-state fluorescence response using silica gel and sapphire beads (individually and combined), applied to the surface of moist sea sand contaminated at 100 ppm U. A publication entitled "Directed Fluorescence Sensor Element for Standoff Detection of Uranium in Soil" (D. Pestov, C. Chen, J. Nelson, J. Anderson, and G. Tepper) has recently been published in Sensors and Actuators B (Pestov, Chen et al. 2009). The majority of the fluorescence data collected under this first main focus area has been in the form of time-resolved spectral data and lifetime decay measurements.

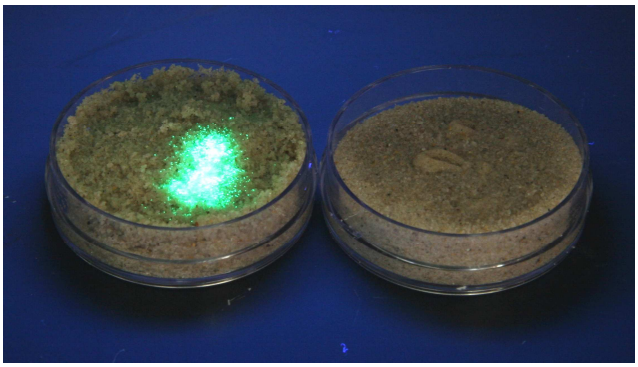

Figure 5. Sand standard contaminated with 100 ppm U, with silica gel on the surface (left) and lacking silica gel (right), under UV (254 nm) irradiation.

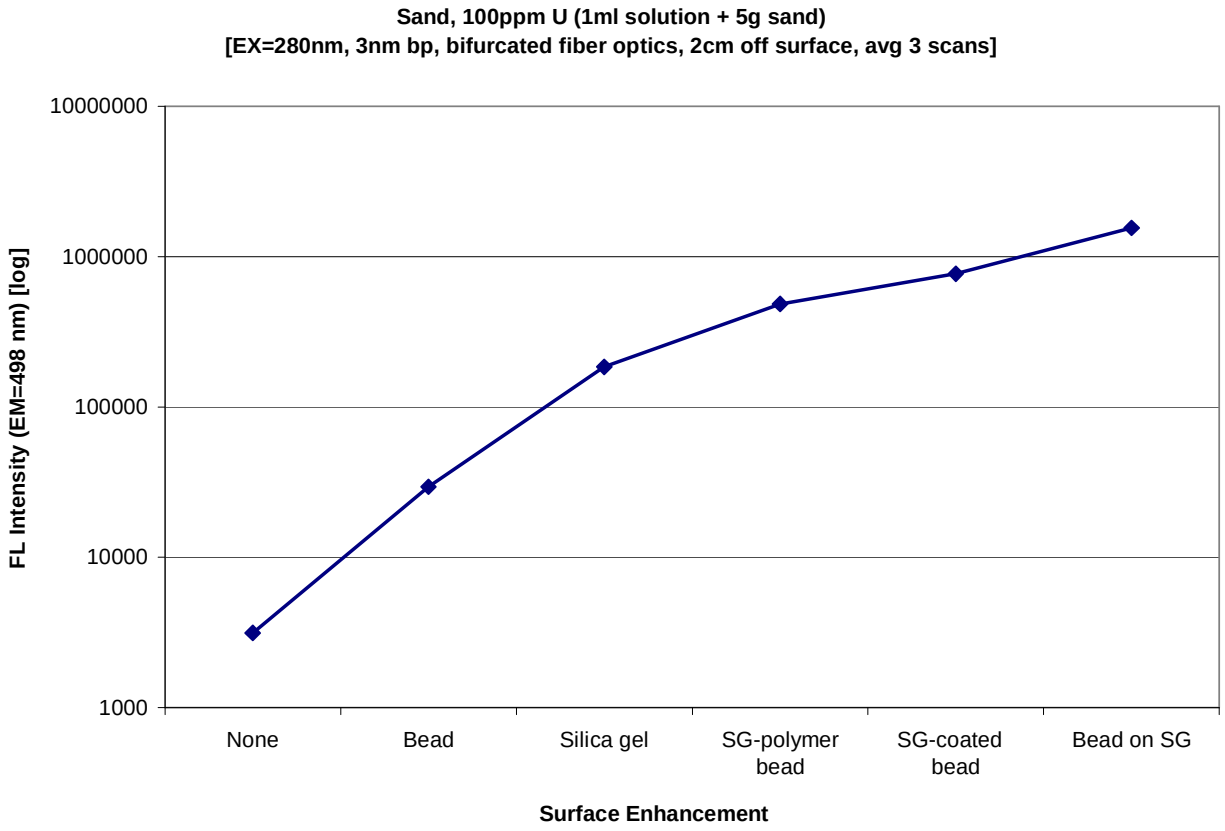

Figure 6. Enhancement effect on uranyl fluorescence using silica gel and sapphire beads (individually and combined) on the surface of sand contaminated with 100 ppm U.

The dissertation research described in this document is primarily aimed at the second main focus area described above. An in-depth literature review was conducted and was critical for defining: 1) the nature of U contamination in the environment (verifying the prevalence of contamination at the soil surface and U contamination levels of importance), 2) the present state of uranyl detection scenarios and the need for improved in-field remote sensing procedures, and 3) the key environmental parameters with strong potential to affect uranyl's fluorescence detection (directly or indirectly) utilizing a distributed sensor as described above. Factors directly affecting uranyl fluorescence would include the presence of and interaction with quenchers and the formation of non-fluorescent species, as well as natural background spectral

interferences. Factors indirectly affecting uranyl's fluorescence detection would include those features limiting uranyl's capability to exist in and move through the solution phase of the soil samples where it can be absorbed by and interact with the silica gel sensor present on the soil surface. The key influential parameters selected for further study, based on literature review and preliminary studies, are described in detail below, and will be investigated in conjugation with U concentration effects and time-dependence of reactions. The majority of the fluorescence data collected under this second main focus area will be in the form of steady-state spectral data.

This research will *not* result in the development of a protocol for specific identification of U concentration or U speciation per say (typically accomplished in conjugation with laboratory wet-chemistry extraction procedures using leaching agents or cryogenic spectroscopic characterization). However, the goal of this work *is* to improve the remote detection and positive identification of uranyl's diagnostic fluorescence emission at the surface of complex environmental samples.

1.7 Key Features of Environmental Samples

1.7.1 Introduction

In complex environmental systems, matrix effects co-exist which typically result in not isolated but integrated influences that can be difficult to fully comprehend. As previously stated, several factors have already been identified and studied under this work and under work by others, demonstrating a capability to potentially affect the fluorescence detection of uranyl (directly or indirectly) utilizing a distributed sensor as described above. Undesirable direct effects on uranyl's fluorescence emission would be observed as: 1) diminishment of the fluorescence intensity, 2) significant reduction or alteration of the unique spectral band structure,

and 3) masking of the uranyl spectra. Such negative effects would result from the presence of and interaction with quenching agents and the formation of non-fluorescent species, as well as natural background spectral interferences. Uranyl can undergo several complex soil interactions which can indirectly limit its capability to be absorbed and enhanced by a distributed sensor on soil surfaces. Such negative influences would be reflected as limited mobility and the inability of uranyl to bind with enhancing materials due to existing preferential complexes with other natural materials.

In general, many factors influence the retention of contaminants in soils such as soil type and binding sites, presence of particulate matter and competing ions, concentration of the contamination, and the chemistry of the aqueous phase (Johnson, Buck et al. 2004). Several key mechanisms have already been described by which specifically U mobility is retarded in the geologic environment (see Table 5). Many studies focusing on the sorption, solubility and transport of U in contaminated soils describe in detail the physical, chemical and mineralogical properties taken into consideration, often outlining them in a table. These soil property reference tables include information such as: particle size or texture (percent sand, clay, and silt), density and porosity, percent moisture content (% MC), pH, organic content, iron (Fe) content, and electrical conductivity (Barnett, Jardine et al. 2000; Bostick, Fendorf et al. 2002; Johnson, Buck et al. 2004; Um, Serne et al. 2007).

Table 5. Key mechanisms by which U mobility can be retarded in the surface and subsurface geologic environment. Adapted from (Duff, Coughlin et al. 2002).

Mechanism
Precipitation of U(VI) and U(IV) phases.
Sorption of U by organic matter and minerals.
Occlusion by clay and oxide coatings.
Co-precipitation of U with Fe oxides and substitution in silicate clays and carbonates.

The key influential features of environmental soil samples selected for further investigation under this research are: 1) soil texture (based on particle size distribution), 2) moisture content (affected by evaporation, temperature and humidity, and directly related to water potential), 3) pH related effects, 4) soil organic matter (SOM), and 5) iron content. Further details justifying the selection of these five main parameters are described below, with the latter three selections supported more heavily by outside literature.

1.7.2 Soil Texture

Soil texture refers to the relative proportions of various sizes of individual soil particles, and directly affects water movement and storage in the soil system. The USDA classification of soil type based on particle size is shown in Figure 7, as is the commonly referenced soil texture triangle showing the classification of the mixtures of different soil types. A comparison between sand and clay is also described, since these two soil types are considered as the two extremes. The majority of studies related to the transport and mobility of U in soils give some reference or description to the mineralogy and soil texture, often characterizing and separating the collected soil samples based on particle size distribution prior to analysis (Hunter and Bertsch 1998; Um, Serne et al. 2007). Given the soil texture details provided in Figure 7, one would hypothesize that, in the absence of all other influential parameters, it would be more feasible to absorb and accumulate uranyl present in the solution phase of a sand system compared to a clay system. This is intuitive given sand exhibits less surface area for the uranyl to potentially interact with, and larger spaces between the particles enabling aqueous materials to flow more readily through the system. It is well known that clays typically exhibit other features beyond their small particle size that also strongly influence the movement and interaction of the aqueous phase.

Sand	**Clay**
Largest particles (> grain size)	Smallest particles (< grain size)
Lower porosity (< volume of void spaces)	Higher porosity (> volume of void spaces)
Larger spaces between particles	Smaller spaces between particles
Does not 'hold' or retain water well (dries out relatively quickly)	'Holds' or retains water very well (water is tightly bound to clay particles)
Structure DOES allow water and air to move through it well	Structure does NOT allow water and air to move through it well

Soil Type	**Particle Size (mm)** [USDA classification]
Clay	< 0.002
Silt	0.002 – 0.05
Very fine sand	0.05 – 0.1
Fine sand	0.1 – 0.25
Medium sand	0.25 – 0.5
Course sand	0.5 – 1.0
Very course sand	1.0 – 2.0

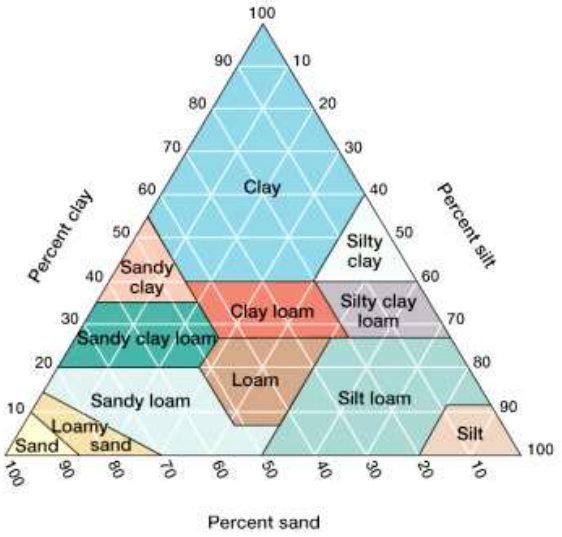

Figure 7. Comparison between sand and clay related to their soil texture and interaction with water (top). Classification of soil types based on particles sizes (bottom left), and the soil texture triangle showing the classification of the mixtures of the different soil types (bottom right).

Numerous studies (typically sorption and surface complexation studies) have specifically focused on the in-depth interaction of uranyl with a variety of different clay minerals. These uranyl – clay studies utilized both laboratory experimental techniques (Turner, Zachara et al. 1996; Benes, Kratzer et al. 1998; Hudson, Terminello et al. 1999; Chisholm-Brause, Berg et al. 2001; Hennig, Reich et al. 2002; Wang, Ainsworth et al. 2002; Chisholm-Brause, Berg et al. 2004; Davis, Meece et al. 2004; Kowal-Fouchard, Drot et al. 2004; Payne, Davis et al. 2004; Catalano and Brown 2005; Krepelova, Brendler et al. 2007), as well as sophisticated modeling techniques (Zaidan, Greathouse et al. 2003; Greathouse and Cygan 2005; Greathouse,

Stellalevinsohn et al. 2005; Greathouse and Cygan 2006). The main clay group names are: 1) smectite, 2) kaolin, 3) illite and 4) chlorite. The smectite group includes: montmorillonite, saponite and nontronite,

while the kaolin group includes: kaolinite, dicktite, halloysite and nacrite.

Clay mineral surfaces are typically characterized by a negative charge and clays therefore have a greater cation exchange capacity (CEC) compared to other natural minerals (Hennig, Reich et al. 2002; Um, Serne et al. 2007). In soil science, the CEC refers to the capacity of the soils for ion exchange of positively charged ions (cations, like uranyl) between the soil particles and the solution phase. Soils and sediments containing a higher percentage of clay-sized fractions, therefore, tend to be characterized by relatively higher CEC values (Um, Serne et al. 2007), strongly affecting uranyl's fate and mobility due to enhanced sorption (Hennig, Reich et al. 2002). The sorption of U on clays is complex since clay minerals exhibit a large variety of potential sorption sites (Barnett, Jardine et al. 2000), which can be either permanently or variably charged sites (Bostick, Fendorf et al. 2002). While a great majority of the uranyl – clay literature assumes that these sorption reactions are primarily attributed to these exchange-site mechanisms, some more recent studies strongly suggest that reactive edge sites play a more dominant sorption role. Under the most relevant environmental conditions (moderate ionic strength and near-neutral pH), highly reactive metal-oxide-like groups (such as silica, SiO and gibbsite, AlO) exist on the surface of clay minerals and act as a sequestering sink for uranyl species. That being said, these reactive edge sites display a strong pH dependency (Chisholm-Brause, Berg et al. 2004).

A study investigating the sorption and solubility of DU in arid soils concluded that clay content was the predominant factor controlling U sorption at this location. A sequential extraction procedure was applied to particles of variable sizes. The extraction of U from the

larger particles (500 – 1000 μm, course sand) was more feasible, showing nearly complete dissolution of the carbonate-bound U via the ammonium acetate extraction step. However the U associated with the smaller particles (53 – 125 μm, fine sand) was non-labile and only removable by the final extraction step involving mixtures of strong acids in conjugation with heating. The decreased U solubility for the smaller arid soil particles was explained by the presence of coatings of amorphous silica and the coexistence with clays (Johnson, Buck et al. 2004).

Other studies have concluded, however, that consideration for soil type and particle size distribution is not sufficient for predicting U sorption and solubility. A detailed study of U surface complexes on heterogeneous soils and sediments from DOE facilities indicated that U sorption was surprisingly similar for widely varying mineralogies, and that clay-sized particle content was not correlated with sorption indicating clay minerals were probably not the primary sorbent (Bostick, Fendorf et al. 2002). Similarly, Fernald site studies indicated that conventional soil-washing and separation-removal methods, predicated on the selective concentration of U contamination with the smallest (clay) fractions, would be ineffective as remediation strategies (Lee and Marsh 1992; Morris, Allen et al. 1996). Soils at this facility are known to be characterized by a wide range of particle sizes, from large sand and gravel chunks (~ 2 – 3 mm diameters) to fine clay-sized particles (Morris, Conradson et al. 1992). Overall, the sand/silt fraction of the soils contained 48 – 79% of the U in the samples, but the dominant size fraction for U contribution did vary somewhat sampling site to sampling site between sand, silt or gravel. These dominant particle size fractions were typically associated with calcium, phosphorous, iron and silicon (Lee and Marsh 1992). The presence of other competitive cations (such as Ca^{2+} and Mg^{2+}) has been proposed as a possible explanation for the apparent lack of strong association of uranyl species with the exchange sites of the clay-sized fraction (Morris, Allen et al. 1996). An

additional explanation was simply that many of the soils were highly disturbed from past construction activities, and that the most course fragments were associated with limestone (indicated also by the high pH of the surface soils), and the majority of U existed as particles cemented to silt, sand and gravel fractions (Lee and Marsh 1992).

Very few papers have mentioned a relationship between soil texture and uranyl fluorescence detection. While a DOE report did describe: 1) a pronounced difference between the structured spectra for uranyl associated with the sand/gravel fraction compared to the clay/silt fraction, and 2) that emission spectra for uranyl-clay systems are typically poorly resolved, the true explanation for the discrepancy was linked to the variation in U speciation (Morris, Conradson et al. 1992).

1.7.3 Moisture Content and Water Potential

The presence of moisture in contaminated surface soils is believed to be an important yet complex parameter related to uranyl detection, and can be both advantageous and disadvantageous, in varying amounts at different times. In summary, water acts as a quencher of uranyl fluorescence, and acts as a generic light scattering media complicating stand-off optical measurements. However, the presence of water is necessary in order for uranyl to exist in a dissolved state in the aqueous phase where it can potentially be absorbed and accumulated by a distributed sensing material. The episodic influx of rain can cause the continued dissolution and reprecipitation of uranyl species, often resulting in the U contamination migrating deeper into the soil. Preliminary studies (discussed in more detail below) have indicated that there is faster kinetic process of free uranyl moving through the system with the flow of water, and there is a slower process of the uranyl migrating through the aqueous phase as it progresses towards

equilibrium. Assuming U contamination is present at the surface of the soil, the initial presence or addition of a certain level of moisture is needed for absorption by distributed accumulating – enhancing material, but the subsequent process of drying due to evaporation can lead to improved uranyl detection. This observation is believed to be due to a gradual increase in the concentration of U absorbed by the distributed material as water is cycled through, however this observation is not strictly held over prolonged periods of time and appears to be dependent upon the nature of the sensor (silica gel for example). An example of a preliminary recommendation would be to take advantage of the natural diurnal cycles, and to distribute an accumulating – enhancing sensor when the immediate surface of soils are typically saturated with dew, and after a defined number of hours enabling migration, reaction and drying, interrogate the target with the fluorescence detection system.

Despite these apparent critical points related to the presence of moisture, very limited attention has been given in the literature to the role and influence of water specifically in U contaminated environmental samples or its fluorescence characterization. In aqueous solutions, the quenching of U luminescence by water molecules is commonly mentioned. Early studies described the dependence of this quenching process on temperature, and suggested that electron transfer due to oxidation – reduction potentials between the uranyl ion and water molecules was the primary mechanism, as opposed to energy transfer (Moriyasu, Yokoyama et al. 1977). Other papers referenced a variety of possible mechanisms including: 1) electron transfer, 2) deactivation by O – H stretching of coordinated water, or 3) exiplex formation (Kaminski, Purcell et al. 1981). Even more recent publications indicate that both: 1) physical deactivation through energy transfer to vibrational modes of water molecules (OH^-), and 2) chemical quenching mechanisms involving electron – transfer or hydrogen atom extraction are possible

explanations for the low QY of uranyl in aqueous solutions (Clark, Conradson et al. 1999; Formosinho Sebastiao, Burrows Hugh et al. 2003).

Regarding uranyl fluorescence of contaminated soil samples, a direct relation with the presence of moisture seems probable but not clearly defined. DOE studies have reported cases of diminishment of the structure of the emission spectra while an overall increase in intensity was observed for samples progressing from wet to dry (Morris, Conradson et al. 1992). Spectral differences between moist and dry samples has been explained by changes in uranyl speciation due to varying amounts of water molecules in the ion's coordination environment, or simply due to changes in the degree of crystallinity of the solution phase (Morris, Conradson et al. 1992; Krepelova, Brendler et al. 2007). Other studies of contaminated sediments have indicated no significant change in the emission intensity of U(VI) species with air drying of the samples (Duff, Morris et al. 2000). Therefore, it is believed that such an observation would be strongly dependent on the specific nature of the sample as well as the analytical methods being utilized.

As previously mentioned, the presence of water is needed in order for uranyl to exist in and move through an aqueous phase where it can potentially be absorbed and accumulated by a distributed sensor. More so than fluorescence studies, those related to uranyl's sorption and dissolution in soils and sediments acknowledge the critical role of the solution phase. Studies of Hanford site sediments describe the importance of the sediment : water (or solid : solution) ratio, and either report the variation in this ratio or percent moisture content (% MC) for collected samples, or verify this ratio was maintained experimentally (Liu, Zachara et al. 2004; Um, Serne et al. 2007). The potential distribution of U in sediments is often described in reference to its distribution coefficient (K_d), which reflects the level at which its mobility is retarded and is controlled by solubility saturation degree, dissolution kinetics, and mass transfer limitation.

Lower K_d values would indicate the uranyl exists in a more mobile form, but K_d values vary significantly with the solid : solution ratio since the amount of U that will dissolve from the solid phase is dependent on the amount of water surrounding it. For the Hanford site sediments, while the adsorption and dissolution studies used sediment : water ratios of 50 g/L and 200 g/L respectively, it is mentioned that much higher ratios (> 2.7×10^4 g/L or ~ 4% MC) exist in the drier vadose zone sediments, which would be characterized by larger K_d values reflective of lower U mobility (Liu, Zachara et al. 2004). For arid soils contaminated by DU penetrators, the lack of saturation and equilibrium conditions limits U transport even more so. As moisture evaporates from the surface soils, the concentration of aqueous U in porewaters exceeds the solubility limit resulting in the precipitation of U (Johnson, Buck et al. 2004).

The soil moisture content is the ratio of the mass of the water (present in the soil sample) to the mass of the dry soil, and is typically presented as a percentage (% MC). The % MC can easily be determined for collected samples by weighing the sample before and after drying (> 24 hours at 105 °C), with the difference equaling the mass of the water. Controlled experiments can be conducted where a defined volume and therefore mass of water is added to dried samples, resulting in the desired level of moisture. At the Hanford site, % MC measurements for samples collected from the saturated zone below the water table ranged from 5 – 33%, while drier vadose zone sediments (above the water table) exhibited moisture contents from 0.8 – 3.6% (Liu, Zachara et al. 2004; Um, Serne et al. 2007).

Despite the fact that soil water potential (WP) measurements do not appear to be mentioned in any of the U literature, it is believed that such measurements would be informative regarding the migration of U with the aqueous phase in surface soils. Soil water potential is directly related to both the amount of water present (% MC) and the soil texture, and plays an

important role in water movement. Soil WP is a measure of the energy status of the soil water (potential energy) relative to reference conditions (pure water). Though total soil WP (ψ) is made up of several component potentials (such as gravitational, osmotic, pressure and matrix), the matrix potential (ψ_m) is the force placed on the water by the soil matrix and normally has the greatest effect on the movement of water through the soil regime. In summary, when water comes in contact with solid particles (such as clay and sand), adhesive intermolecular forces are formed between them. These liquid – solid adhesive forces in combination with the attraction among water molecules themselves result in surface tension and the formation of menisci, which require even stronger forces to break. Soil matrix potential (ψ_m) is a negative pressure measurement (tension or suction) commonly reported in units of milli-Pascals (MPa). The ψ_m measurements are dependent upon the distances between the solid particles (reflected by soil texture) as well as the chemical composition of the solid matrix. Very strong (more negative) matrix potentials bind water to soil particles under drier conditions. In the absence of all other influential parameters, water tends to flow from higher (less negative) potentials to lower (more negative) potentials. Soil water release curves show the relationship between the soil matrix WP (negative value) and water content, with less water resulting in greater tension on the soil particles, reflected as more negative WP readings. However, the soil water release curves can vary substantially for different soil types, with finer-textured soils (such as clays) exhibiting stronger (more negative) potentials for a given % water content, compared to more coarse particles like sand (see Figure 8).

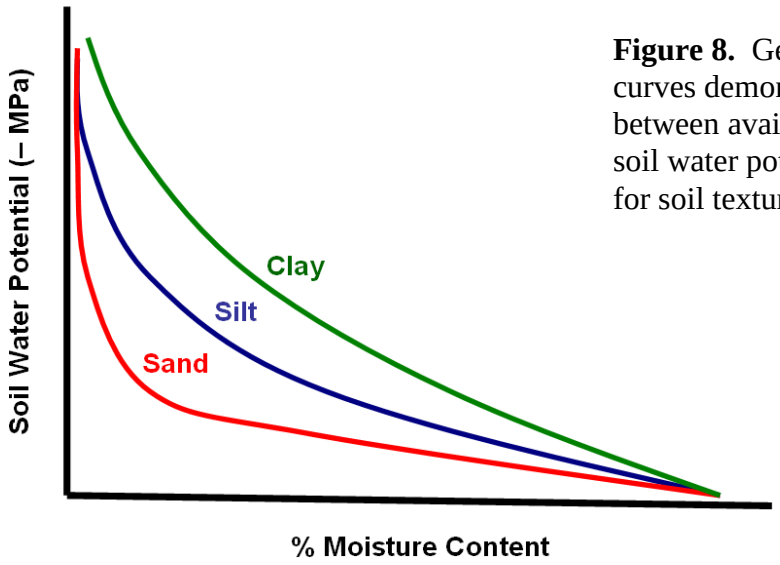

Figure 8. Generic soil water release curves demonstrating the relationship between available water as % MC and soil water potential, with consideration for soil texture.

1.7.4 pH Related Effects

An immense amount of pertinent literature discusses pH effects with regard to: 1) uranyl fluorescence in solution and in soil samples (both based on U speciation), and 2) uranyl – soil interactions (sorption – dissolution processes) affecting its mobility and availability for detection. Some details related to pH effects have already been provided in previous sections pertinent to: 1) various hydrolyzed species of U(VI), 2) U complexation with carbonate under more alkaline conditions [CO_3^{2-}], 3) uranyl – silica species and 4) common leaching procedures for U extraction. While some studies focus entirely on pH effects through experiments where pH is tightly controlled, other studies make reference to the original status of collected samples prior to analysis. In general, soils are characterized by a large range of potential pH values. Surface soil pH maps for the United States and Australia are publically available and show that the great majority of surface soils are characterized by pH values within the 4.5 – 9.0 range, with large disparate areas being predominantly either acidic or alkaline. In natural soils and surface waters,

pH levels below 3 are very uncommon. Table 6 describes the standard soil pH classifications as defined by the USDA Natural Resources Conservation Service, and Table 7 provides reference information for pH levels in environmental soil samples used in U studies previously mentioned.

Changes in pH in aqueous phases directly affect U speciation, in turn affecting its luminescent features. Many studies have focused a great deal on this topic, often times presenting U speciation diagrams as a function of pH pertinent to their specific study (Eliet, Bidoglio et al. 1995; Meinrath 1997; Barnett, Jardine et al. 2000; Billard, Ansoborlo et al. 2003; Formosinho Sebastiao, Burrows Hugh et al. 2003; Kirishima, Kimura et al. 2004; Walter, Arnold et al. 2005; Arai, McBeath et al. 2006), with some showing speciation for U sorbed to solid materials such as silica and clay (Gabriel, Charlet et al. 2001; Payne, Davis et al. 2004). While these pH – speciation diagrams for U can vary and strongly depend on the chemical composition of the solution phase, the concentration of solutes and temperature, a general pattern is typically observed for different forms of U most commonly encountered in aqueous phases. Figure 9 presents a generalized diagram showing the predominant trends of U aqueous speciation as a function of pH.

Table 6. Standard soil pH classifications. Adapted from USDA NRCS public information.

pH Classifications	**pH values**		**pH Classifications**	**pH values**
Extremely Acid	< 4.5		Neutral	6.6 – 7.3
Very Strongly Acid	4.5 – 5.0		Slightly Alkaline	7.4 – 7.8
Strongly Acid	5.1 – 5.5		Moderately Alkaline	7.9 – 8.4
Moderately Acid	5.6 – 6.0		Strongly Alkaline	8.5 – 9.0
Slightly Acid	6.1 – 6.5		Very Strongly Alkaline	> 9.0

Table 7. Reference information for pH levels in environmental soil samples used in U studies.

Site / Details	**Approx. pH**
Common range for soils.	3.5 – 9
Fernald Environmental Management Site, Ohio (DOE) Reference topsoils. [a] Core samples and homogenized blends having large concentrations of calcite [$CaCO_3$] and dolomite [$CaMg(CO_3)_2$]. [a]	 5.4 – 6.3 7.0 – 8.5
Hanford Reservation, Washington (DOE) Subsurface (1 m) media. [b] Aquifer sediments. [c]	 ~ 6.8 ~ 7.5
Oak Ridge Field Research Center, Tennessee (DOE) Soil-saprolite core. [d] Fill material. [d]	 4.5 – 8 7.0 – 10.5
Kosovo (following 1999 conflict) Topsoils in the close vicinity of DU penetrators and impact zones. [e]	 7.1 – 8.8
DU penetrator test range (Upper Mojave Desert) Alkaline desert soils. [f]	 8.5 – 10.5

[a] (Morris, Allen et al. 1996)
[b] (Bostick, Fendorf et al. 2002), [c] (Um, Serne et al. 2007)
[d] (Moon, Roh et al. 2006)
[e] (Di Lella, Nannoni et al. 2005)
[f] (Johnson, Buck et al. 2004)

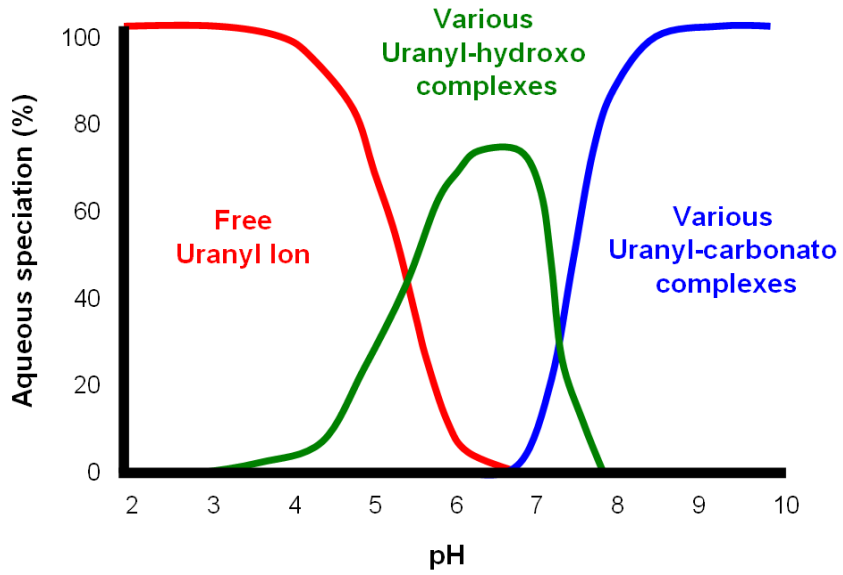

Figure 9. Generalized diagram showing the predominant trends of U(VI) aqueous speciation (%) as a function of pH.

Under the most extreme acidic conditions (pH < 3), the free uranyl ion (UO_2^{2+}) prevails as the dominant U(VI) form, however such conditions would unlikely be encountered in natural systems. Under strongly to moderately acidic conditions (pH 4.5 – 6), a mixture of free ion and hydroxyl forms of U co-exist, with a variety of different uranyl-hydroxo complexes present in the pH 4 – 8 range, dominating the neutral range (Eliet, Bidoglio et al. 1995; Billard, Ansoborlo et al. 2003; Formosinho Sebastiao, Burrows Hugh et al. 2003; Kirishima, Kimura et al. 2004). In the neutral region, uranyl-carbonato complexes begin to form and co-exist with hydroxyl forms, but in the moderately to extremely alkaline range (pH 8 – 10) other uranyl-carbonte forms prevail (Meinrath 1997; Barnett, Jardine et al. 2000; Billard, Ansoborlo et al. 2003; Arai, McBeath et al. 2006). Table 8 summarizes the key hydroxyl and carbonate forms of U(VI) most commonly encountered in aqueous phases, and their corresponding optimal pH. Note the predominance of cationic species under acidic conditions and anionic species under alkaline conditions. Several studies presented detailed spectroscopic characterizations of different forms of aqueous U through pH experiments, and these studies demonstrated both the emission spectra

and lifetime decay values can vary substantially (Eliet, Bidoglio et al. 1995; Billard, Ansoborlo et al. 2003). For example, U fluorescence is known to be quenched through its reaction with carbonate radicals under neutral and alkaline pH conditions (Meinrath 1997).

Table 8. Chemical formulas for commonly encountered hydroxyl and carbonate forms of U(VI) in aqueous phases and their corresponding approximate optimal pH values.

Chemical formula	Optimal pH		Chemical formula	Optimal pH
UO_2^{2+}	< 5		$UO_2CO_3^{\circ}$	7
UO_2OH^{+}	5		$UO_2(OH)_3^{-}$	7 – 8
$(UO_2)_2(OH)_2^{2+}$	5		$(UO_2)_2CO_3(OH)_3^{-}$	7 – 8
$(UO_2)_3(OH)_5^{+}$	6 – 7		$UO_2(CO_3)_2^{2-}$	7 – 8
$UO_2(OH)_2^{\circ}$	6 – 7		$UO_2(CO_3)_3^{4-}$	> 8.5

The speciation of uranyl adsorbed to the surfaces of solid materials (such as kaolinite), can mirror the U speciation changes in the aqueous phase, with UO_2^{2+}, UO_2OH^{+} and $UO_2CO_3^{\circ}$ adsorbed at lower, intermediate and higher pH levels respectively (Payne, Davis et al. 2004). However, luminescent studies of solid U – containing minerals have to take into consideration the direct relationship between pH and U sorption. A study presenting total integrated intensities for optical emission spectra for uranyl sorbed to soil smectites (clays) demonstrated that even though there was some variation due to electrolyte concentration, a similar general trend was observed for sorbed U fluorescence based on pH. This trend was reflective of the amount of U present on the surface of the solid material, and showed intensities rising as the pH progressed from 4 to neutral, and then dropping around pH 8, though decent uranyl emission spectra were still obtainable at pH 4 and 8. The variation of uranyl sorption on smectites with pH and ionic strength was further explained by: 1) competition for fixed – charge sites on the basal planes, 2) activation of pH – dependent variable charge sites on the clay edges, and 3) the pH dependent

uranyl solution speciation (Chisholm-Brause, Berg et al. 2004). Indeed the solution speciation of U largely determines how it partitions within the solid phase (Bostick, Fendorf et al. 2002).

The effect of pH on uranyl's interaction with soil particles, with specific reference to sorption reactions and inversely dissolution and diffusion reactions, has been heavily studied (Mason, Turney et al. 1997; Barnett, Jardine et al. 2000; Chen and Yiacoumi 2002; Chisholm-Brause, Berg et al. 2004; Liu, Zachara et al. 2004; Payne, Davis et al. 2004; Tokunaga, Wan et al. 2004; Arai, McBeath et al. 2006; Chang, Korshin Gregory et al. 2006). Most data from these studies, both experimental and modeled, depict the same commonly referenced trend relative to total U uptake with regard to pH, with percent U sorption steadily rising in the pH 3 – 6 range, peaking in the neutral to slightly alkaline range, and dropping quickly in the pH 8 – 9 range. The opposite trend is described for U dissolution and diffusion, as would be expected (Liu, Zachara et al. 2004; Tokunaga, Wan et al. 2004). Figure 10 presents this generalized trend of U sorption (%) as a function of pH, and Table 9 summarizes the findings of various U sorption, dissolution and diffusion studies accounting for pH. This explains why both acidic and alkaline leaching solutions are commonly used to extract U from natural solid materials (as previously described).

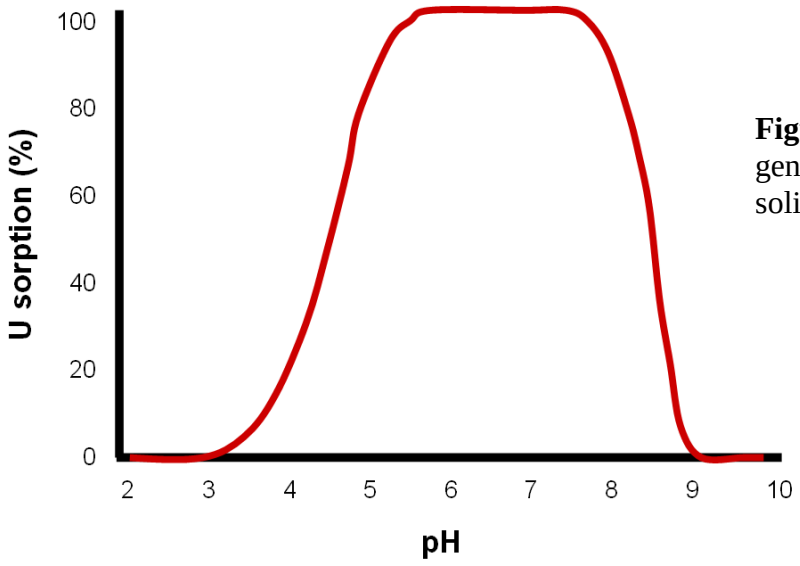

Figure 10. Diagram showing the general trend of U sorption (%) on solid materials as a function of pH.

Table 9. Summary of U sorption, dissolution and diffusion studies and their findings associated with pH changes.

Study Description	Findings
Adsorption of U on a clay standard (kaolinite) as a function of pH (3 – 10) and [U]. (Payne, Davis et al. 2004)	Both experimental and modeled data showed: U uptake increased with pH (log linear relationship for 3.5 – 5.5 range), reaching a maximum in the near-neutral range; Sorption decreased rapidly at higher pH values (8 – 9) due to presence of aqueous uranyl – carbonate complexes; Sorption curves varied somewhat with regard to [U], but exhibited similar trends.
Adsorption of U on Hanford site aquifer sediments varying in mineralogy. (Um, Serne et al. 2007)	U adsorption decreased with increasing concentrations of dissolved carbonate, due to formation of strong anionic aqueous U – carbonate complexes under highly alkaline conditions.
U adsorption and transport in natural, heterogeneous soils from DOE sites. (Barnett, Jardine et al. 2000)	Aqueous phase pH was the controlling factor for U adsorption; Exhibited classic pH adsorption edge in the 4.5 – 5.5 range; Degree of adsorption decreasing sharply in the 7.5 – 8.5 range, due to increased dissolved carbonate, resulting in increased U – carbonate complexes; Adsorption edges varied somewhat for different soil samples, but exhibited a similar trend.
U adsorption on the surface of gibbsite (aluminum hydroxide mineral). (Chang, Korshin Gregory et al. 2006)	Both experimental and modeled data showed: U adsorbed via outer – sphere complexation on mineral surfaces, with adsorption increasing rapidly at ~ pH 5, peaking at ~ pH 8, and then dropping drastically at pH 8 – 9.
Modeling DU transport in natural subsurface systems. (Chen and Yiacoumi 2002)	The pH of soils plays a critical role with regard to the immobilization of DU through sorption; Equilibrium modeling showed DU sorption increasing sharply from 0 – 100% in the pH 3.5 – 5 range, with immobilization maximized above pH 5.
U dissolution from Hanford sediments under alkaline (pH 7 – 9.5) conditions. (Liu, Zachara et al. 2004)	Rate and extent of U dissolution was influenced by uranyl mineral solubility, carbonate concentration, and mass transfer from intraparticle regions; Dissolved [U] was constant at pH < 8.2 and increased at pH > 8.2; Assumes influence of pH is the result of variable bicarbonate concentration.
U diffusion into slightly alkaline soils from concentrated acidic and alkaline solutions. (Tokunaga, Wan et al. 2004)	Soils provided pH buffering, resulting in diffusion at nearly constant pH despite the extreme differences in pH of the original solutions; U transport is greatest at high [U] and non-neutral pH values; U diffusion is lowest at low [U] and neutral pH values where sorption is strongest.

While the sorption of U to soils is a relatively fast process, the subsequent dissolution and mobilization of U is a much slower process, both strongly dependent on U concentration. For fifty year old DOE contaminated subsurface sediments, experiments indicated that uranyl dissolution was extremely slow over a long period of time for pH < 7.5, but this rate was much higher at pH 9. Over a 200 day period in the pH 9 electrolyte solution, a rapid initial release of U was observed for ~ 50 days, with the overall release rate decreasing with increasing equilibrium time, and ~ 60 – 93% of total U dissolved by day 200 (Liu, Zachara et al. 2004). As indicated in Table 9, the influence of pH on U adsorption or dissolution under alkaline conditions is believed to be due the formation of anionic uranyl – carbonate complexes. In fact, DOE studies focusing on identifying soil mineral types more likely to retain U contamination, thereby limiting its mobility, concluded that calcite ($CaCO_3$, a carbonate mineral and weathering product of concrete – based structures for containing wastes) was not a suitable material for long – term sequestering of U (Reeder, Nugent et al. 2000). DOE reports on the Fernald site discuss how the soils at certain locations contain course fragments were limestone was used as fill, cover and road construction materials, and the presence of limestone was reflected by the relatively high pH of the surface soils (Lee and Marsh 1992; Morris, Conradson et al. 1992).

With regard to the luminescent characterization of contaminated soils, the DOE – Fernald reports mentioned above described the fluorescence emission spectra obtained for a variety of samples. The only sample for which no structured luminescence was observed was a sample obtained from the drum storage area consisting of concrete pads (Morris, Conradson et al. 1992), despite the surface soils at this location contained high levels of U (Lee and Marsh 1992). Our preliminary studies have similarly shown a loss in the structure of the uranyl emission in the presence of concrete, and it has been brought to our attention by experts in this field that U

contaminated soils near concrete structures pose issues regarding uranyl fluorescence detection. In particular, two commonly occurring U(VI) minerals are reported as typically displaying weak, broad structureless emission spectra: rutherfordine and schoepite (Morris, Conradson et al. 1992; Morris, Allen et al. 1996; Duff, Morris et al. 2000). Rutherfordine is a uranyl – carbonate mineral [UO_2CO_3], while schoepite is a uranyl – hydroxide mineral [$UO_2(OH)_2 \bullet H_2O$], yet both appear to exist predominantly in the neutral pH range (refer back to Tables 3 and 8). That being said, another study demonstrated it is very feasible to obtain good fluorescence data from samples characterized by U species present in the neutral pH range. This detailed TRLF study of U bound to gibbsite (AlO) in the absence of carbonate, revealed the presence of four primary U species through spectral deconvolution (Chang, Korshin Gregory et al. 2006). Species 'A' was predominant at pH < 5 and its emission spectrum was characterized by both good structure and intensity. Species 'B' climbed in the pH 4 – 6 region, remained through the neutral region, and its emission spectra had good intensity but its vibronic structure was not as clearly defined as species 'A'. Species 'C' was most abundant in the pH 7 – 8 region but was much less abundant overall than species 'A' and 'B'; yet its emission spectra was the most highly resolved and was 'blue-shifted' (shifted to shorter wavelengths) compared to species 'A' and 'B'. Species 'D' contributed very little to the overall spectra, but was most abundant in the neutral range, and its emission spectra was characterized by poor structure and low intensity. Based on these results, the authors concluded that species 'A' and 'B' were mononuclear surface complexes in the forms of $\equiv AlO–(UO_2)^+$ and $\equiv AlO–(UO_2)OH°$. Species 'C' however was believed to correspond to electrostatically bound uranyl complexes, primarily the $UO_2(OH)_3^-$ form, because it revealed properties similar to that of a UO_2^{2+} – montmorillonite system. Lastly, species 'D' was believed to be the presence of schoepite, $UO_2(OH)_2^\circ$. These conclusions are consistent with the

information in Table 8, and indicate that it is the specific nature of the interaction (i.e., mononuclear, polynuclear, electrostatic, etc.) that determines its luminescent properties more so than pH directly.

Figure 9 gave the impression that various hydroxyl and carbonate forms of U are primarily observed in aqueous phases in addition to the free uranyl ion. However, as Table 3 indicated, phosphate and silicate forms are also commonly observed in natural mineral phases. Contrary to uranyl carbonate ternary surface complexes which begin to form at neutral pH, uranyl phosphate complexes are formed in more acidic environments (Bostick, Fendorf et al. 2002). For the Fernald site studies, the majority of the uranyl species that gave rise to strong structured green emission spectra were believed to be the uranyl phosphate mineral meta-autunite [$Ca(UO_2)_2(PO_4)_2 \bullet 2\text{-}6H_2O$] (Morris, Conradson et al. 1992; Morris, Allen et al. 1996). Similar studies have been conducted for uranyl silicate forms. Descriptions for the room temperature fluorescence emission spectra of various uranyl silicates are presented in Table 10.

Table 10. Descriptions for the room temperature fluorescence emission spectra of various uranyl silicates. Adapted from (Wang, Zachara et al. 2005).

Mineral Name	**Chemical Formula**	**Spectra Descriptions**
Boltwoodite	$K(UO_2)(SiO_3OH)\ (H_2O)_{15}$	Strong, well resolved emission spectra exhibiting typical vibronic features.
Uranophane	$Ca(UO_2)_2(SiO_3OH)_2\ (H_2O)_5$	
Haiweeite	$Ca(UO_2)_2[Si_5O_{12}(OH)_2](H_2O)_3$	
Soddyite	$(UO_2)_2(SiO_4)\ (H_2O)_2$	Broad, essentially unstructured spectra spanning the uranyl region.
Weeksite	$K_2(UO_2)_2(Si_2O_5)_3\ (H_2O)_4$	
Cuprosklodowskite	$Cu(UO_2)_2(SiO_3OH)_2\ (H_2O)_6$	Essentially non-fluorescent in the uranyl region, lacking intensity and structure.
Sklodowskite	$Mg(UO_2)_2(SiO_3OH)_2\ (H_2O)_6$	
Kasolite	$Pb(UO_2)(SiO_4)(H_2O)$	

Clearly, the structure of the emission spectra is strongly dependent on the samples' composition. One observation would be that all the uranyl – silicate minerals characterized by a lack of fluorescence in the typical uranyl region all contained another divalent metal in their

crystal structure (Wang, Zachara et al. 2005). Another observation would be that minerals noted for yielding structured emissions (uranophane, haiweeite, meta-autunite, liebigite and bedquerelite) often contain calcium or are characterized by a ternary structure (Morris, Allen et al. 1996; Wang, Zachara et al. 2005).

1.7.5 Soil Organic Matter (SOM)

Similar to pH related effects, the interactions between U and organic materials (OM) is a heavily studied area. Over 200 years ago, A. Bucholz in 1805 gave the first reported description of the photochemical reaction involving uranyl and organic substrates, and since then countless studies have been generated regarding this topic (Formosinho Sebastiao, Burrows Hugh et al. 2003). The majority of U related OM literature has four main focuses important to understanding its potentially strong interference with uranyl's fluorescence detection: 1) spectral interference and overlap, and utilizing time – discriminating analytical techniques, 2) decreased luminescence due to complex formation, 3) effects on sorption and mobility, and 4) fractionation of OM.

Broadly described, natural organic matter (NOM) is a poly-functional conglomeration of organic molecules of varying molecular weights, sizes and structures, ubiquitous in the natural environment (Frimmel 1998; Singhal, Kumar et al. 2005). That being said, a wide variety of other terms are used throughout the literature in reference to organic substances: soil organic matter (SOM), organic content (OC), total organic content (TOC), dissolved organic content (DOC), humic substances (HS), humic acid (HA) and fulvic acid (FA). The most commonly studied organic compounds in natural systems are the humic and fulvic acids, which are degradation products of organic matter (Singhal, Kumar et al. 2005). Figure 11 depicts how

different types of humic substances in soils are further classified as being either humic or fulvic acids based on their solubility, and additional characteristics of each. Due to the disparity of their chemical structures, NOM in general play a multifunctional role in the environment with specific regard to complexation with metals and adsorption onto mineral surfaces, in turn greatly affecting the migration of actinides like U (daSilva, Machado et al. 1996; Frimmel 1998; Singhal, Kumar et al. 2005; Bednar, Medina et al. 2007).

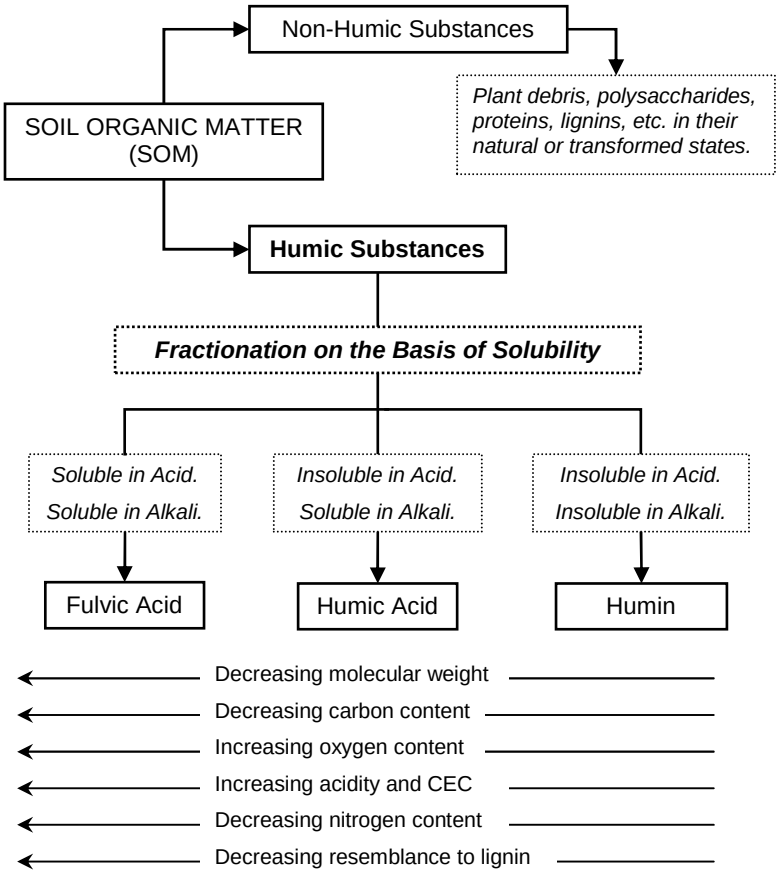

Figure 11. Soil organic matter (SOM) fractionation diagram. Adapted from the Soil Science Society of America's (SSSA) book series No. 5, Methods of Soil Analysis, Part 3, Chemical Methods (Organic matter characterization), p. 1025 (Swift 1996).

Humic substances are characterized by a variety and abundance of functional groups including carboxylic and hydroxilic structures (-COOH, -OH, -NH_2) which serve as electron donors resulting in metal ion coordination and colloid formation (daSilva, Machado et al. 1996; Lubal, Fetsch et al. 2000). Lubal *et al.* (2000) provided a comprehensive review of studies on humate complexation with the uranyl ion, and detailed reaction schemes are described for uranyl with different HA functional groups, resulting in the formation of either 1 : 1 or 1 : 2 (metal : ligand) complexes for U : HA. For the most part, humic and fulvic acids are soluble in the typical pH range of natural systems, and are characterizes by pronounced redox properties potentially influencing the oxidation state of metal ions (Krepelova, Brendler et al. 2007; Mibus, Sachs et al. 2007). One study discussed how sediments supplied with high levels of organic content resulted in 80% of the U(VI) being reduced to the insoluble, non-luminescent U(IV), with subsequent reoxidation (Tokunaga, Wan et al. 2008). With regards to the highly oxidizing surface soil conditions relevant to this research, the prevalence of organic materials in surface soils makes OM an important issue of concern. Studies comparing and contrasting organic – rich (8 – 12% OC) versus organic – poor (< 2% OC) U contaminated soils and sediments (or stratifications) verified: 1) significant levels of organic bounded U were most abundant in the surface soils (Duff, Morris et al. 2000; Radenkovic, Cupac et al. 2008), and 2) U was strongly associated with the organic phase, more so in organic – rich samples, even in the presence of both amorphous and crystalline iron (Fe) phases (Hunter and Bertsch 1998).

Regarding steady-state luminescence characterization, when organic substances are prevalent in environmental samples, their typically broad and unstructured overlapping fluorescence may swamp or mask the uranyl emission, making it difficult to detect. This is most notable when longer excitation wavelengths (such as 420 nm) are utilized, however still applies

when UV excitations are used (such as 280 nm), with the OM fluorescence strongest in the blue spectral region yet still stretching over through uranyl's green – yellow region (see preliminary studies below). Fluorescence studies of U – contaminated environmental samples commonly mention the presence of broad luminescent profiles in these spectral regions and indicate their likely attribution to the presence of organics (Morris, Allen et al. 1996; Duff, Morris et al. 2000). For this reason, most studies utilize time – discriminating detection techniques (such as TRLFS) which can focus on the longer decays characteristic of uranyl species (microsecond (μs) to millisecond (ms) range) while ignoring the shorter decays typical of organics (nanosecond (ns) range) (Kaminski, Purcell et al. 1981; Meinrath 1997; Duff, Morris et al. 2000).

While time domain analytical techniques are advantageous for separating various co-occurring and overlapping spectra characterized by different fluorescence decays, their application is still limited with regard to the quenching or diminishment of the uranyl fluorescence due to complex formation with organics. Studies often describe how the absence of the characteristic U emission is not necessarily positive evidence for the lack of U in the samples since many naturally occurring agents (such as organics and other heavy metals) are capable of substantially quenching the uranyl emission (Morris, Conradson et al. 1992; Meinrath 1997). The complexation of U with organics results in quenched fluorescence intensities (for both) and shorter measured lifetimes for uranyl (Duff, Morris et al. 2000; Krepelova, Brendler et al. 2007).

An entire separate realm of literature (typically pertinent to water quality) focuses on the fluorescence attributes of NOM themselves, including both steady-state and lifetime characterizations (Frimmel 1998). From this different perspective, many of these studies discuss the quenching of the NOM fluorescence due to complexation with metal ions, specifically with uranyl in many cases (Kumke, Tiseanu et al. 1998). The complexation of U(VI) specifically

with humic acids and fulvic acids has been the subject of many investigations. In aqueous systems, U complexation with organic ligands competes with the formation of hydroxo complexes (Singhal, Kumar et al. 2005). For the pH 4 – 5 range, both humic and fulvic acids (from natural river waters) can be strongly bound with U(VI), with humic acids forming slightly stronger complexes with U and demonstrating a greater pH dependence (Lenhart, Cabaniss et al. 2000). Studies utilizing size fractionation techniques for NOM analysis have observed: 1) dissolved organic content (DOC) consisted mainly of fulvic acid, and 2) U complexation was most prominent with lower molecular weight fractions of humic colloids and humic acids (Saito, Nagasaki et al. 2002; Singhal, Kumar et al. 2005).

The quenching of both uranyl and OM fluorescence due to their complex formation is referred to as static quenching (daSilva, Machado et al. 1996; Sachs, Brendler et al. 2007). The quenching process induced on OM fluorescence due to varying concentrations of uranyl have been described through in-depth Stern – Volmer quenching profiles for both humic acids (Takumi, Shinya et al. 2001; Saito, Nagasaki et al. 2002) and fulvic acids (daSilva, Machado et al. 1996). Regarding uranyl complexation with soil FAs, the data suggested the predominance of one type of binding structure, that the stability of these complexes are relatively high, and indicated FA highly influence U speciation in acidic soils (daSilva, Machado et al. 1996). The importance of FAs with regard to U speciation in acidic soils is likely to be due to the fact that FAs are soluble under acidic conditions whereas HAs are not, making FAs a more likely candidate to react with aqueous uranyl species. Sachs *et al.* (2007) provided an in-depth investigation of U(VI) complexation with HAs in solution using TRLFS. This study indicated the predominant formation of ternary uranyl – hydroxo – humate complexes under near-neutral pH conditions: $UO_2^{2+} + H_2O\ [OH^-] \rightarrow UO_2OH^+$; $UO_2OH^+ + HA(I)^- \rightarrow UO_2(OH)HA(I)$

[neutral] where (I) indicates one proton exchanging functional group of the HA participating in the reaction. Their speciation diagrams show the $UO_2(OH)HA(I)$ form being highly abundant in the near-neutral pH range, with a less abundant $UO_2HA(II)$ form existing in the pH 3 – 5 range, peaking at pH 4.

The effects of NOM on the speciation of U, in turn affecting its sorption and mobility in environmental samples, have been studied by many. Table 11 summarizes the findings of several studies examining the influence of HA on U sorption or mobility for varying pH conditions, for different mineral types. In comparison to the typical pH – dependent U sorption curve (refer to Figure 10), the presence of HA enhances U sorption under more acidic conditions, and either decreases sorption, increasing mobility, or has little to no effect under neutral to alkaline conditions, depending on the mineral type. That being said, these studies also indicated that in these ternary systems (mineral – U – HA) there appears to be a preference for U to bind directly to the mineral surfaces rather than binding to adsorbed HA, or they bind to the mineral surfaces as uranyl – humate complexes (Lenhart and Honeyman 1999; Krepelova, Brendler et al. 2007; Krepelova, Reich et al. 2008). This is further supported by the observation that when mineral surface sites are in excess, the influence of HAs on U sorption is less pronounced (Lenhart and Honeyman 1999).

Given the evidence that aqueous complexation between uranyl and HA results in the formation of quenched or non-luminescent species, and that U is typically sorbed to mineral surfaces as uranyl – humate complexes, it is not surprising that the presence of HA affects the fluorescence of uranyl sorbed to mineral surfaces. TRLFS data for U sorbed on kaolinite surfaces showed that, in the absence of HA, the spectra yielded six and five emission bands for binary and ternary systems respectively, and these bands were shifted to higher wavelengths

compared to free uranyl solutions. However, in the presence of HA, while the number and position of emission bands did not appear to be affected, the fluorescence intensities of the samples were greatly reduced for the entire pH 5 – 8 range (Krepelova, Brendler et al. 2007).

Table 11. Summary of U sorption and mobility studies and their findings associated with the presence of humic acid (HA).

Study Description	**Findings**
Migration of U in a quartz sand system in the presence of HA. (Mibus, Sachs et al. 2007)	Under near-neutral pH conditions, the mobility of U is significantly enhanced in the presence of HA for a quartz sand system.
U(VI) sorption onto kaolinite (clay) in the presence and absence of HA. (Krepelova, Sachs et al. 2006)	U sorption was influenced by pH, [U] and presence of HA; In the acidic pH range, U uptake was enhanced in the presence of HA (compared to a HA-free system), initially believed to be due to the presence of additional binding sites from HA adsorbed on kaolinite surfaces; In the near-neutral pH range, U sorption was reduced in presence of HA, believed to be due to formation of aqueous uranyl – humate complexes.
Structural characterization of U(VI) surface complexes on kaolinite in the presence of HA. (Krepelova, Brendler et al. 2007; Krepelova, Reich et al. 2008)	Subsequent studies revealed that in the ternary kaolinite – U – HA system, U prefers direct binding on kaolinite surfaces rather than to HA bound to the clay surface, or it is sorbed as a uranyl – humate complex; Significant parts of the kaolinite surface were not covered by HA in this study.
U(VI) sorption on hematite in the presence of HA. (Lenhart and Honeyman 1999)	U sorption by hematite was enhanced at low pH values and slightly decreased at more alkaline values in the presence of HA; When hematite surface sites are in excess, the influence of the NOM is less pronounced.
U adsorption on ferrihydrite and effects of HA. (Payne, Davis et al. 1996)	The addition of HA increased U uptake on ferrihydrite at pH values less than neutral, with little effect at higher pH values.

1.7.6 Iron Content

The interactions of U with various iron phases (including iron oxides such as hematite, iron hydroxides, and iron oxide – hydroxides such as ferrihydrite and goethite) in both pure mineral and highly amorphous forms have been heavily studied (Payne, Davis et al. 1994; Waite, Davis et al. 1994; Payne, Davis et al. 1996; Murakami, Ohnuki et al. 1997; Ohnuki, Isobe et al. 1997; Reich, Moll et al. 1998; Moyes, Parkman et al. 2000; Waite, Davis et al. 2000; Giammar and Hering 2001; Duff, Coughlin et al. 2002; Catalano, Trainor et al. 2005; Um, Serne et al. 2007; Tokunaga, Wan et al. 2008). The importance of iron (Fe) with regard to its ability to interfere with uranyl's remote fluorescence detection falls under three main focus areas: 1) its potential to directly quench uranyl fluorescence, 2) the capability of Fe^{3+} or Fe^{2+} to effectively oxidize or reduce U respectively, in turn affecting its solubility and luminescence, and 3) enhanced U sorption to Fe phases, thereby limiting its mobility.

Several papers have given the impression that high levels of iron in environmental samples can result in the quenching of uranyl luminescence (Sowder, Clark et al. 1998; Duff, Coughlin et al. 2002). For solution studies, metal ions in general can often quench uranyl fluorescence, with both the ferrous (Fe^{2+}) and ferric (Fe^{3+}) oxidative forms of iron commonly being mentioned (Moriyasu, Yokoyama et al. 1977; Burrows, Cardoso et al. 1985; Blackburn and Almasri 1994). The quenching reaction of uranyl luminescence by Fe^{2+} is diffusion – controlled and is due to electron transfer from the Fe^{2+} to the uranyl ion, UO_2^{2+} (Moriyasu, Yokoyama et al. 1977; Burrows, Cardoso et al. 1985). A photophysical study of the excited uranyl ion in aqueous solutions indicated the effect of metal ions follows typical Stern – Volmer quenching behaviors, and is probably explained by reversible crossing between two energetically close excited states (Burrows, Cardoso et al. 1985). Another study was of ferrous ions being

added to a uranyl solution (pH 3) containing poly(vinylsulfonate) [PVS, polymer] and indicated the quenching process was complex due to the Fe^{2+} ions initially displacing the uranyl ions from polymer binding sites, followed by Fe^{2+} ions quenching the liberated uranyl ions (Morawetz and Taha 1971). Similar to ferrous ions, ferric ions (Fe^{3+}) have also been cited as an interfering quencher of uranyl luminescence, limiting detection of U in aqueous samples when utilizing pulsed – source fluorescence spectrometers (Williams and Miller 1983). An in-depth study of sample matrix quenching affecting the measurement of trace [U] in solutions described how, of all the cations examined, the transition metals demonstrated the greatest interferences (in the order of: $Cr^{3+} > Ni^{2+} > Cu^{2+} > Fe^{3+}$), and that quenching due to Fe^{3+} resulted in a significant decrease in the phosphorescence lifetime (Sowder, Clark et al. 1998). Meinrath's detailed publication (1997) on the application of fluorescence spectroscopy for characterizing U speciation in environmental samples describes how inorganic ions (including Fe^{3+} and Cl^{-}) can reduce the emission yield of the excited uranyl species by either: 1) abstracting the excited electron from the uranyl entity, or 2) transferring an electron to the electronically excited U(VI) (Meinrath 1997).

Literature related to luminescence characterization of U – containing minerals with regard to iron content is limited. A study of U co-precipitation with iron oxide minerals acknowledged that iron can quench the U emission, yet claimed in this case U concentrations on the surface of the precipitates were high enough to detect its fluorescence (Duff, Coughlin et al. 2002). Similarly, a study of contaminated Fernald soils noted that monolayer surface adsorption of U to iron oxyhydroxy phases can lead to deactivation of the luminescence through quenching, however they observed the luminescence from U grains physically associated with the goethite

mineral phase (α – FeOOH) in a multilayer manner did not completely quench the luminescence (Morris, Allen et al. 1996).

As mentioned in previous sections, the oxidative state of U is very important in that: 1) U(VI) species (including uranyl forms) exhibit the natural, long-lived fluorescence while other oxidative states [such as U(IV)] are generally non-luminescent (Sowder, Clark et al. 1998), and 2) the solubility of U(VI) species is much greater than that of U(IV) species (Bostick, Fendorf et al. 2002; Tokunaga, Wan et al. 2008). Therefore, from the perspective of this research mission, it is important U exists in the 6+ oxidative form so there is greater chance of absorbing it from the solution phase in addition to it being fluorescent. The oxidation of U to the hexavalent state is as follows: $UO_2 - 2e^- \rightarrow UO_2^{2+}$. The continual oxidation of U is often achieved in the presence of ferric ions as: $UO_2 + 2\ Fe^{3+} \rightarrow UO_2^{2+} + 2\ Fe^{2+}$ where the ferric ions must be renewed by continual oxidation of the ferrous (Fe^{2+}) ions (Stork, Smartt et al. 2006). In a state of equilibrium, U existing in the presence of goethite [an iron(III) phase] will exist in the hexavelent form since the UO_2/UO_2^{2+} oxidation potential is considerably lower than that for Fe(II)/Fe(III) (Morris, Allen et al. 1996). A study of contaminated sediments undergoing bioreduction, however, demonstrated that Fe(III) can persist as an electron accepter even under reducing conditions, resulting in the reoxidation of U(IV) (Tokunaga, Wan et al. 2008).

Under oxidizing conditions, as would be expected in most surface soils and aquatic systems, U would predominantly exist in the U(VI) form. For iron, typical Eh – pH stability diagrams indicate that for oxidizing conditions, the following Fe(III) forms predominate: Fe^{3+} (pH < 2), $Fe(OH)^{2+}$ (pH ~ 2 – 3.5), $Fe(OH)_2^+$ (pH ~ 3.5 – 4), $Fe(OH)_3$ (pH ~ 4 – 11.5), and $Fe(OH)_4^-$ (pH ~ 11.5 – 14). Recalling the typical pH range for soils is ~ 3.5 – 9, one would

expect pure iron phases to exist primarily as the $Fe(OH)_3$ form, with $Fe(OH)_2^+$ present under more acidic conditions.

Sorption of U to pure crystalline iron minerals as well as to amorphous iron oxide forms has been heavily studied (Murakami, Ohnuki et al. 1997; Barnett, Jardine et al. 2000). In iron – rich soils, U exhibits a strong affinity for the Fe surfaces, resulting in its significant occlusion and therefore limited transport in the environment (Barnett, Jardine et al. 2000; Duff, Coughlin et al. 2002). Table 12 summaries studies describing the strong association between U and Fe – phases resulting in enhanced sorption and reduced mobility. The presence of Fe oxides in soils is important because they commonly occur as grain coatings (see Table 12) resulting in increased surface areas and greater sorption capacities due to their porous nature and small particle size (Reich, Moll et al. 1998; Bargar, Reitmeyer et al. 2000; Um, Serne et al. 2007). A study on the influence of iron oxides on the surface area of soil confirmed that both amorphous and crystalline iron oxides are significantly correlated with increased surface areas, while specific surface areas can vary from soil to soil (Borggaard 1982). Both surface complexation and surface precipitation have been described as different mechanisms of U retention in the presence of iron oxides and hydroxides [‘iron hydr(oxides)’], which depend on mineral type, [U] and pH. The precipitation of iron oxides themselves notably occurs under acidic conditions (Anderson 1996; Reich, Moll et al. 1998). U uptake and incorporation into Fe hydr(oxides) occurs predominantly by surface complexation until the point of surface saturation, after which precipitation of U(VI) results in the formation of discrete crystalline uranyl phases (Moyes, Parkman et al. 2000; Duff, Coughlin et al. 2002). Several independent studies examining the nature of U sorption on iron minerals (such as ferrihydrite) describe the formation of inner-

sphere, mononuclear surface complexes for a wide pH range (~ 4 – 8) (Waite, Davis et al. 1994; Reich, Moll et al. 1998; Moyes, Parkman et al. 2000; Bostick, Fendorf et al. 2002).

Table 12. Summary of studies describing the strong association between U and Fe – phases resulting in enhanced sorption and reduced mobility.

Site/Study Description	**Findings**
DOE Savannah River site, SC. (Wang, Zachara et al. 2005)	Most of the sediment U(VI) was associated with poorly crystalline iron oxides and particulate OM.
DOE Hanford site aquifer sediments. (Um, Serne et al. 2007)	Samples were dominated by sand and gravel fractions, yet high iron content correlated to heavy iron – oxide coatings, resulting in strong U(VI) adsorption; Concluded iron oxides were the key sorbent affecting U(VI) fate and mobility in this study.
Heterogeneous media (pH varied) from DOE facilities. (Barnett, Jardine et al. 2000; Bostick, Fendorf et al. 2002)	Media was dominated by sand-sized quartz minerals with iron oxide coatings; U sorption was highly correlated to iron content (as opposed to clay, OM and Mg oxides); Concluded iron hydr(oxides) were primarily responsible for the observed adsorption properties.
Western Kosovo topsoils, following 1999 conflict. (Di Lella, Nannoni et al. 2005)	High and rather uniform percentages of U content (24 – 36%) were determined to be associated with poorly crystalline iron oxides phases in the soils.
DU contaminated soils in Southern Serbia. (Radenkovic, Cupac et al. 2008)	Soils characterized by: ~ 80% sand, neutral pH, low clay and humus content; Fe and Mg oxides, as well as carbonates, were the prevailing substrates for DU sorption.

While some studies generally claim dissolved U sorbs Fe – oxide minerals (such as goethite and hematite) over a wide range of pH conditions (Duff, Coughlin et al. 2002), other studies confirm and define the pH – dependency of this interaction more clearly. Iron hydr(oxides), including ferrihydrite, goethite, hematite and amorphous forms, do typically sorb U(VI) strongly under neutral to slightly basic conditions (Bostick, Fendorf et al. 2002). That being said, the adsorption decreases sharply in the narrow pH range of ~ 7.5 – 8.5 (referred to as

the reverse adsorption edge, refer to Figure 10). Based on these observed adsorption properties, a study demonstrating similar U sorption to a variety of heterogeneous media from DOE sites concluded iron hydr(oxides) were the dominant pH dependent charged surface on these soils since the total Fe contents were similar in these samples (Barnett, Jardine et al. 2000). While U sorption on iron phases tends to follow the general trend depicted in Figure 10, increasing the concentration of Fe surface sites in the sample (from limited to excess) results in a broadening of the sorption curve, from an initial range of pH 4 – 9 to a final range of pH 3 – 10. This observation combined with fact that U prefers to bind directly to Fe surfaces in ternary systems (such as $\equiv FeOH–UO_2–HA$) explains why the presence of NOM is not as influential on U sorption when Fe surface sites (such as hematite) are in excess (refer to Table 11) (Lenhart and Honeyman 1999).

Similar to when OM is prevalent, in the presence carbonates (CO_3^{2-}) U also prefers to bind directly to Fe surfaces as uranyl – carbonato ternary complexes [such as $\equiv FeO_2–UO_2–CO_3^{2-}$], and this has been confirmed for a variety of Fe – bearing phases including highly heterogeneous mixtures of goethite, hematite and amorphous iron hydr(oxides) (Waite, Davis et al. 1994; Reich, Moll et al. 1998; Bargar, Reitmeyer et al. 1999; Bargar, Reitmeyer et al. 2000; Bostick, Fendorf et al. 2002; Davis, Meece et al. 2004; Catalano, Trainor et al. 2005). As described in previous sections, U complexation with carbonate is a dominant geochemical reaction, typically resulting in significant desorption of U from soil particles, and was described as the key reason for observing the reverse absorption edge in the alkaline pH range (refer to Table 9). Carbonate anions can absorb and change the electrical double layer charge and potential of iron oxides, influencing U adsorption (Davis, Meece et al. 2004). While previously U sorption on iron minerals was described as involving the formation of inner-sphere,

mononuclear surface complexes (pH ~ 4 – 8), in the presence of carbonates, ternary surface complexation is bidentate (involving two binding sites) or binuclear involving binding with adjacent singly coordinated oxygen sites on the iron mineral surface (Waite, Davis et al. 1994; Catalano, Trainor et al. 2005).

Despite that the presence of Fe – phases, in general, typically results in increased surface areas and enhanced sorption of U in soils, the specific nature of the interaction is dependent upon the structure of the Fe phase, and whether it exists in an amorphous or crystalline form. One study utilizing a sequential extraction procedure and examining the fractions of U associated with different co-existing phases showed that for an organic – poor sample, a much larger fraction of U was associated with the amorphous Fe phase (extracted first) compared to the crystalline Fe phase (Hunter and Bertsch 1998). However, a different study utilizing a selective extraction procedure for static systems of U sorbed to either amorphous or crystalline Fe (such as goethite) showed that the fraction of U desorbed from the amorphous Fe minerals was lower that that extracted from the crystalline minerals. That being said, they also examined the changes in U sorption characteristics for a dynamic system where amorphous Fe minerals were undergoing crystallization. These tests demonstrated that during the crystallization of amorphous iron minerals, most of the U associated with the amorphous phase is not released into solution but is fixed (to a degree) within the forming crystalline iron minerals (Ohnuki, Isobe et al. 1997).

The variation in the nature of the interaction between U and different Fe forms appears to also influence the uranyl luminescent features. The above mentioned study which utilized a sequential extraction procedure also demonstrated that the fluorescence spectra of contaminated sand particles varied depending on the Fe forms present. Specifically, with the extraction and removal of the amorphous Fe phase, the new emission spectra (representing the U bound to

crystalline Fe) was somewhat decreased in intensity yet exhibited an overall improvement in its structure (line width resolution) as well a 'blue-shift' (shift in bands to shorter, higher energy wavelengths) (Hunter and Bertsch 1998). These observations correspond well with those of Chang *et al.* (2006) who studied U bound to gibbsite (AlO) (see previous section). They reported the presence of a 'species C' that was less abundant than other species present yet exhibited a highly-resolved and 'blue-shifted' emission spectra, corresponding to electrostatically bound uranyl complexes (Chang, Korshin Gregory et al. 2006). Clearly, variations in U adsorption to Fe phases can be caused by differences in surface charge, substrate structure, the electronic structure of surface functional groups, as well as U(VI) aqueous speciation (Catalano, Trainor et al. 2005).

1.7.7 Summary and Hypothesis Statements

While numerous environmental parameters co-exist and can potentially limit the fluorescence detection of uranyl on soil surfaces, some seem potentially more influential and are more heavily supported by outside literature. Table 13 summarizes the key influential features of environmental samples selected for further investigation and important points related to each.

All of the parameters selected affect U sorption and migration in the soil environment, indirectly affecting its ability to be absorbed and enhanced by a distributed sensor. Similarly, most of the selected parameters also are capable of affecting the fluorescence response of U directly. Notably, these parameters often behave as matrix effects exhibiting overlapping and integrated influences. One example would be the direct relationship between soil texture, moisture content and water potential. Another example would be the increase in sorption of U to particles that is seen at somewhat lower pH values for both organic – rich and iron – rich soils.

Table 13. Key influential features of environmental samples selected for further investigation.

Parameter	Comments
Soil Texture [1]	Based on particles sizes and porosity. Affects water content, flow, and potential. Clay: surfaces more abundant and typically characterized by greater CEC and reactive edge sites, resulting in increased U sorption.
Moisture Content [1,2]	% MC: Directly affected by temperature, evaporation and humidity, and related to WP. Characterized by strongly time – dependent, dynamic effects; both faster kinetic flow processes and slower molecular movements within (affects U sorption, dissolution and precipitation). Water: quenches U FL and absorbs/scatters light; affects crystallinity of samples and U speciation, affecting FL.
Water Potential [1]	WP: Directly related to both % MC and soil texture, and affected by chemical composition of the solid matrix. Strongly affects water movement (and therefore soluble U movement) through the soil regime.
pH Related Effects [1,2]	Affects U speciation, in turn affecting both FL response and mobility. Direct relationship to U sorption versus dissolution, with sorption strongest in the near-neutral range, and desorption/dissolution greatest under more acidic and alkaline conditions (slow process). Affects charge of uranyl species and soil surfaces, thereby affecting the type of binding interactions, in turn affecting the FL spectrum. Complexation with carbonates under alkaline conditions results in reduced FL. Free uranyl ion (strongly acidic conditions) exhibits lower FL compared to hydroxo species (slightly acidic conditions).
Soil Organic Matter [1,2]	Affects U adsorption/desorption to soil particles and mobility. Sorption of U is enhanced under acidic conditions in the presence of HA (sorption begins at pH ~ 3 v. ~ 4, unless mineral surface sites in excess), while U sorption is decreased (mobility increased) in near-neutral pH conditions, in the presence of HA. Directly affects U FL via spectral overlap (steady-state analyses), and complex-formation resulting in static quenching. Both aqueous and sorbed uranyl – humate complexes exhibit diminished FL.
Iron Content [1,2]	Often exists as soil grain coatings, resulting in enhanced U sorption due to greater surface areas and stronger affinity for uranyl species. Commonly identified as the key sorbent responsible for U adsorption properties. Higher Fe content results in widening of the pH dependent sorption curve. Presence of Fe^{3+} and Fe^{2+} results in quenched U FL.

[1] Affects U migration, indirectly affecting its potential fluorescence – based surface soil detection.

[2] Directly affects U fluorescence (FL) response.

An additional influence for consideration would be seen in comparing the pH dependencies of U sorption to natural solid materials, and the fluorescence response of uranyl when it interacts with silica gel (the selected accumulating and enhancing material) in the absence of carbonates (see Figure 12). This figure gives the impression that for the pH region most ideal for uranyl – silica gel fluorescence, the sorption of U to the solid soil matrix will be strong, limiting available soluble U, especially for low U contamination levels. The general similarities between these curves is likely due to the fact that the interaction of uranyl with silica gel in solution follows a similar sorption trend as U to natural materials in the environment, and therefore there would most likely be a slow competitive sorption process for uranyl between its affinity for natural minerals and the newly introduced silica gel sorbent on the soil surface.

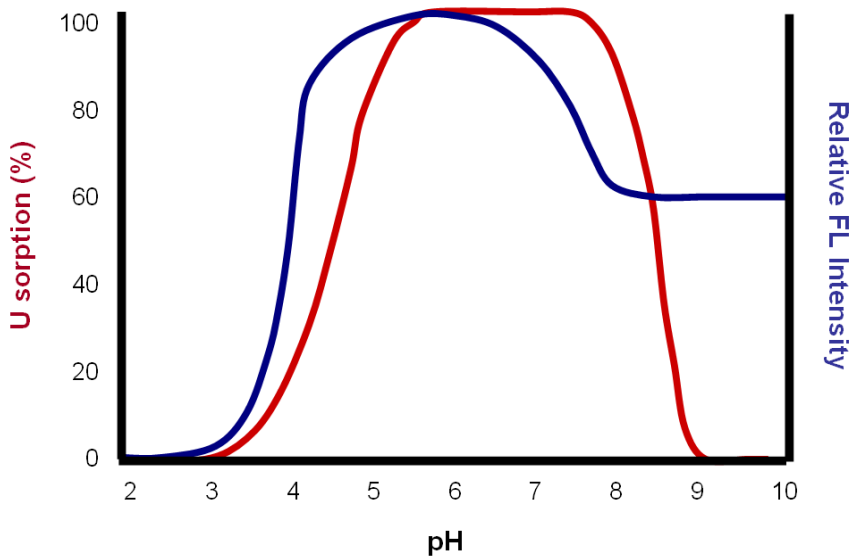

Figure 12. Diagram showing the general trend of U sorption (%) on natural solid materials as a function of pH (red), in comparison to the pH dependent trend of uranyl – silica gel solution fluorescence intensity, in the absence of carbonates (blue).

From a comprehensive perspective, most all the parameters selected in some way help define the 'U speciation' (the specific form of the uranyl complex), which in turn determines how it will interact with the soil matrix in addition to its luminescent response. The majority of the fluorescence data collected for this dissertation research was in the form of steady-state spectral data. Undesirable direct effects on uranyl's fluorescence emission would be observed as: 1) significant diminishment of the fluorescence intensity, 2) significant reduction or alteration of the unique spectral band structure, and 3) masking of the uranyl spectra. Both temporal effects as well as U concentration effects were examined in conjugation with the selected key environmental parameters. Combined effects demonstrating realistic phenomena were studied through examining collected field samples that were further characterized with regard to their soil texture, pH, organic matter, iron content and CEC. A preliminarily proposed 'best-case' scenario would likely be a highly contaminated, moist, organic and iron poor sand sample of pH 4 – 5 (see Table 14 for further details).

Based on all the background information and justifications described previously, the following hypotheses were generated for further testing and validation with regard to uranyl fluorescence – based detection at ground – level soil surfaces, typically utilizing a distributed silica gel – based sensor.

<u>Comprehensive Hypothesis Statements:</u>

1. The fluorescence detection of uranyl compounds is dependent upon key environmental parameters including: soil texture, moisture content, soil pH, organic matter, iron content and cation exchange capacity (CEC).

2. The fluorescence detection of uranyl compounds is strongly dependent upon the concentration of uranium present in the soil matrix (0 ppm, 10 ppm, 100 ppm and 500 ppm).

3. The fluorescence detection of uranyl compounds is dependent upon time, following the application of the distributed silica gel – based sensor.

Table 14. A proposed best-case scenario for uranyl fluoresce detection at soil surfaces with a silica gel – based distributed sensor, and detailed explanations related to environmental factors.

Explanation related to:	**Proposed best-case scenario:** Highly contaminated, moist, organic and iron poor, sand sample of pH 4 – 5.
U contamination level	The lower the [U] in the soils, the harder it will be to detect because less U will exist in the aqueous phase where it can be easily absorbed by a distributed sensor, and less U absorbed by the sensor in general will result in a weaker FL return.
Moisture content	Both a perfectly dry and saturated sample would be more troublesome. In the complete absence of water, the U is immobile and cannot be absorbed by the distributed sensor. Under saturated conditions, the overabundance of water would result in increased quenching and light scattering, as well as limit the amount of U that would potentially flow with water (faster kinetic process) from the soil to the silica gel.
Soil texture	In the absence of other factors, detection in a sand system is more feasible and timely than in a silt or clay sample since the water flow is faster. Clays are characterized by greater surface area and surface charge, making it a more difficult medium to extract U from.
pH	The uranyl – silica gel complex is essentially non-FL at pH $\leq$ 3. Under near-neutral conditions, U sorption is strongest to soil particles, making absorption of aqueous U by the distributed sensor more difficult and time demanding. Under soil alkaline conditions (pH 8 – 10), while the U is less likely to be bound to soil particles, uranyl's complexation with carbonates may result in not only quenched FL but also limited sorption of U by silica gel.
Organic matter	In organic – rich soils, not only will U sorption to soil particles be stronger under slightly acidic soil conditions, U will exist as uranyl – humate complexes which exhibit greatly diminished FL.
Iron content	In iron – rich soils, not only will U sorption to soil particles be stronger under both slightly acidic and alkaline soil conditions, soil texture will not be as important in that the iron typically exists as soil coatings characterized by high surface area and strong affinity for U. In addition, the presence of aqueous Fe ions may result in collisional quenching of U FL.

CHAPTER 2: EMPIRICAL INVESTIGATIONS

2.1 Preliminary Studies

2.1.1 Introduction

A wide variety of studies have previously been conducted which are relatable to the defined key features of environmental samples potentially limiting uranyl fluorescence detection in the environment. Data resulting from several of these preliminary studies are discussed below, and helped identify general patterns and potential influential factors. For all these studies, the source of U for sample spiking was uranyl nitrate hexahydrate [$UO_2(NO_3)_2$ x $6H_2O$], which was typically dissolved in nanopure water to make a 10 mM stock solution. The majority of the early preliminary studies used the Sea sand standard (SDc) as a model system, while some more recent studies utilized collected environmental soil samples. Table 15 lists the detailed chemical composition of the KGa-1b clay (kaolinite) standard sample to be used in subsequent studies, while Table 16 provides a detailed list of the soil samples utilized in discussed studies. The KGa-1b clay standard was obtained from the Clay Mineral Society, Source Clays Repository in Columbia, USA, and is a commonly used clay-kaolinite standard (Payne, Davis et al. 2004; Krepelova, Brendler et al. 2007). For this clay standard, note the high percent composition of SiO_2 and Al_2O_3, and recall that under relevant environmental conditions these highly reactive metal-oxide-like groups on the surfaces of clays act as a sequestering sink for uranyl species, but display a strong pH dependency (Chisholm-Brause, Berg et al. 2004).

The environmental samples listed in Table 16 were characterized with regard to their soil texture, soil pH and percent organic matter. The sample from the Contrary Creek main stream (CCms) is known to contain a high degree of iron precipitates (indicated by its orange color) in addition to being acidic and containing Fe^{3+} and Fe^{2+} forms of iron (Anderson 1996). The sample from the James River stream bed (JA3) is predominantly silt, and contains a relatively high percentage of organic matter. The closer to neutral pH of this sample made it a very important sample for further analysis. Based on the background information described in the previous section, an additional important environmental sample would be one characterized by a high pH and the prevalence of carbonate species, due to the breakdown of concrete materials.

Table 15. Chemical composition (wt. %, dry) of KGa-1b clay (kaolinite) standard sample, obtained from the Clay Minerals Society, Source Clays Repository in Columbia, USA. Adapted from (Payne, Davis et al. 2004).

SiO_2	45.2		MgO	0.05
Al_2O_3	39.1		CaO	0.02
TiO_2	1.64		Na_2O	0.04
Fe_2O_3	0.21		K_2O	0.02

Table 16. List of soil samples utilized for discussed studies.

Sample code	Soil texture [a]	Color / %OM [b]	Sample collection	Typical condition / Environmental neighboring	Soil pH [c]
SDc (SC)	Sand	light tan / 0%	Fisher Scientific (Sea Sand standard) Purchased 2007	*N/A*	5.5
KGa-1b (KB)	Clay	white / 0%	Clay Mineral Society (Clay standard) KGa-1b, Georgia kaolinite Purchased 2008	*N/A*	4.5
SPf (SF)	48% Sand 31% Silt 21% Clay Loam	brown / 2.4%	Eastern Piedmont soil, Montpelier VA Semi-permanent flood zone Est. soil penetration: 6 in Collected Feb 2008	Wet zone / wooded area	4.6
UPc (UC)	54% Sand 17% Silt 29% Clay Sandy Clay Loam	dark tan / 0.7%	Eastern Piedmont soil, Montpelier VA Upland area Est. soil penetration: 6 in Collected Feb 2008	Dry zone / wooded area	4.2
JA3 (JA)	44% Sand 45% Silt 11% Clay Loam	dark brown / 4.1%	James River stream bed Hopewell VA Bottom of a shallow channel Est. soil penetration: 1 ft Collected Feb 2008	Submerged / nature preserve, downriver from industrial area	6.1
CCdr (CR)	92% Sand 2% Silt 6% Clay Sand	golden brown / 0.8%	Contrary Creek drainage site Mineral VA Drainage pool beside creek Est. soil penetration: 1 in Collected July 2008 Recollection Aug 2009	Wet zone, submerged / drainage pool, wooded area, acid mine drainage site	4.9
CCms (CS)	94% Sand 2% Silt 4% Clay Sand	orange / 1.9%	Contrary Creek stream bed Mineral VA Bottom of shallow steam Est. soil penetration: 1 in Collected July 2008 Recollection Aug 2009	Wet zone, submerged / stream bed in wooded area, acid mine drainage site	3.3
Yma (YA)	87% Sand 7% Silt 6% Clay Loamy Sand	orange brown / 0.3%	Alluvial plain area Yuma AZ Est. soil penetration: 3 ft Collected Sept 2007	Dry desert soil / sparsely vegetated	8.3
RCsw (RW)	49% Sand 26% Silt 25% Clay Sandy Clay Loam	very dark brown / 2.4%	VCU Rice Center Charles City County VA Adjacent to old spillway Est. soil penetration: 1 ft Collected Aug 2009	Wet zone / wooded area	5.2
RCdh (RH)	34% Sand 44% Silt 22% Clay Loam	brown / 4.8%	VCU Rice Center Charles City County VA Adjacent to old dining hall Est. soil penetration: 1 ft Collected Aug 2009	Dry zone / wooded area	4.7

Table 16. (Continued).

Sample code	Soil texture [a]	Color / %OM [b]	Sample collection	Typical condition / Environmental neighboring	Soil pH [c]
Rcof (RF)	38% Sand 40% Silt 22% Clay Loam	golden brown / 5.9%	VCU Rice Center Charles City County VA Open field Est. soil penetration: 1 ft Collected Aug 2009	Dry zone / open-grass field	4.5
NMws (NS)	96% Sand 0% Silt 9% Clay Sand	opaque white / 0.1%	White Sands NM Collected Oct 1994	Gypsum desert sands	7.3
NMjp (NP)	78% Sand 15% Silt 7% Clay Loamy Sand	orange / 0.1%	Jornada Experimental Range Las Cruces NM Collected *unknown*	Playa lake bed sands	7.8
Sad (SD)	54% Sand 31% Silt 15% Clay Sandy Loam	orange brown / 1.3%	Saudi Arabia (near Riyadh) Collected 1992	Dune sands	7.9
Camo (CO)	93% Sand 3% Silt 4% Clay Sand	very dark brown / 2.4%	Montana de Oro state park Los Osos CA Collected *unknown*	Dune sands	5.5

[a] Soil textures verified through standard particle-size analysis by hydrometer (A&L Eastern Laboratories, Inc.).
[b] Organic matter (% OM) verified through routine colorimetric determination (A&L Eastern Laboratories, Inc.).
[c] Soil pH verified through standard 1:1 potentiometric soil-slurry procedure (A&L Eastern Laboratories, Inc.).

2.1.2 Steady-state Fluorescence Spectroscopy

Steady-state fluorescence data were collected using a Fluorolog®-3 spectrofluorometer (Jobin Yvon Inc., Edison, NJ, USA) with DataMax for Windows ™ as the driver / controller software. A 1000 W xenon arc lamp was used as the excitation source, and the emission data were corrected for monochromater aberrations and detector response. All spectra were obtained at room temperature. Aqueous samples were analyzed in 1 cm^2 quartz cuvettes placed inside the sample compartment, while solid samples were analyzed using a bifurcated fiber optics, positioned at nadir to the sample surface and consistently maintained at approximately 2 cm above the surface of the samples. For these emission scans, an excitation wavelength (λ_{Ex}) of

280 nm was primarily used, however λ_{Ex} of 300, 355 and 420 nm were used in some of these preliminary studies for a variety of reasons. The emission window (λ_{Em}) was defined as the 400 – 650 nm range (typically 1 nm resolution). For several of the later studies, a long-pass filter (320 nm, Edmund Optics #46421), was placed in front of the emission detector in order to minimize second degree order effects in the emission spectra. This enabled the use of shorter, more ideal excitation wavelengths (such as 280 nm v. 300 nm). Post-processing of the emission data was typically performed using Microsoft Excel, OriginPro® v8, and MATLAB.

2.1.3 Data Related to Key Features of Environmental Samples

It is intuitive that variation in moisture content in soil samples could affect the remote fluorescence detection of uranyl in a variety of ways, and that the amount of moisture in the samples is directly affected by evaporation, temperature and humidity. One early study specifically focused on comparing the difference in spectral response for 'high' (75 – 85%) versus 'low' (20 – 30%) relative humidity conditions (see Figure 13). Sand samples were prepared (120 ppm U, NaF powder placed on surface, consistent initial % MC) and placed in humidity chambers for 18 hours. This study clearly indicated that drier conditions (lower humidity) resulted in improved signal intensity and spectral shape for these samples.

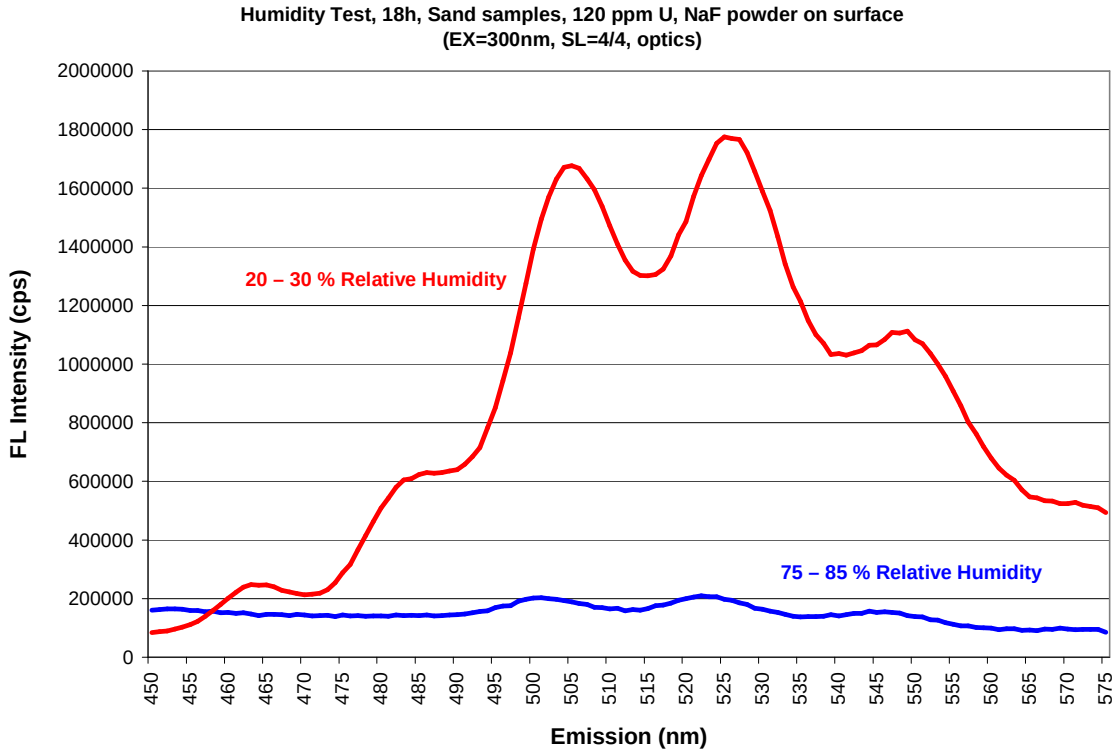

Figure 13. Steady-state fluorescence emission scans demonstrating the effect of variation in humidity on uranyl detection when enhanced by NaF powder on sand samples contaminated with 120 ppm U.

While Figure 13 indicated that drier conditions are better for detection, it is important to remember that an adequate level of moisture must first be present as a delivery mechanism to bring the uranyl to the absorbing–enhancing material on the soil surface, and *subsequent* drying appears to be advantageous. With regards to uranyl migration and moisture in soils, there is a faster kinetic process of free uranyl moving through the soil *with* the flow of water, and there is a slower process of the uranyl migrating *through* the aqueous phase as it progresses towards equilibrium. One previous study attempted to visually demonstrate (through detected florescence) this rapid kinetic process of U migrating with water through sand. In this study, water was introduced (from below) to dry contaminated sand having silica gel on its surface. Figure 14 shows the results of this continual wave analysis test (CWA, single point intensity

counts). Once the water flowing through the sand system reached the silica gel, the fluorescence rapidly increased over a short period of time (~ 30 sec) until reaching a point of saturation, after which a very slow increase in intensity was observed for several minutes. While the initial rapid increase in intensity was due to uranyl being absorbed by the silica gel along with the water, the slower subsequent increase in intensity was most likely due to: 1) gradually more uranyl being introduced to the silica gel via its migration through the aqueous phase, and/or 2) uranyl slowly forming more fluorescent complexes with the silica gel and being isolated in its protective pores.

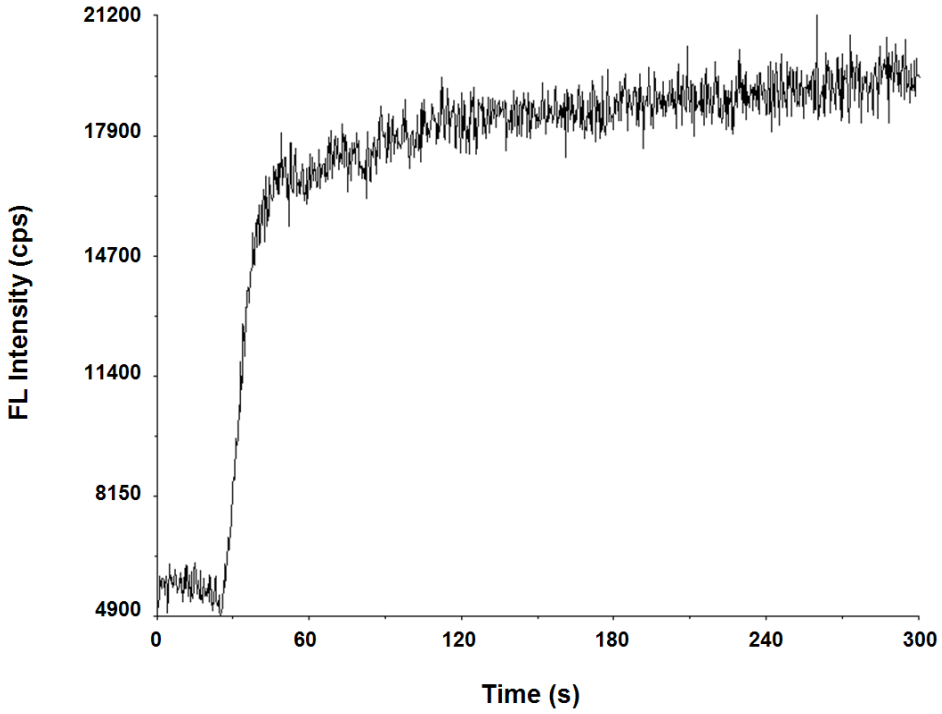

Figure 14. Single-point fluorescence intensity counts demonstrating the rapid migration of U with water through sand (λ_{Ex} = 300 nm, λ_{Em} = 519 nm, 3 nm bp). Water was added (10 mL at ~0.1 mL/sec) to dry sand (30 g) previously contaminated with 100 ppm U, with silica gel on the surface.

Once the silica gel has absorbed all the local moisture and uranyl it has access to, the slower subsequent process of drying through evaporation also affects the uranyl detection. Figure 15 shows the gradual increase in uranyl fluorescence intensity with time (t = 0, 20, 120 min). This observed increase was most likely a combined result of both the drying of the sample and the time-dependent interaction between the uranyl and silica gel as described above.

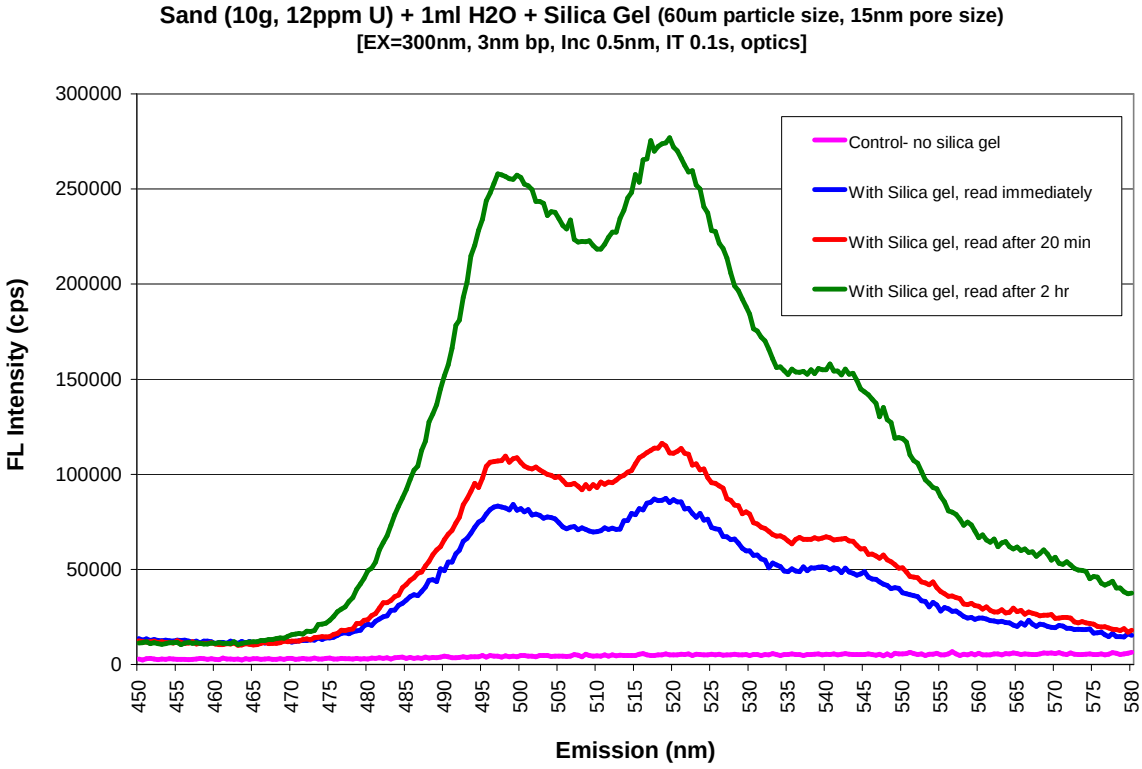

Figure 15. Steady-state fluorescence emission scans demonstrating the time dependence of uranyl detection when enhanced by silica gel on sand samples contaminated with 12 ppm U.

A later study was aimed at examining variations in uranyl fluorescence detection with time for different soil samples, varying in initial moisture content (see Figure 16). This data (single peak intensity counts) clearly indicates a strong dependence on soil type (sand standard compared to two environmental loam samples), initial moisture content (5, 10, 15%), and time (day 0 versus day 12). These samples were stored in sealed dishes, and the % MC was fairly

well maintained over the 12 day period. Therefore, the differences seen between day 0 and day 12 were primarily due to time-dependent interactions between uranyl and the silica gel, rather than effects due to drying. All the samples yielded a significant increase in fluorescence response after 12 days. That being said, the sand samples in general yielded much higher intensity counts on day 0 compared to the environmental samples as would be expected. A similar pattern related to % MC was seen between the two environmental loam samples, which was clearly distinct from that seen for the sand standard. For day 12, higher initial % MC resulted in improved fluorescence response from the loam samples, whereas the opposite pattern was seen for the sand samples. This observation may be tied to the fact that water potentials vary based on soil texture, and tend to vary within the 5 – 15% moisture content range for the loam samples, whereas < 5% MC would be more influential for sand samples. A possible explanation could be that 5% MC may be more than adequate for uranyl transport in a sand sample and additional moisture results in greater quenching, where as in loam samples (capable of holding more water) the higher % MC may result in a greater capacity for the uranyl to migrate to the silica gel. While this study demonstrated the influence of time, it should not be assumed that it would take such a long period of time to be able to detect this level of U in a sample containing silt or clay. Subsequent experiments showed 100 ppm U could be detected in the environmental samples (SPf, UPc and JA3) within a few days. However, for this same experiment, the James River sample (JA3) yielded no observable fluorescence response on day 0 (data not shown). The fact that the JA3 sample was more difficult than the UPc and SPf samples with regards to uranyl detection indicates that more than soil texture was playing a role. This observation can probably be explained by the facts that the JA3 sample was characterized by a

near-neutral pH (whereas the others were slightly acidic) in addition to containing the highest amount of OM.

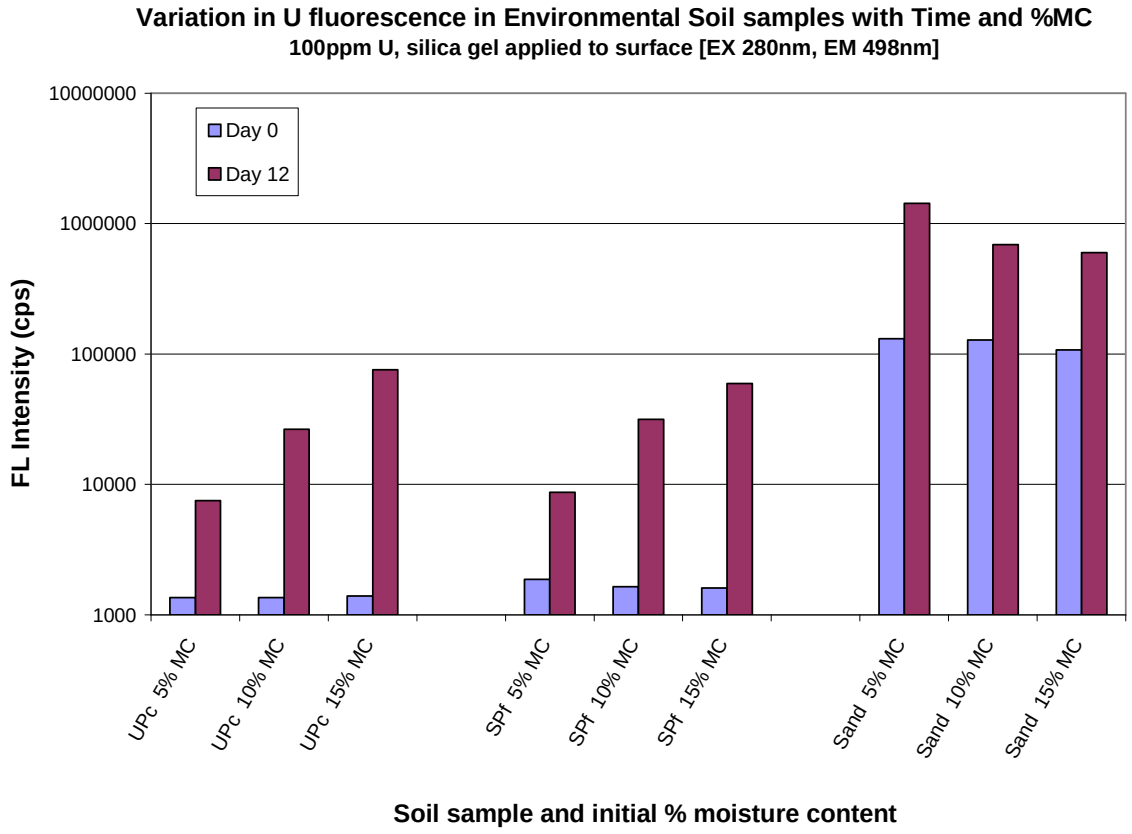

Figure 16. Effect of moisture content and time on detected uranyl fluorescence enhanced by silica gel for varying soil samples.

The observation that the James River sample (JA3) was more challenging with regards to detecting uranyl fluorescence compared to the other environmental samples (UPc and SPf), which themselves were more challenging than the sand standard sample (SDc), is somewhat reflected in the pattern of the water potential curves for these samples. Figure 17 displays their water potential readings relative to % MC. It is important to note that for these readings, the samples were completely air-dried initially, with controlled amounts of water subsequently

added to the samples and allowed to absorb overnight. Therefore, any potential effects due to the chemical nature of the original solution phase would not be present.

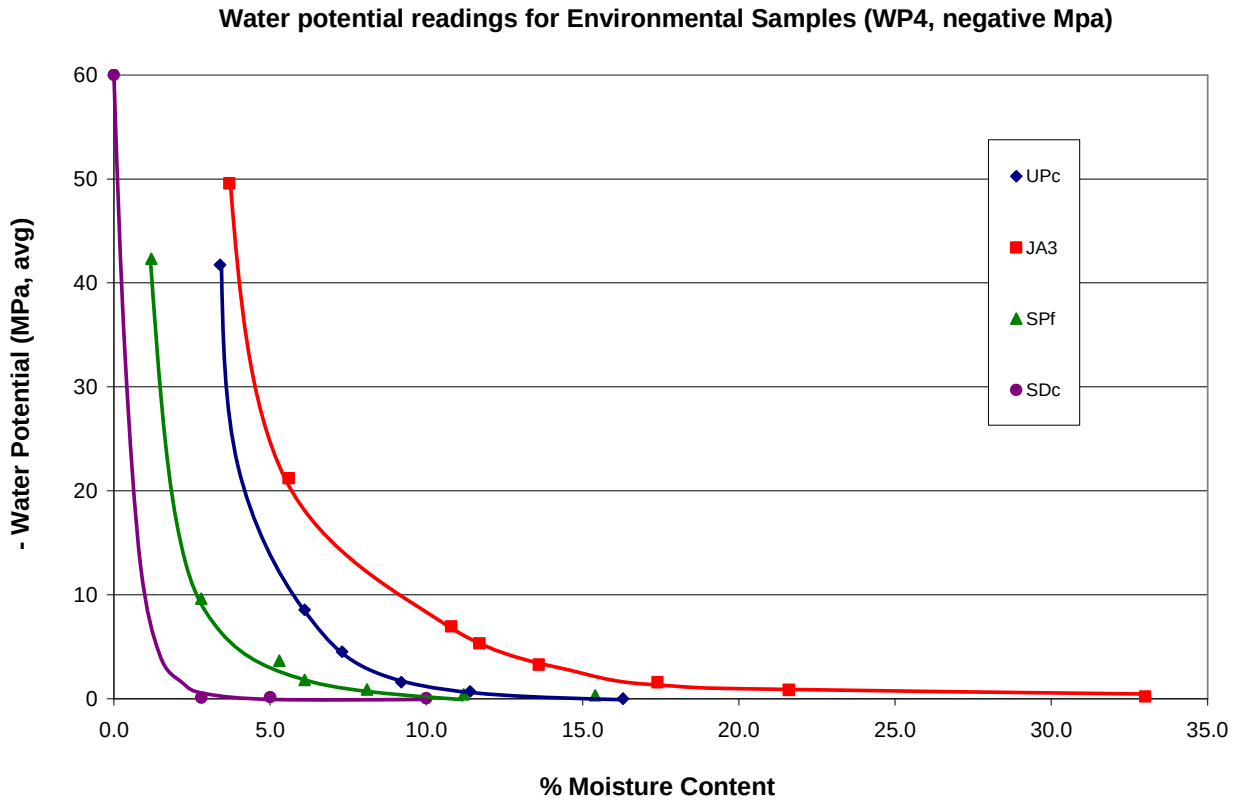

Figure 17. Water potential readings related to % MC for varying soil samples.

The sand standard yielded the expected steepest drop in water potential with increasing % MC (refer to Figure 8), displaying the greatest variation in the < 5% MC range as previously described. The environmental samples containing 20 – 30% clay (UPc and SPf) yielded distinct curves, however these curves essentially overlapped in the 10 – 15% MC range. Despite their clear differences in WP at 5% MC, no obvious differences were seen in the fluorescence data for these samples at 5% MC (refer to Figure 16). However, the JA3 sample (predominantly silt) yielded the broadest WP curve, displaying the greatest variation of all the samples in WP for the 5 – 15% MC range. This observation may, in part, be related to why this sample seems to be the

most challenging of the environmental samples examined. Also, the fact that these samples do not necessarily display the anticipated pattern relative to soil texture (see Figure 8) further indicates that more than soil texture is affecting the WP properties of these samples, such as the chemical properties of the soil particles.

While the detection challenges presented by the environmental samples are clearly related to the physical and chemical nature of the solid soil matrix, and reflective of specific U – soil particle interactions, the aqueous phase of the soil samples themselves alone can be highly influential. The aqueous phases of the environmental samples were collected as soil supernatants after centrifugation, followed by 0.22 μm filtration (samples were all clear), prior to the addition of U. Figure 18 demonstrates the variation in unenhanced uranyl detection in clear aqueous samples where only the chemical properties and dissolved constituents (originating from the initial soil conditions) play a role. For this experiment, nanopure water (NP, pH 6.9) was used as a control. The large variation in the uranyl fluorescence emission observed for these samples is believed to be due to the integrative effects of pH, OM, and iron content. Clearly, again, the JA3 sample stands out as being the most challenging. In this case, however, any effects due to pH are not reflective of U – soil particle interactions. Also notable is the approximate neutral pH of the control sample yielding the best results, as well as other previous studies that did not indicate that neutral conditions alone would cause a substantial decrease in aqueous uranyl fluorescence. However, the emission spectrum displayed by the JA3 sample is indicative to the strong presence of OM. That being said, the neutral pH of this sample may affect the amount and type of dissolved OM present. Recall while fulvic acids (Fas) are soluble under both acidic and alkaline conditions, humic acids (HAs) are insoluble under acidic conditions (refer to Figure 11). Therefore, any HAs potentially present in the more acidic environmental samples (UPc, CCdr,

CCms) were most likely insoluble and filtered out, whereas soluble HAs were most likely strongly abundant in the aqueous filtered JA3 sample. This observation is also supported by the general U(VI) speciation diagrams in the presence of HA as a function of pH (Sachs, Brendler et al. 2007), which indicated the predominant formation of ternary uranyl-hydroxo-humate complexes under near-neutral pH conditions, with $UO_2(OH)HA(I)$ as being highly abundant in the near-neutral pH range and a less abundant $UO_2HA(II)$ form existing in the pH 3 – 5 range (see previous section).

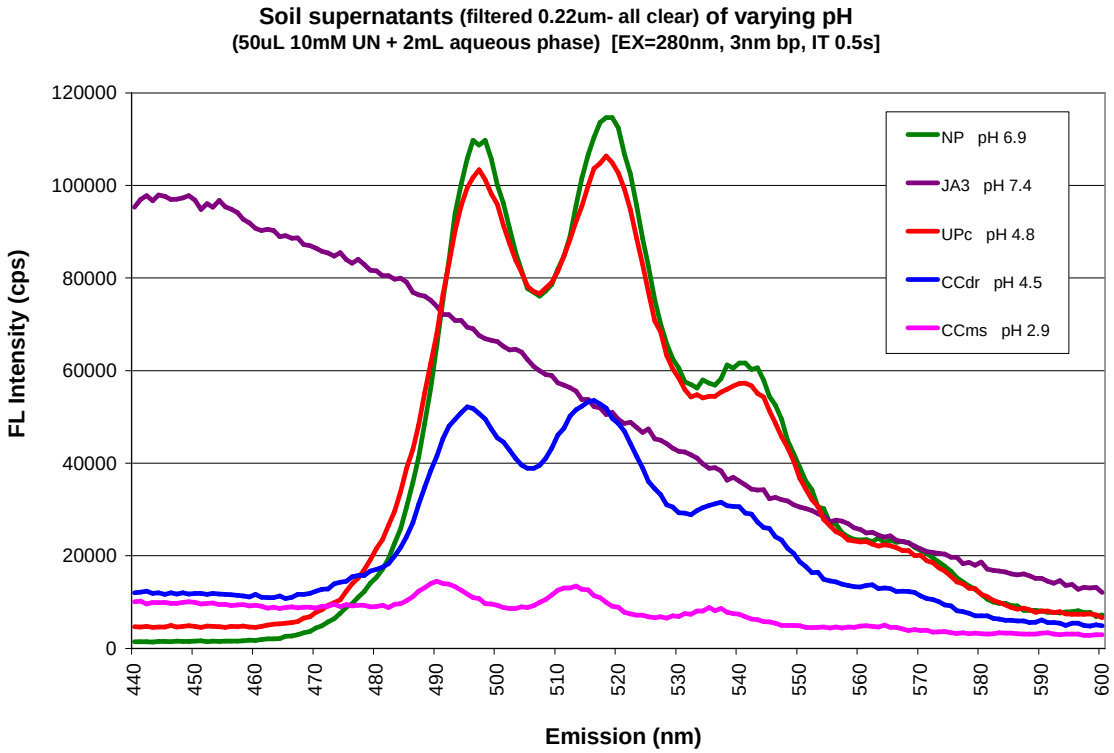

Figure 18. Steady-state fluorescence emission scans for filtered soil supernatants demonstrating the variation in uranyl detection in the aqueous phase, aside from U – soil particle interactions.

As described in a previous section, when organic substances are prevalent in environmental samples, their typically broad and unstructured overlapping fluorescence may swamp or mask the uranyl emission, making it difficult to detect. This is most notable when

longer excitation wavelengths are utilized (such as 420 nm, see Figure 19), however still applies when UV excitations are used (such as 280 nm), with the OM fluorescence strongest in the blue spectral region yet still stretching over through uranyl's green – yellow region (see Figure 18, JA3 sample). Figure 19 shows the typical HA fluorescence peak, and demonstrates not only the spectral overlap of the HA and uranyl emissions but also clearly depicts the static quenching of both the uranyl and HA fluorescence.

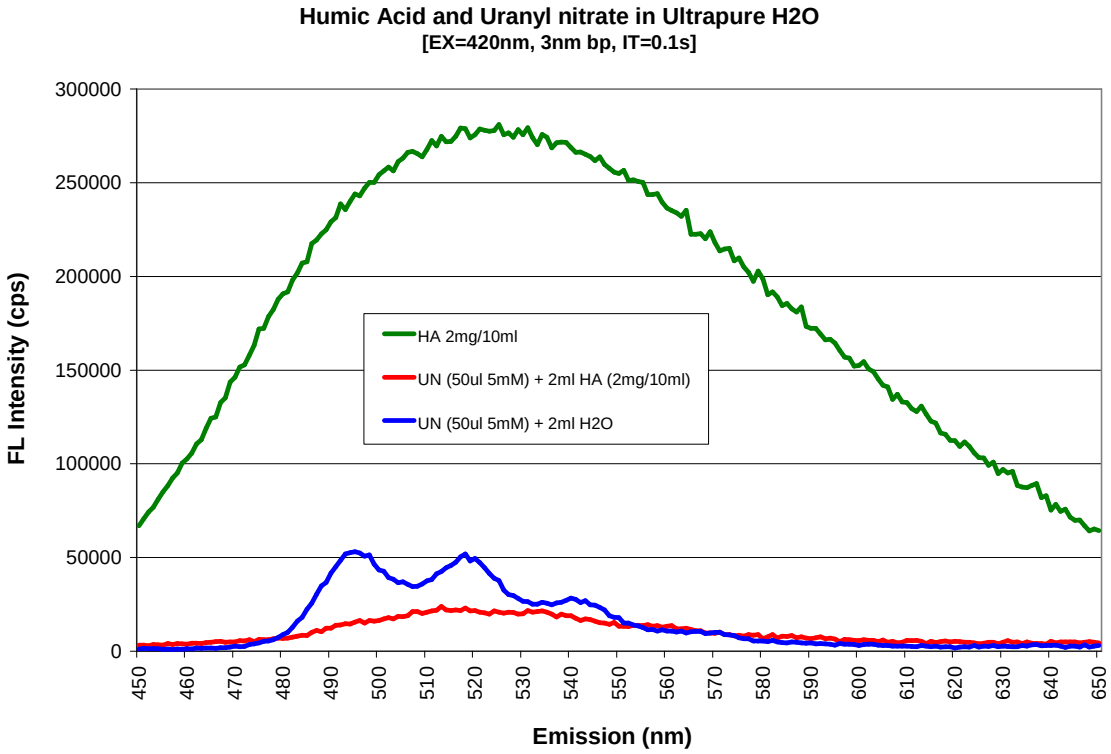

Figure 19. Steady-state fluorescence emission scans demonstrating both the spectral overlap and static quenching of humic acid and uranyl (λ_{Ex} = 420 nm).

In order to further investigate the feasibility of detecting uranyl in the challenging JA3 filtered sample (see Figure 18), this aqueous sample was acidified through the addition of sulfuric acid, thereby reducing the pH from 7.4 to 1 (see Figure 20). These results should not be surprising given the previous discussion of acid leaching and enhancement techniques. Figure

21 further demonstrates the acidification enhancement for a control nanopure water sample. Recall the acidification – enhancement effect on uranyl fluorescence is not specifically due to the low pH of the sample, but rather the shielding of the uranyl ion from nonradiative decays (Kaminski, Purcell et al. 1981). Also, the addition of sulfuric acid not only isolates the uranyl ion initially but subsequently forms uranyl sulfate species which exhibit enhanced spectral properties (Stork, Smartt et al. 2006).

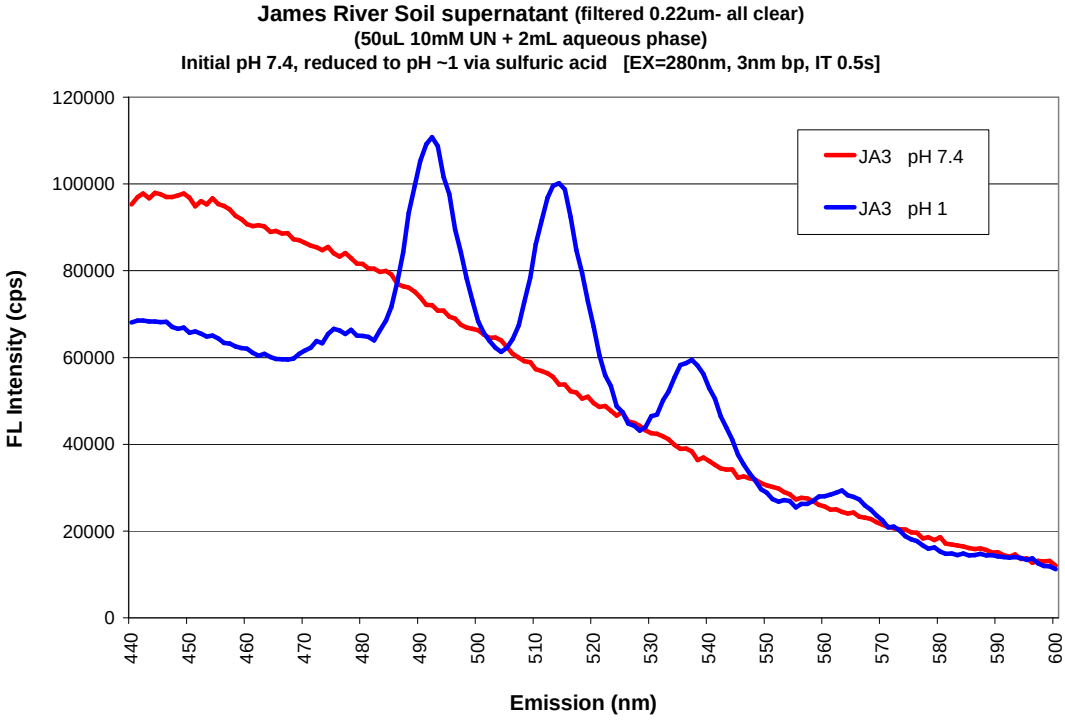

Figure 20. Steady-state fluorescence emission scans for a filtered James River soil supernatant demonstrating the effect of acidification on uranyl detection.

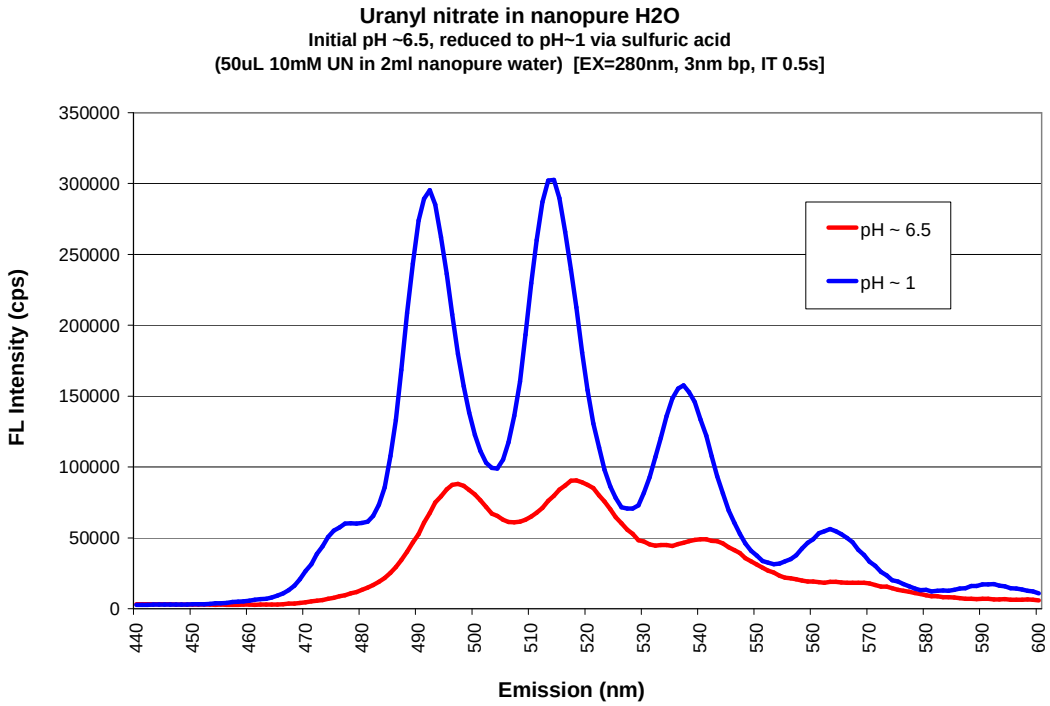

Figure 21. Steady-state fluorescence emission scans demonstrating the effect of acidification on uranyl detection in aqueous solution.

All the filtered soil supernatant samples displayed in Figure 18, as well as the acidified JA3 sample shown in Figure 20, were re-analyzed prior to and following the addition of U. Specifically, single peak intensity counts were recorded for the first uranyl peak (λ_{Ex} = 280 nm, λ_{Em} = 495 ± 5 nm) as well as the typical OM peak (λ_{Ex} = 350 nm, λ_{Em} = 440 nm), and are displayed in Table 17.

Several observations can be made from this table. First note the OM peak intensities for the various samples. The JA3 sample clearly is characterized by the greatest amount of OM, with the CCms and CCdr samples having intermediate concentrations, and the UPc sample having the lowest, with the nanopure control sample obviously having none. There is a general pattern indicating an inverse relationship between the intensities of the OM and U peaks (i.e.,

higher OM peaks tend to result in lower U peaks due to complex formation and quenching). For example, sample UPc had the lowest OM peak originally, and its U peak was only slightly lower than that of the nanopure control. In comparison, sample CCdr had a larger OM peak originally, and in turn its U peak was much lower. For sample JA3, a very large OM peak was still seen after the addition of U, and in turn no U peak was observed. It was only after this sample was acidified that the U peak could be detected. Note the reduction in the OM peak upon acidification, most like due to the insoluble nature of HAs under acidic conditions. Sample CCms did not follow the pattern described above. This sample's OM peak was between that of UPc and CCdr originally, however: 1) its OM peak was not reduced with the addition of U, and 2) its U peak was the smallest one observed (see also Figure 18). Both of these observations are believed to be tied to the fact that this sample was characterized by a very low pH of ~ 3. The first observation (no OM peak reduction) is probably explained by the facts that U tends to exist as the free uranyl ion under extremely acidic conditions and that U-HA complexes typically do not exist below pH 3. The second observation (lowest U peak) is most likely explained by the prevalence of Fe^{3+} and Fe^{2+} in this sample and their tendency to quench uranyl fluorescence.

Table 17. Approximate intensity counts for U or OM fluorescence peaks in filtered (0.22 μm) soil supernatants.

	Nanopure		UPc		CCms		CCdr		JA3	
	no U	*w/ U*	*no U*	*w/ U*	*no U*	*w/ U*	*no U*	*w/ U*	*w/ U*	*w/ U acidified*
U 1st Pk λ_{Ex} = 280 nm λ_{Em} = 495 ± 5 nm	no pk	103 x10^3	no pk	88 x10^3	no pk	14 x10^3	no pk	44 x10^3	no pk	111 x10^3
OM Pk λ_{Ex} = 350 nm λ_{Em} = 440 nm	no pk	no pk	20 x10^3	15 x10^3	46 x10^3	51 x10^3	65 x10^3	47 x10^3	624 x10^3	357 x10^3

Samples containing U: 50 uL of 10 mM uranyl nitrate solution added to 2 mL aqueous samples.

As previously stated, future studies should include the analysis of an additional sample type – one characterized by the prevalence of carbonate species and being more alkaline, as would be expected from the weathering of concrete materials. In summary, an abundance of carbonate species (typical under alkaline conditions) results in both decreased absorption of U to solid materials as well as decreased uranyl fluorescence. Also, several previously mentioned DOE studies described the occurrence of weak, broad and structureless emission spectra for certain uranyl-carbonate minerals as well as for contaminated soils near concrete structures. Preliminary studies (see below) have similarly shown a loss in the structure of the uranyl emission in the presence of concrete. Figure 22 shows the fluorescence emission spectra for solid concrete samples spiked with a high concentration of U, and a control (no U). While fluorescence from uranyl was detectable within the typical emission range, and similarly was enhanced in terms of its intensity in the presence of the Uraplex^{TM} phosphate-based complexant, the spectra lacked its typical vibronic band structure. To the best of our knowledge, this specific type of observation has not been explained. However, it is suspected that the loss of the vibronic structure in the emission would be related to the specific nature of the binding interactions in the uranyl's local coordination environment. For example, while U sorption on iron minerals was described as involving the formation of inner-sphere, mononuclear surface complexes (pH ~ 4 – 8), in the presence of carbonates, ternary surface complexation is bidentate (involving two binding sites) or binuclear involving binding with adjacent singly coordinated oxygen sites on the iron mineral surface (Waite, Davis et al. 1994; Catalano, Trainor et al. 2005).

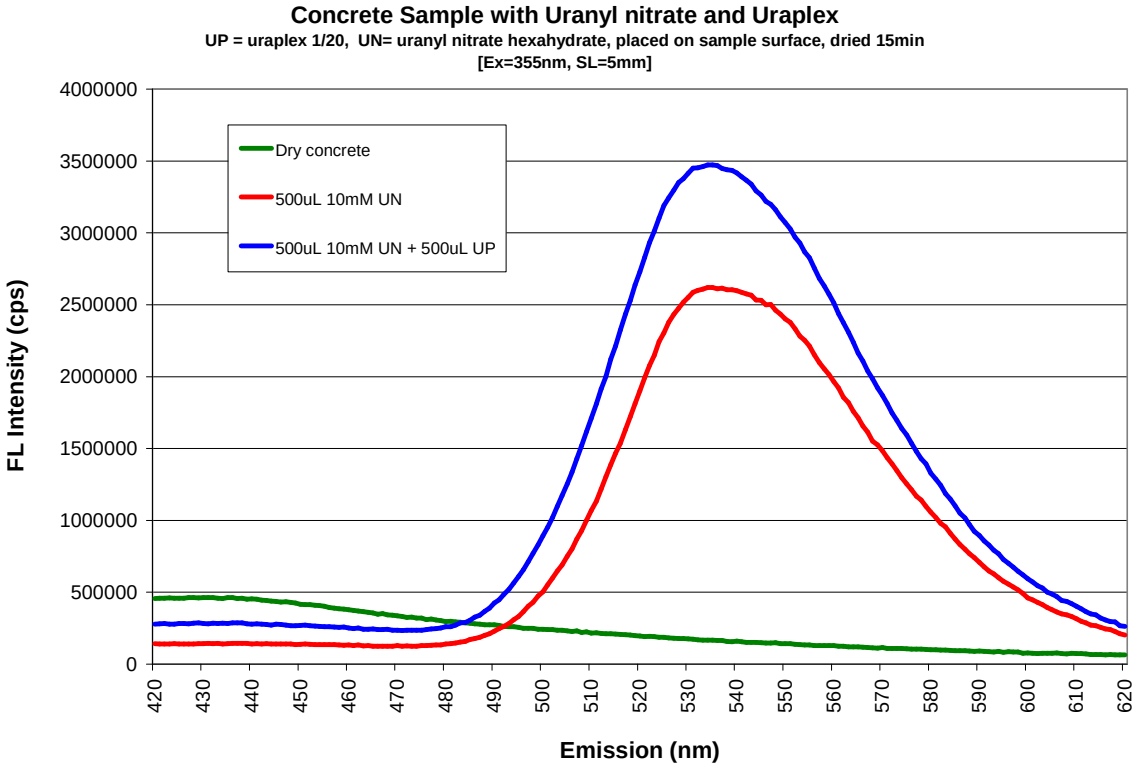

Figure 22. Steady-state fluorescence emission scans demonstrating the loss of band structure in the uranyl spectra in the presence of concrete.

2.2 Research Design

2.2.1 Introduction

The preliminary studies discussed above were very insightful with regards to key features of environmental samples and uranyl fluorescence detection. However, in order to confidently test the previously listed hypotheses simultaneously (1. key soil parameters, 2. U concentration and 3. time-dependence) a well-defined, tightly controlled and comprehensive experimental matrix was employed. This way, tests on different soil samples are directly comparable to each other, as well as the resulting steady-state fluorescence data.

2.2.2 Luminescence Detection and Spectral Scoring – Test Dataset

This section describes investigated techniques for analyzing the steady-state emission spectra collected on a variety of uranyl sample types. While numerous studies by others have focused on information that can be exploited from detailed analysis of U fluorescence emission spectra, including uranyl species identification, the purpose of this work is to improve the positive identification of the uranyl diagnostic fluorescence emission (in general) in environmental samples. There are two key features of the uranyl emission spectrum that are most important: 1) fluorescence intensity and 2) band structure. The generation of single numerical values representing the quality of the U spectral response is desired, essentially 'scoring' the uranyl emission spectra based on fluoresce intensity and band structure.

Previously, most of the uranyl fluorescence emission spectra were first visually screened regarding whether or not they displayed any detectable band structure typical of uranyl species. If the uranyl band structure was observable at all, the spectra were then compared based on their peak intensities. However, this approach was somewhat subjective, and did not result in single numerical values representing the quality of the U spectral responses. Subsequent experiments explore key environmental parameters influencing U spectral properties, either directly or indirectly, including: soil texture, pH, moisture content, water potential, iron content, organic content and cation exchange capacity (CEC). With these quasi-observational studies, these parameters vary naturally for collected environmental samples. A comprehensive data matrix was generated describing these parameters, and it was desired that single numerical response variables could be inserted into this data matrix in order to explore relationships between these environmental parameters, as well as their effects on the uranyl steady-state fluorescence emission.

The fluorescence intensity was typically presented as the intensity of the highest uranyl peak, which was usually either the first (~ 497 nm) or the second (~ 519 nm) observable uranyl band, depending on the sample. While from a remote sensing perspective the intensity of the uranyl emission is important, for analysis of spectral response, the band structure is also critical. For the purpose of this project, 'band structure' will essentially refer to how well defined are the diagnostic 'peaks and valleys' of the uranyl emission spectra, rather than details such as exact band locations and band widths that are more heavily influenced by specific uranyl speciation. It is not uncommon for uranyl emissions to be masked by other background emissions in environmental samples. Therefore, in some cases a low intensity yet well-defined uranyl spectrum is preferred to a strong emission in the 'green region' that lacks typical uranyl band structure for positive identification (see Figure 23 as an example).

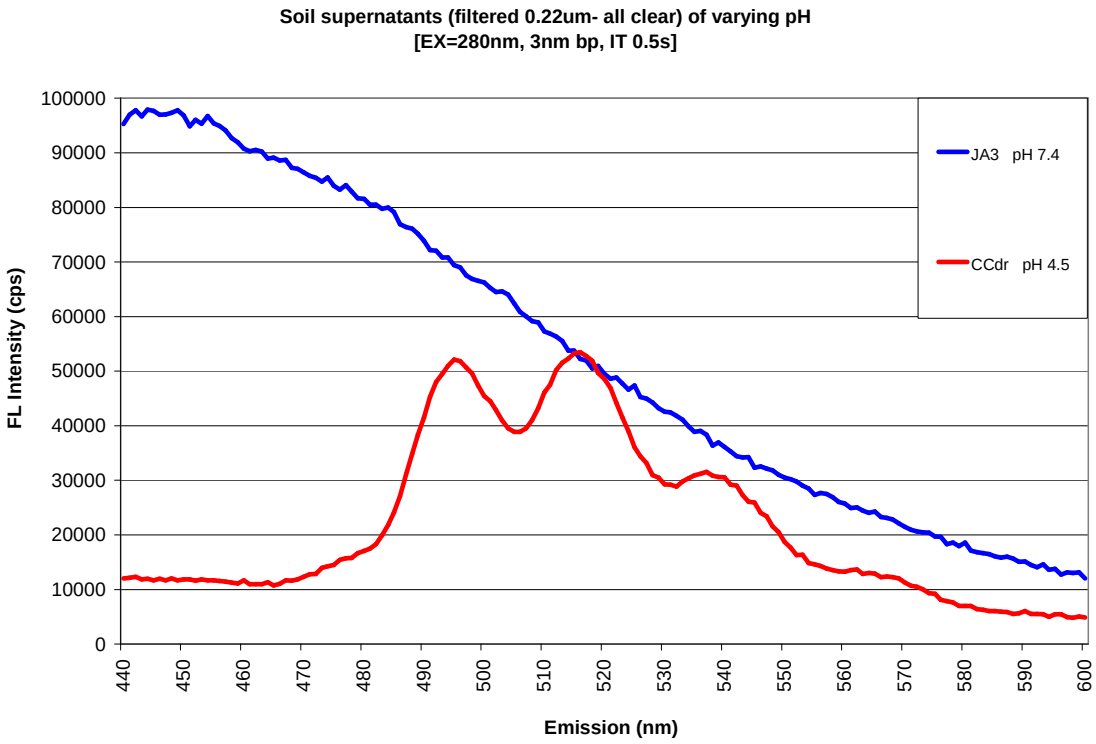

Figure 23. Emission spectra for aqueous environmental samples containing comparable levels of U, demonstrating the importance of uranyl detection based on band structure.

A sample set of uranyl emission spectra representing the diversity of possible and typically observed responses was gathered and used here as a dataset for testing (see Figure 24). It is important to note that the spectrum labeled 'Ref' was used here as a best case scenario, reference spectrum. This spectrum was generated from an aqueous sample where uranyl nitrate was enhanced by the phosphate-based complexant Uraplex^{TM}. Also notable is that two of the sample spectra completely lack U band structure: the sample labeled 'UP' and the sample labeled 'JA3' (not to be confused with 'JA3-pH1', the acidified-enhanced sample).

It was decided to use only the data present in the ~ 490 – 555 nm range, which was more specific to the key uranyl peaks typically observed from these types of samples. Data at wavelengths less than 480 nm were typically too heavily influenced by the background (such as organic matter) and were resulting in fluorescence intensity scores not truly representative of uranyl fluorescence. That being said, a scoring procedure was desired where the spectra did not need to go through an initial screening process to determine if the emission was due to uranyl or another source, and therefore each spectrum received an intensity score regardless. The intensity score was derived from the highest intensity reading within the 490 – 555 nm range, which *typically* corresponded to the intensity of either the first (~ 497 nm) or the second (~ 519 nm) uranyl band, depending on the sample. This approach is advantageous in that the intensity of the uranyl signal is not necessarily defined by a previously selected single wavelength position. However, if no uranyl peaks were present (e.g., JA3 or UP), simply the highest intensity count in that emission region was recorded. The recorded intensity values were in units of counts per second (cps), and typically ranged from approximately $1x10^4$ (background) to $2x10^6$. If you divide these intensity counts by 10^5, the resulting intensity scores range from 0.11 to 1.54 for this test dataset, with higher values indicating a better score.

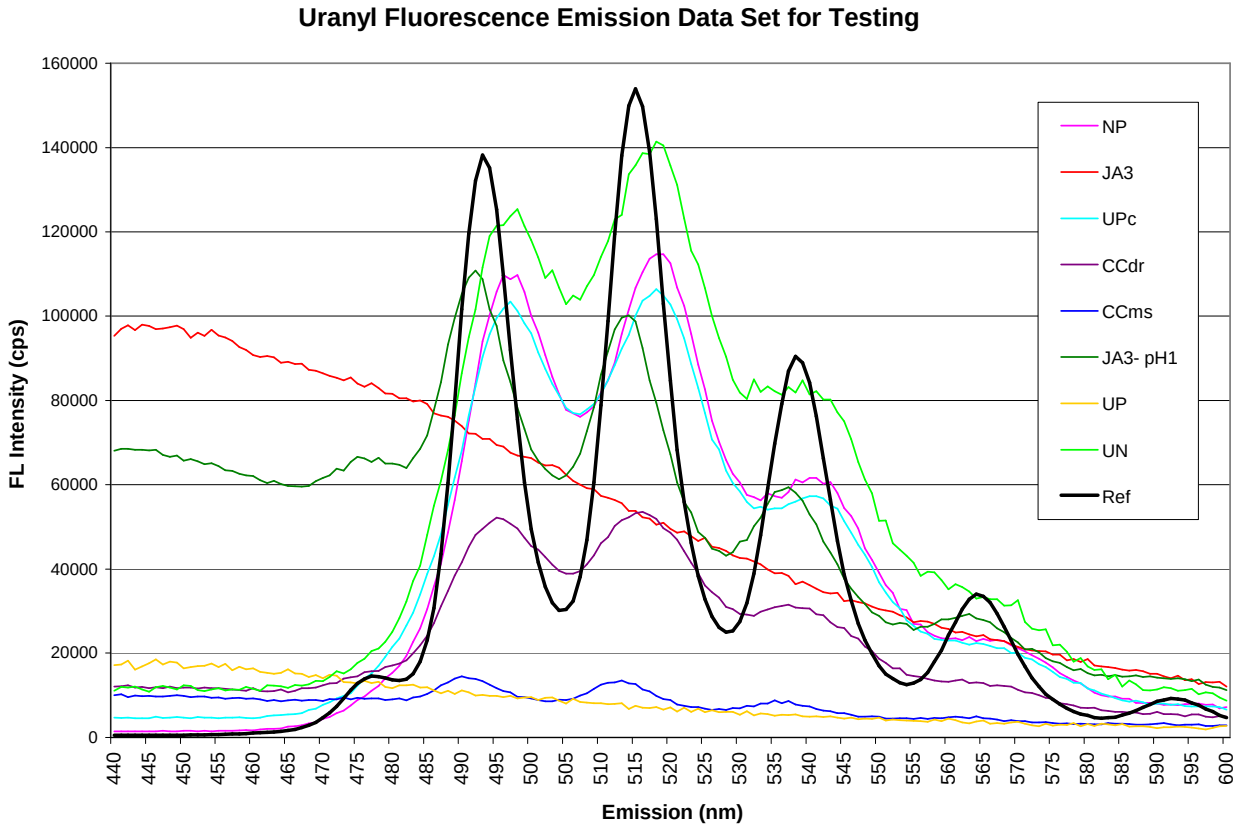

Figure 24. A sample set of uranyl emission spectra representing the diversity of possible and typically observed responses, used here as a dataset for testing a new scoring procedure.

While deriving a spectral score based solely on fluorescence intensity would be fairly simple, deriving a score representing band structure can be more challenging, especially if you are trying to avoid allowing features such as specific band location and band widths to heavily influence your score. The goal of this effort was to come up with a fairly simple strategy for scoring each spectrum such that the values generated represented how well defined the uranyl 'peaks and valleys' appeared when the spectra were normalized for intensity. More importantly, this technique would ideally result in scores for the 'structureless' samples (i.e., JA3 and UP) that are easily distinguishable (i.e., outliers) from scores for spectra visually displaying any degree of structure.

The three main uranyl peaks were identified as ~ 497 nm, ~ 519 nm and ~ 542 nm, while the two main uranyl valleys were identified as ~ 509 nm and ~ 533 nm. Note that other longer wavelength peaks as observed in the original reference spectrum are typically not well defined in these sample spectra. Also, it was determined that after reviewing the appearance of a large number of spectra collected over the life of this project, depending on the sample conditions, the first (~ 497 nm) and third (~ 542 nm) main peaks were on occasion not well defined, sometimes appearing as a 'shoulder'. However, for samples visually displaying any level of band structure, the center peak was always definable and varied within the 510 – 525 nm range. Therefore, all the spectra in this test dataset were normalized such that the center peak occurring in this narrow range was adjusted to the 519 nm position (average position), and relabeled as 'adjusted emission wavelength'. This allowed for the main uranyl peak locations to essentially line up, and minimize error due to variations in specific band locations. Figure 25 shows the steady-state fluorescence emission spectra for the uranyl samples (490 – 555 nm range, normalized for intensity and center peak position, smoothed using weighted averages – OriginPro v8), while Table 18 summarizes preliminary attempts at scoring these uranyl emission spectra for band structure.

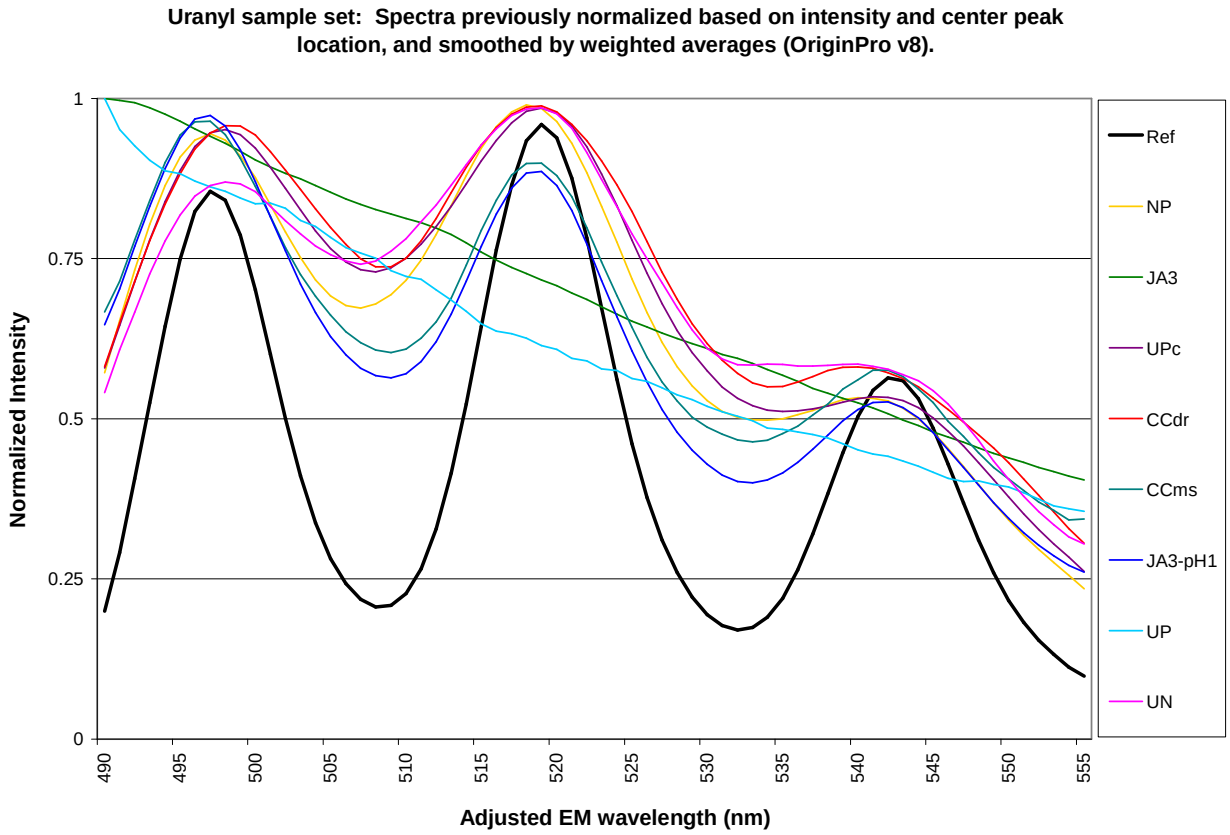

Figure 25. A sample set of steady-state fluorescence emission spectra for uranyl samples (490 – 555 nm range, normalized for intensity and center peak position, smoothed using weighted averages).

Table 18. Attempted procedures for scoring steady-state uranyl fluorescence band structure.

Procedure	Comments
Calculated the ratio of the average of the three main uranyl peak intensities to the average of the two main uranyl valley intensities.	Resulted in scores logically ordered, however this technique averages the intensities of peaks and valleys that can vary substantially.
Calculated the sum of the square of the differences between the reference spectrum and the sample spectra for the adjusted 490 – 555 nm emission range.	Resulted in the structureless UP sample having a score not distinguishable from other samples of poor structure (e.g., UN and CCdr). Technique was too heavily influenced by band widths, resulting in greater differences than desired between the reference spectrum and promising sample spectra.
Calculated the sum of the square of the differences between the reference spectrum and sample spectra for key peak and valley wavelengths (497, 509, 519, 533, and 542 nm).	Resulted in scores logically ordered, with the structureless UP and JA3 samples having the highest scores. However, these scores were very progressive with: 1) not as large a difference seen as would be expected between the best-case reference spectrum and sample spectra, and 2) the structureless sample scores still not clearly distinct from samples characterized by some level of structure.
Calculated the sum of the absolute values of the differences between the reference spectrum and sample spectra for key peak and valley wavelengths (497, 509, 519, 533, and 542 nm).	Resulted in more promising scores, with scores for the structureless samples (UP and JA3) being clearly distinct from scores of the other samples characterized by varying levels of structure, with the ideal reference sample also being clearly distinct.
Calculated the deconvolution values (FFT, OriginPro) using each sample spectrum as the convoluted 'signal' and the reference spectrum as the 'response'.	Resulted in improved scores, with: 1) scores for the structureless spectra (UP and JA3) being even more distinct from spectra characterized by some level of structure, and 2) not as drastic a difference between the best-case reference spectrum and promising sample spectra. However, involved questionable application of deconvolution calculations.
Calculated the sum of the square of the differences between the reference spectrum and the sample spectra for the adjusted 490 – 555 nm emission range, with the lowest normalized intensity values (555 nm) previously adjusted to zero.	Resulted in ideal scores, with scores for the structureless spectra (UP and JA3) being obvious outliers from spectra characterized by some level of structure; a difference greater that that seen between these promising sample spectra and the best-case reference spectrum.

As indicated in the bottom row of Table 18, the spectra displayed in Figure 25 were further modified such that the lowest normalized intensity value for each spectrum (at 555 nm) was adjusted to zero (see Figure 26).

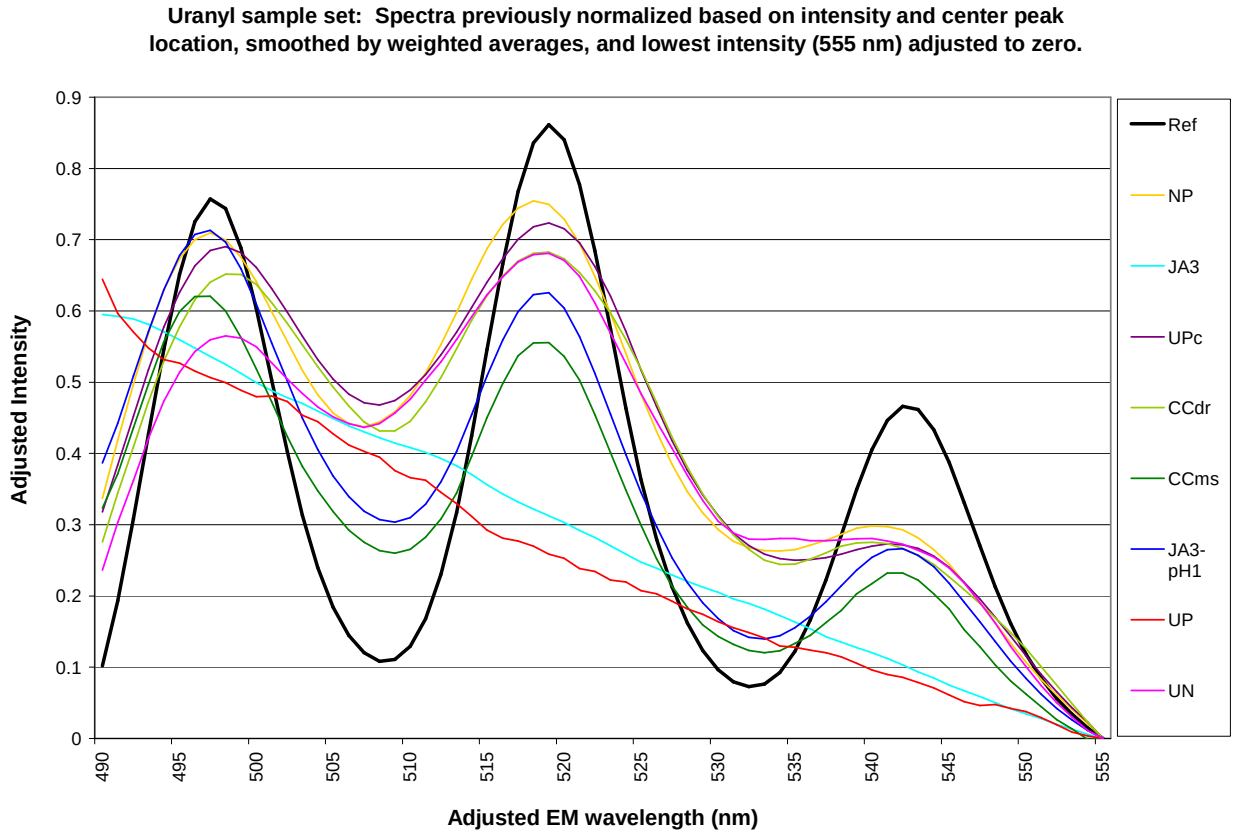

Figure 26. A sample set of steady-state fluorescence emission spectra for uranyl samples (490 – 555 nm range, normalized for intensity and center peak position, smoothed using weighted averages, with the lowest normalized intensity values at 555 nm adjusted to zero).

The spectra displayed in Figure 26 were then used to calculate the sum of the square of the differences between the reference spectrum and each sample spectrum. Using this approach with this modified dataset resulted in ideal scores for band structure. Figure 27 depicts the scores for the structureless spectra (UP and JA3) as obvious outliers from spectra characterized by some level of structure; a difference greater than that seen between these promising sample

spectra and the best-case reference spectrum. Obviously, the sum of the square of the differences between the adjusted reference spectrum and itself is zero (perfect match). The scores for sample spectra visually displaying some level of band structure ranged from approximately 1.1 to 2.1, while the scores for the structureless spectra were > 4.

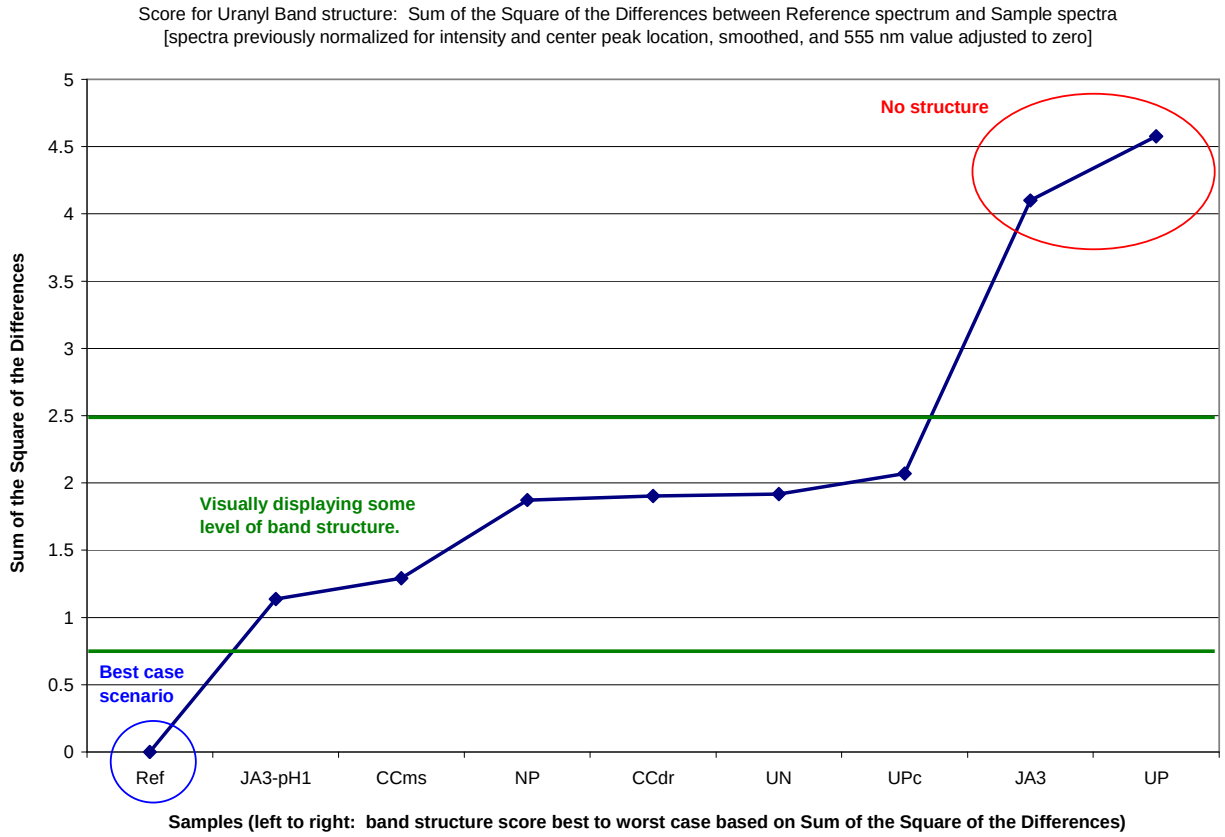

Figure 27. Scores for uranyl emission band structure based on the sum of the square of the differences between the reference spectrum and sample spectra, for the adjusted uranyl spectral test dataset.

As mentioned above, the overall quality of the uranyl spectral response is important, considering both fluorescence intensity and band structure. Figure 28 depicts both the band structure scores (x-axis) and the fluorescence intensity scores (y-axis) for the samples in this test

dataset. From this plot, it is easy to identify which samples result in the most promising spectra based on both of these critical features.

As a comparison to the above described band structure scoring procedure, the 'Peak Analyzer' function in OriginPro v8 (using the Guassian based calculations) was employed for the uranyl steady-state fluorescence emission spectra (490 – 555 nm range, normalized for intensity and center peak position, smoothed using weighted averages). Table 19 summarizes the results of this analysis. It is important to note that if the data were not smoothed prior to this procedure, the results depicted a large number of inaccurate peaks due to noise, inherent to low-intensity spectra.

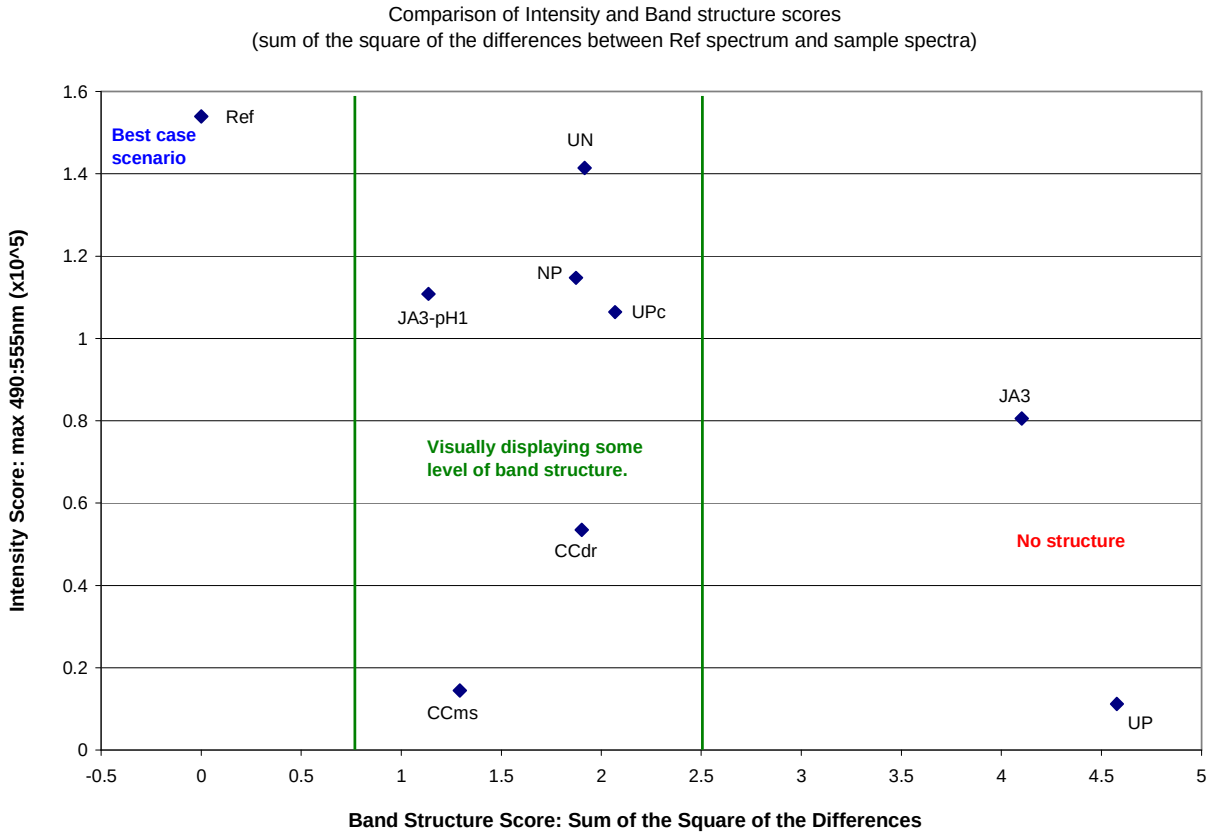

Figure 28. Comparison of fluorescence intensity and band structure scores for the adjusted uranyl spectral test dataset.

Table 19. Uranyl peaks successfully identified by the 'Peak Analyzer' function in OriginPro v8 (Guassian based calculations) for sample emission spectra (490 – 555 nm range, normalized for intensity and center peak position, smoothed using weighted averages).

Sample	Peaks Successfully Identified
Ref	[3] ~ 497 nm, ~ 519 nm, ~ 542 nm
JA3-pH1	[3] ~ 497 nm, ~ 519 nm, ~ 542 nm
CCms	[3] ~ 497 nm, ~ 519 nm, ~ 542 nm
NP	[3] ~ 497 nm, ~ 519 nm, ~ 542 nm
UPc	[3] ~ 497 nm, ~ 519 nm, ~ 542 nm
CCdr	[3] ~ 497 nm, ~ 519 nm, ~ 542 nm
UN [a]	[2] ~ 497 nm, ~ 519 nm
UP	[0]
JA3	[0]

[a] Sample UN: 3rd uranyl peak was not discernable by this method, yet this sample was given the best score for intensity and a comparable score for band structure.

While the above described methods for generating scores, reflective of: 1) fluorescence intensity, or 2) band structure for uranyl steady-state emission spectra were very promising, additional methods were subsequently investigated. These spectral scores were then used as response variables in a comprehensive data matrix containing information related to environmental sample parameters that can influence the luminescence detection of U.

2.2.3 Experiments for Testing Hypotheses

Subsequent experiments utilized all fifteen different soil samples previously described in Table 16, and shown below in Figure 29. Commonly practiced soil preparation procedures were utilized for drying (overnight at ~ 40°C), mixing, and sieving (2 mm) soil samples prior to submitting for further analyses.

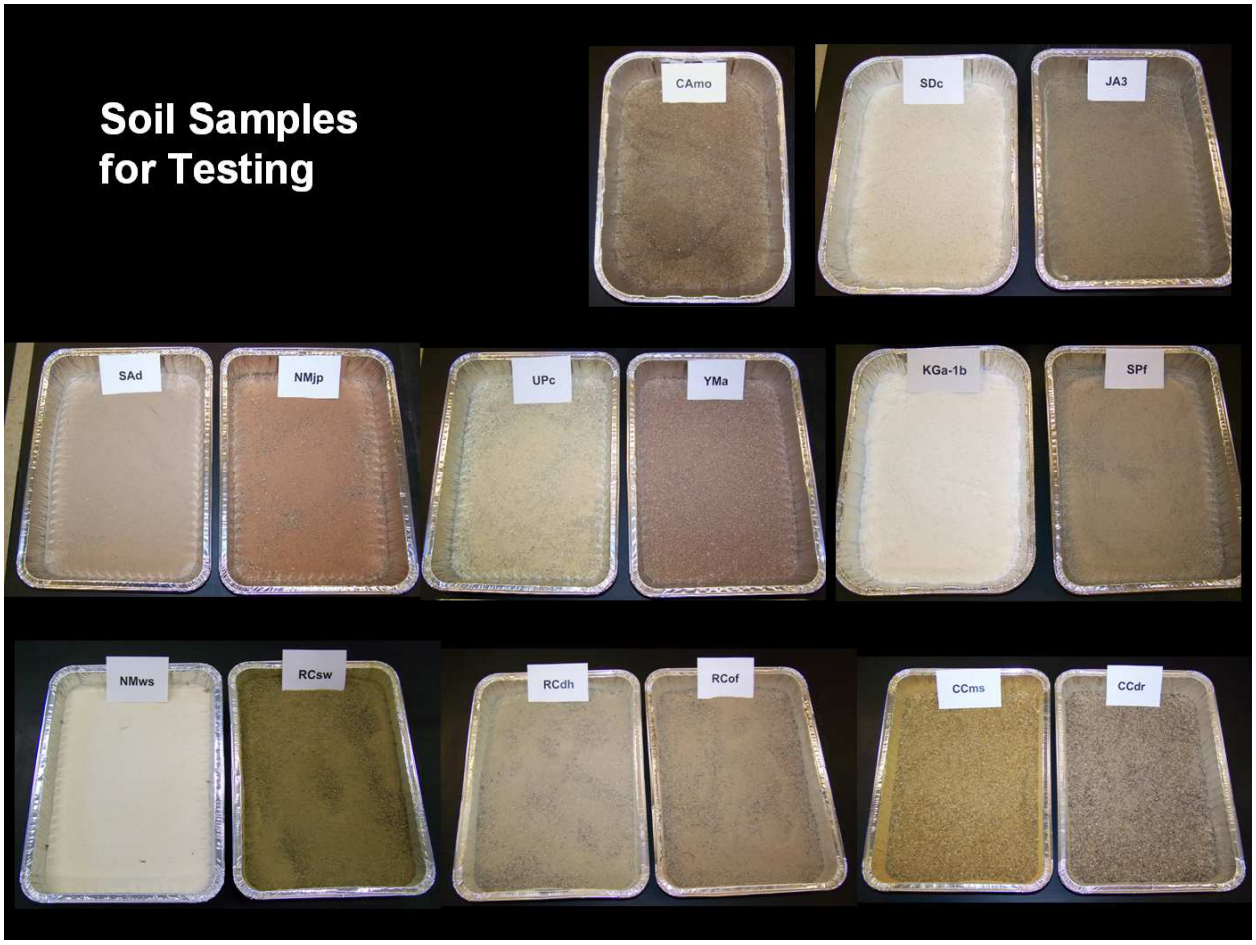

Figure 29. Digital photograph of soil samples utilized for discussed studies, previously air-dried, mixed, and sieved (2 mm).

A subsample of each soil sample was submitted to A&L Eastern Laboratories, Inc. (Richmond, VA) for chemical and physical analyses (see Table 20). The commonly used Mehlich III procedure listed in Table 20 uses an extraction solution which is a combination of acids (acetic and nitric), salts (ammonium fluoride and ammonium nitrate), and EDTA chelating agent (Mehlich 1984). The cation exchange capacity (CEC), which essentially refers to the amount of cations a soil can hold (such as UO_2^{2+}), was also investigated as key soil parameter. The CEC is expressed in milliequivalents per 100 grams of soil (meq/100g), and can vary based

on the other previously defined key parameters, including organic matter (increasing OM content typically increases the CEC).

Table 20. Soil sample analyses performed by A&L Eastern Laboratories Inc., Richmond, VA.

Soil Analysis	**Comments**
Soil pH	Standard 1:1 potentiometric soil-slurry procedure. Refer to Chapter 3, http://ag.udel.edu/extension/agnr/soiltesting.htm (Eckert and Sims 1995).
Soil texture	Particle-size analysis by hydrometer. Reported as: % sand, % silt, % clay, and resulting classification.
Organic matter (%)	Routine colorimetric determination of soil organic matter. Refer to Chapter 8, http://ag.udel.edu/extension/agnr/soiltesting.htm (Schulte 1995).
CEC, total (meq/100g)	Method: SW-846-9081[a], based on sodium saturation at pH 7.
Iron (ppm)	Mehlich III: multi element soil extraction procedure.
Iron, total (mg/kg, ppm)	Method: SW-846-3051/6010C [a].

[a] Test Methods for Evaluating Solid Wastes, Physical / Chemical Methods (SW-846 4th Edition), US EPA.

The majority of the previously defined key parameters varied naturally for these soil samples, including soil texture, pH, organic matter, iron content and CEC, while initial moisture contents were controlled. Water potential curves (relating WP4 readings to % MC) were generated for the remaining soil samples, similar to those previously shown in Figure 17 (data not shown). Based on these individual WP curves, two initial moisture content percentages were selected for U detection experiments (low and high). The % MC was initially controlled (Initial % MC) and then tracked gravimetrically (Estimated % MC), where the soil water content is defined as: $\theta_m = M_w / M_s$ where θ_m is the mass of the water content, M_w is the mass of the water evaporated ($\geq$ 24 hours at 105 °C), and M_s is the mass of the dry soil. Subsets of samples previously dried at ~ 40 °C were further dried at 105 °C for $\geq$ 24 hours to determine what small amounts of moisture were still present and needed to be accounted for in the % MC estimations.

For all these studies, the source of U for sample spiking was uranyl nitrate hexahydrate [$UO_2(NO_3)_2$ x $6H_2O$], which was dissolved in nanopure water to make a 100 mM stock solution. Very small amounts of this U stock solution were mixed with larger volumes of water, and then added and thoroughly mixed into the individual soil sample preps when introducing the initial desired moisture content. The amounts of U stock solution added to small 5 g soil preps were varied such that the resulting U concentrations were: 10 ppm, 100 ppm and 500 ppm, in addition to control samples where no U had been added. Once the water – uranyl solutions had been mixed into the soil sample preps, they were sealed in zip-lock baggies (excess air removed), and stored in the refrigerator for 48 hours to ensure adequate contact time for the moisture and U to interact with the soil matrix.

Silica gel powder (Fisher AC36003, ultra-pure, 40 – 60 μm diameter, 40 angstrom pore size) was added in small amounts (~ 70 mg) to the surface of each soil sample, in a single spot location, immediately prior to initial spectral analysis. The silica gel was added to the samples in a controlled and timely manner, such that the application and amount was consistent, using a commercially available ammunition powder measuring – dispensing device (Lee Perfect Powder Measure, Cabela's Item No. 9IS-214003). Weight measurements (for estimating % MC) were quickly obtained for each sample just prior to any spectral reading.

The interactions between the uranyl and silica gel enhancer are believed to be time dependent, in addition to moisture changes. Therefore, a series of time-point spectral measurements were collected for each prepared soil sample: t = 1 min, 15 min, 30 min, 1 hr, 2 hr, 3 hr and 24 hr. Throughout these time points, the sample dishes were left open enabling them to air dry. A previously designed steady-state fluorescence emission scan was used for all spectral readings, keeping all parameters consistent (see previous section). The bifurcated fiber

optics was positioned at nadir and consistently maintained at given distance above the surface of the samples (~ 2 cm). However, two measurements were collected from each soil dish; one directly above the silica gel spot, and one above an area where no enhancer was present on the surface (bare soil). Two replicates of each unique sample condition were prepared and analyzed.

2.3 Comprehensive Experimental Matrix and Data Analysis

2.3.1 Introduction

The integrative experimental matrix was employed, testing different soil samples, generating steady-state fluorescence spectra, and building a comprehensive dataset which was then utilized to simultaneously test the previously listed hypotheses. The three hypotheses state that the fluorescence detection of uranyl compounds is *dependent* upon: 1) key soil parameters (soil texture, moisture content, soil pH, organic matter content, iron content and CEC), 2) the concentration of U contamination, and 3) time of analysis, specifically following the application of silica gel enhancing material.

The total number of collected sample spectra, or sample size (*n*), was 3360 (15 soil samples, 4 concentrations of U, 7 time points, 2 initial moisture content levels – low or high, 2 readings per dish – over silica gel or bare soil, and 2 replicate samples). Figures 30 and 31 show examples of sample spectra in their original form. More specifically, Figure 30 displays the relationship between U soil concentration and positive detection for soil KGa-1b, at the 24 hr time point, over bare soil, with high initial % moisture content. Figure 31 demonstrates the importance of adequate initial moisture content levels necessary for silica gel – based enhancement for soil SDc, at the 24 hr time point, with [U] = 500 ppm.

Data analysis was performed for the comprehensive dataset using the JMP statistical software (version 8, by SAS). A variety of different statistical approaches were employed to examine in detail: response (Y) variables, predictor (X) variables, and relationships between predictor and response variables, progressively working towards developing optimized regression-based predictive models for this dataset. Data analysis results include: bivariate plots, correlation tables, principal components analysis (PCA), comparison of means, simple linear regression (dependency, single X, single Y), multiple linear regression (dependency, multiple X's, single Y), multivariate regression (dependency, multiple X's, multiple Y's), as well as investigation of predictor variable interaction terms and multicollinearity issues through examination of variance inflation factors (VIF).

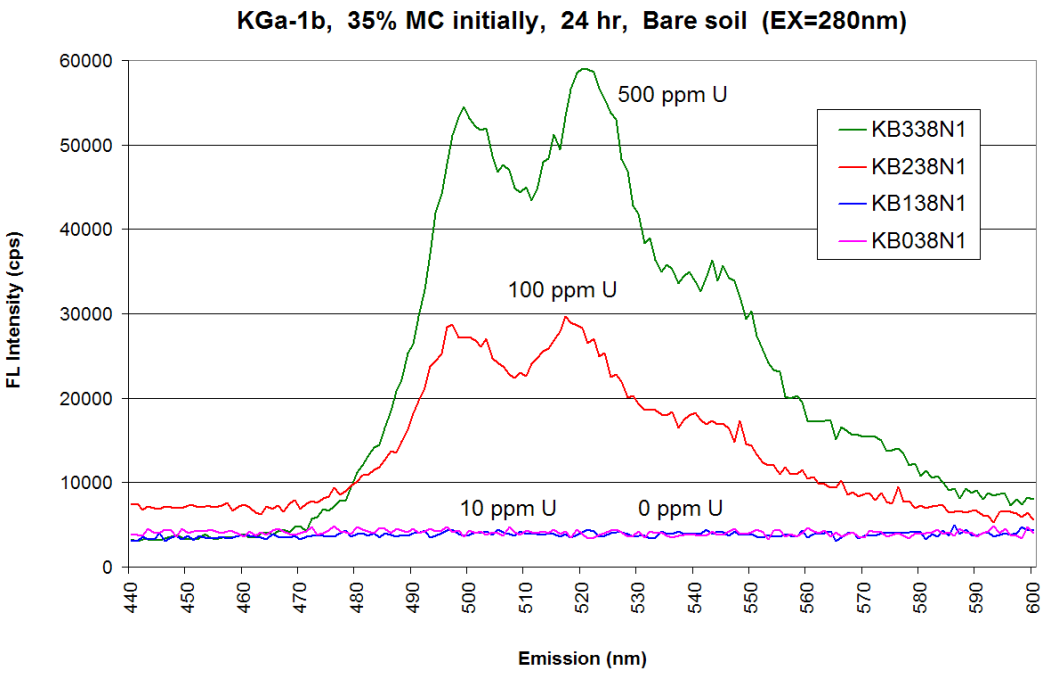

Figure 30. Steady-state fluorescence emission scans for soil sample KGa-1b, displaying the relationship between U soil concentrations and detection.

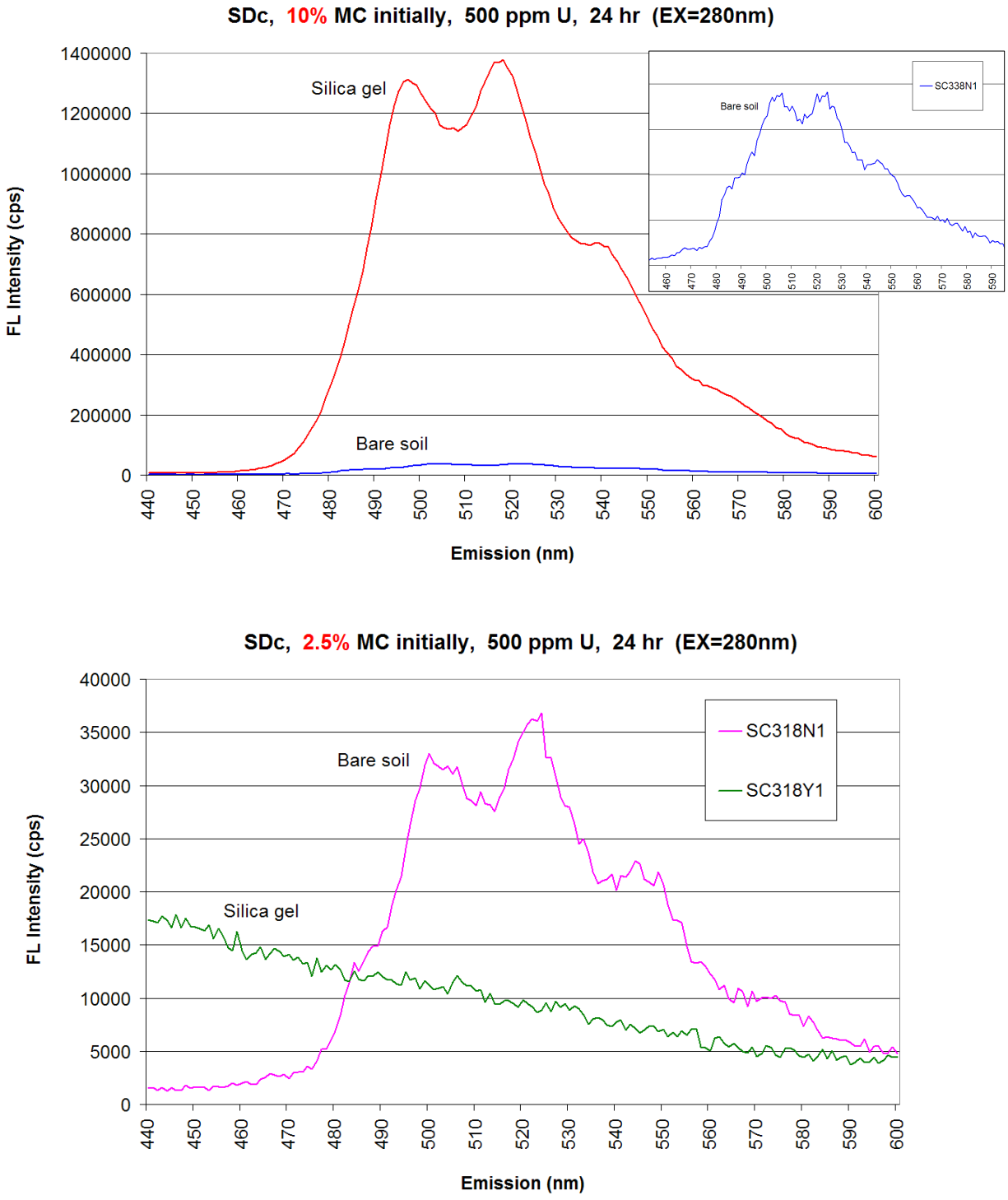

Figure 31. Steady-state fluorescence emission scans for soil sample SDc, demonstrating the importance of adequate initial moisture content levels, necessary for silica gel – based enhancement (top: 10% initial MC, bottom: 2.5% initial MC).

2.3.2 Statistical Variables

The tables in this section present highly-relevant information pertinent to the experimental variables contained within the comprehensive data matrix. Table 21 describes each variable explored through subsequent statistical analyses, and defines their role. More in-depth details regarding specific variables are provided in subsequent tables. Table 22 lists the 'low' and 'high' initial percent moisture contents selected for the various soil samples, based on each soil's individual water potential curve (data not shown). Table 23 displays the results of soil sample analyses, relevant to key soil parameters.

Table 21. Variables utilized for statistical analyses.

Variable Role	**Variable Description**
Predictor (X) Factor (controlled) Continuous	[U] (ppm) Uranium concentration introduced to soil samples. 0 ppm (controls), 10 ppm, 100 ppm, 500 ppm.
Predictor (X) Factor (controlled) Categorical	Over SG Spectral reading taken over silica gel vs. bare soil. Yes (Y), No (N)
Predictor (X) Factor (controlled) Categorical	Read Time Time of analysis following application of silica gel. 1 min, 15 min, 30 min, 1 hr, 2 hr, 3 hr, 24 hr
Predictor (X) Factor (controlled) Continuous	Initial % MC Initial percent moisture content introduced to soil samples. Selected a low and high % depending on the soil. See Table 22.
Predictor (X) Covariate (observed) Continuous	Est. % MC Estimated percent moisture content (tracked gravimetrically) for each sample, at each time point. Values steadily dropped with time as samples continued to air dry.
Predictor (X) Covariate (observed) Categorical	Soil text. class. Soil texture classification, based on % Sand, Clay and Silt. Same for a given soil sample. See Table 23.

Table 21. (Continued).

Variable Role	Variable Description
Predictor (X) Covariate (observed) Continuous	% Sand Percentage of Sand, based on particle size distribution. Same for a given soil sample. See Table 23.
Predictor (X) Covariate (observed) Continuous	% Silt Percentage of Silt, based on particle size distribution. Same for a given soil sample. See Table 23.
Predictor (X) Covariate (observed) Continuous	% Clay Percentage of Clay, based on particle size distribution. Same for a given soil sample. See Table 23.
Predictor (X) Covariate (observed) Continuous	Soil pH Dry soil pH estimation by 1:1 potentiometric procedure. Same for a given soil sample. See Table 23.
Predictor (X) Covariate (observed) Continuous	Total CEC Total cation exchange capacity, by standard EPA methods. Same for a given soil sample. See Table 23.
Predictor (X) Covariate (observed) Continuous	% OM Percentage of organic matter, by routine colorimetric determination. Same for a given soil sample. See Table 23.
Predictor (X) Covariate (observed) Continuous	Iron (ppm), Mehlich III Iron content estimation by Mehlich III soil extraction procedure. Same for a given soil sample. See Table 23.
Predictor (X) Covariate (observed) Continuous	Total Iron (ppm) Total iron content, by standard EPA methods. Same for a given soil sample. See Table 23.
Response (Y) (observed) Continuous	Intensity score (LN, cps) Fluorescence intensity score, generated from each individual sample emission spectrum. See Table 24.
Response (Y) (observed) Continuous	Structure score Emission band structure score, generated from each individual sample emission spectrum. See Table 24.

Table 22. Low and high initial percent moisture contents (% MC) selected for soil samples.

Soil	SC	CO	CR	CS	NS	NP	YA	SF	UC	JA	RW	SD	RF	RH	KB
Low	2.5	2.5	2.5	2.5	2.5	2.5	2.5	5	5	5	5	5	5	5	2.5
High	10	10	10	10	10	10	10	25	25	25	25	25	35	35	35

Table 23. Results of soil sample analyses, relevant to key soil parameters.

Soil code	**Soil texture** [a]	**% Sand** [a]	**% Silt** [a]	**% Clay** [a]	**Soil pH** [b]	**Total CEC** [c] **(meq/100g)**	**% OM** [d]	**Iron** [e] **(ppm)**	**Total Iron** [f] **(ppm)**	**Initial U levels** [g] **(ppm)**
CO	Sand	93	3	4	5.5	3.1	2.4	19	8940	0.99
CR	Sand	92	2	6	4.9	1.1	0.8	374	4300	0.29
CS	Sand	94	2	4	3.3	1.1	1.9	448	53000	0.38
JA	Loam	44	45	11	6.1	7.2	4.1	603	26500	1.2
KB	Clay	0	0	100	4.5	1.1	0.1	16	97	0.45
NP	Loamy Sand	78	15	7	7.8	5.6	0.1	36	6420	0.5
NS	Sand	96	0	9	7.3	0.2	0.1	56	447	<0.08
RF	Loam	38	40	22	4.5	3.5	5.9	125	12100	0.12
RH	Loam	34	44	22	4.7	3.1	4.8	118	5160	1.23
RW	Sandy Clay Loam	49	26	25	5.2	4.2	2.4	564	18400	1.05
SC	Sand	100	0	0	5.5	0.4	0.1	27	839	0.12
SD	Sandy Loam	54	31	15	7.9	9.1	1.3	46	10700	0.49
SF	Loam	48	31	21	4.6	2.4	2.4	404	2510	0.74
UC	Sandy Clay Loam	54	17	29	4.2	6.5	0.7	127	5320	0.12
YA	Loamy Sand	87	7	6	8.3	6.9	0.3	224	18000	0.21

[a] Soil textures verified through standard particle-size analysis by hydrometer (A&L Eastern Laboratories, Inc.).
[b] Soil pH verified through standard 1:1 potentiometric soil-slurry procedure (A&L Eastern Laboratories, Inc.).
[c] Total CEC verified through method SW-846-9081, US EPA (A&L Eastern Laboratories, Inc.).
[d] Organic matter (% OM) verified through routine colorimetric determination (A&L Eastern Laboratories, Inc.).
[e] Iron content verified through Mehlich III multi element soil extraction procedure (A&L Eastern Laboratories, Inc.).
[f] Total iron verified through method SW-846-3051/6010C, US EPA (A&L Eastern Laboratories, Inc.).
[g] Background U levels verified by EPA 6000/7000 series methods (ERDC Environmental Chemistry Branch).

Table 24 summarizes the steps taken in generating the response variables (fluorescence intensity scores and emission band structure scores) from the samples' steady-state emission spectra, using MATLAB data processing software. Referring back to the preceding 'Luminescence Detection and Spectral Scoring' section, minor revisions were made to the previously described scoring procedures based on what proved most promising for this large dataset (see step 6, followed by Figure 32).

Table 24. Summary of procedure for generating response variables from collected sample fluorescence emission spectra.

Step	Description
1	Generate emission spectra (λ_{Ex} = 280 nm, λ_{Em} = 440 – 600 nm, 1 nm increments, 320 nm long-pass filter, consistent slit widths, bifurcated fiber optics – nadir to sample surface at consistent distance of ~ 2 cm, solid-standard for daily calibration). {x-axis = EM wavelength, y-axis = FL Intensity (cps)}
2	Smooth emission spectra using weighted averages (evenly weighted across 5 nm windows). Minimizes high degree of noise inherent in low intensity spectra.
3	**Record Intensity Score:** Highest intensity value (cps) within the 490 – 555 nm range (focusing on the three predominant uranyl peaks). The corresponding natural log (ln) values were utilized for this dataset, and ranged from 7.32 to 15.51 (equivalent to $1.5x10^3$ to $5.5x10^6$ cps).
4	Normalize for center peak position: Center peak occurring within 510 – 525 nm range adjusted to the 519 nm position. Allows for the main uranyl peaks to align, minimizing error due to variations in specific band locations. {x-axis = Adjusted EM wavelength, y-axis = FL Intensity (cps)}
5	Normalize intensity scale. Allows for spectra to fall on the same general scale. {x-axis = Adjusted EM wavelength, y-axis = Normalized Intensity}
6	Centralize band structure variation within the reference spectrum: For each sample spectrum, identify the y-axis midpoint between the 519 nm peak and the 505:513 nm valley, and align this mid-point value with the mid-point value of the reference spectrum (0.61). See Figure 32. {x-axis = Adjusted EM wavelength, y-axis = Adjusted Intensity}
7	**Record Structure Score:** Calculate the sum of the square of the differences between the reference spectrum and each new sample spectrum for the adjusted 490 – 555 nm emission range. The resulting structure scores ranged from 1.46 to 9.54 for this dataset, with the reference spectrum score equal to zero, a perfect match.

Figure 32. A promising sample spectrum (green) centralized for band structure variation within the reference spectrum (blue). See Table 24, step 6.

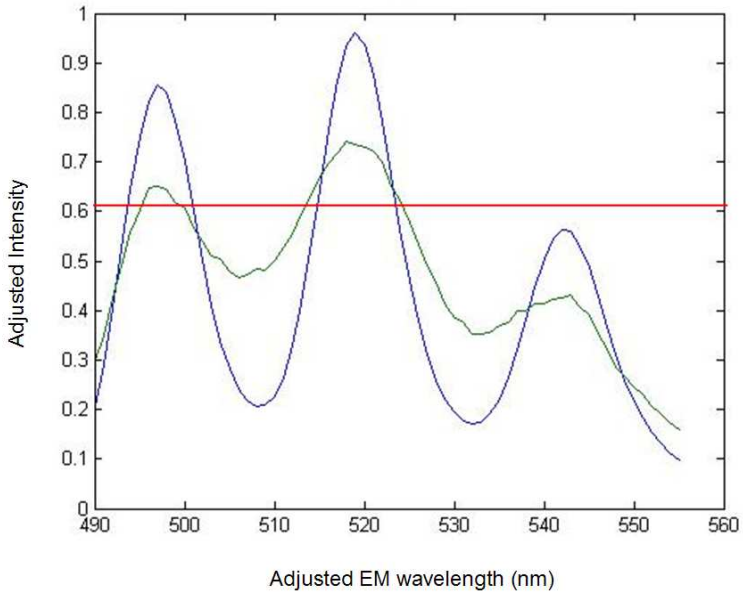

2.3.3 Response (Y) Variables

The generated response variables (intensity scores and structure scores) were examined and compared. Figures 33 and 34 are bivariate plots showing the relationship between the different score types, while Figure 35 and Table 25 display distribution details for these response variables individually. More specifically, Figure 33 focuses on the control samples ([U] = 0 ppm, n = 840), while Figure 34 displays scores for the entire dataset (n = 3360). Recall that the original intensity counts (cps) were converted to natural log (ln) values, resulting in intensity scores ranging from 7.32 to 15.51 (see Table 25). The calculated structure scores ranged from 1.46 to 9.54, with the reference spectrum score equal to zero (a perfect match). The multivariate routine (JMP v8) indicated the generated response variables, intensity score and structure score, are negatively correlated (– 0.68). The negative correlation value simply indicates there is a tendency for structure score to decrease (closer to the reference) as intensity score increases.

The pattern displayed in Figure 33 by the control (0 ppm) samples can be explained in part by whether the reading was collected over silica gel or bare soil. Structure scores for control

samples ranged from 3.94 to 5.88 for silica gel, and from 4.22 to 9.54 for bare soil. This indicates that using silica gel helps control the variation in structure score. This also indicates, however, that for structure scores of ~ 4 and above, that progressively higher scores do not indicate diminishing structure. Intensity scores for control samples ranged from 7.97 to 11.85 for silica gel, and from 7.32 to 10.31 for bare soil. These intensity scores for control samples, however, were influenced by moisture levels and soil sample identity (color for example).

In comparing Figure 34 to Figure 33, it is clear that the introduction of U contaminated samples results in structure scores extending into the ~ 1.5 to 4 range, and intensity scores into the ~ 11.9 to 15.5 range for this dataset. Close examination of individual sample spectra confirmed that a structure score of 3.2 or less displays some level of visible band structure, while structure scores in the range of 3.2 – 4 are questionable. Given this observation and that 3.23 is two standard deviations below the mean for control samples, this structure value was selected as a confident detection threshold for structure. Contrary to structure scores, a confident detection threshold for intensity scores was harder to define, due to the relatively high intensities that could be displayed by control samples. That being said, an intensity score of 10.43 represents the upper 97^{th} percentile of control samples, and this value was selected as a detection threshold for the following section examining populations of spectra achieving desired detection.

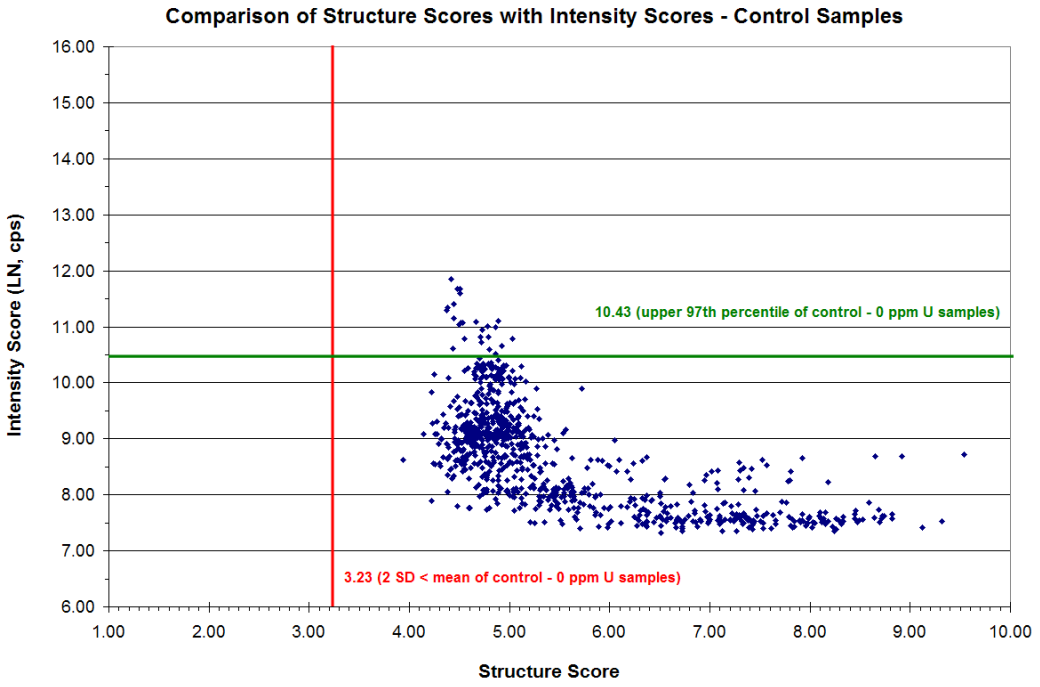

Figure 33. Comparison of fluorescence intensity and band structure scores for the control samples, [U] = 0 ppm (n = 840).

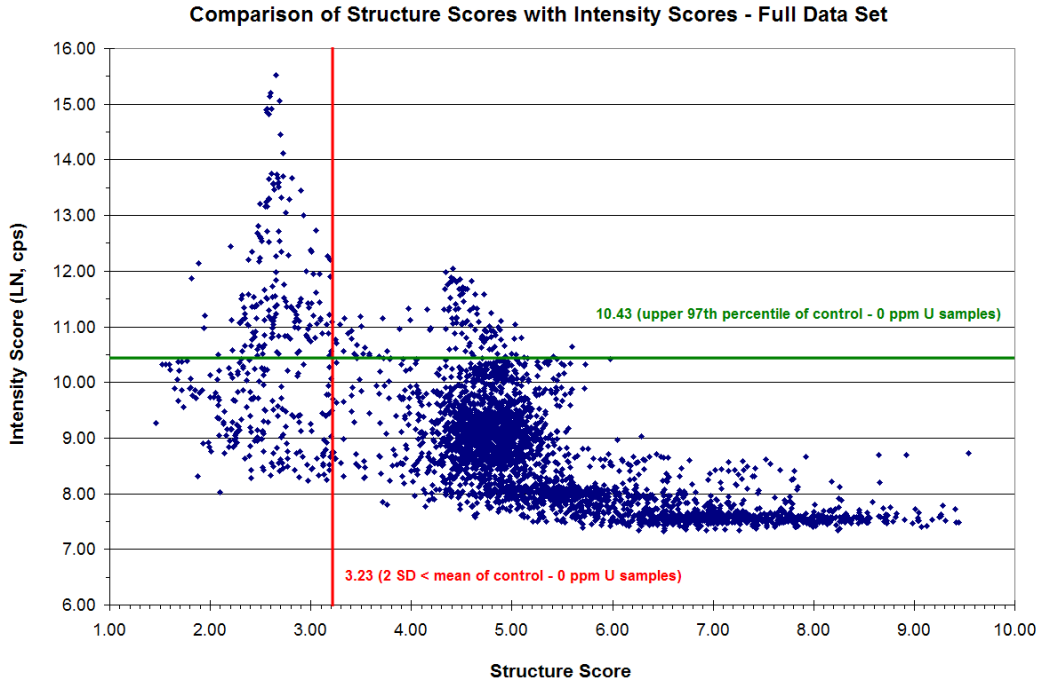

Figure 34. Comparison of fluorescence intensity and band structure scores for the comprehensive dataset (n = 3360).

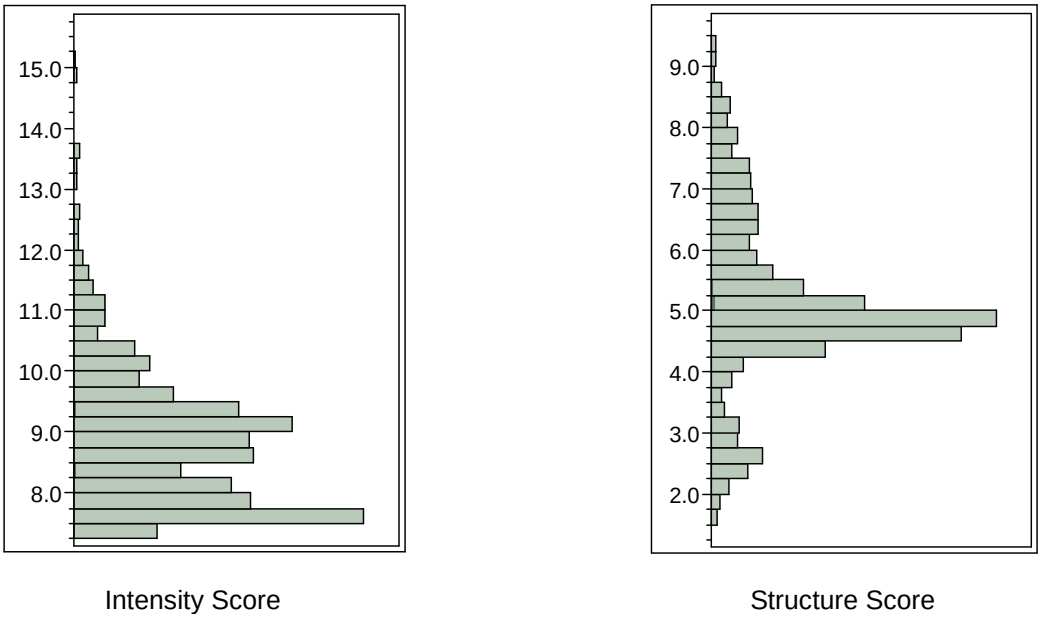

Figure 35. Distribution plots for the generated response variables, Intensity score and Structure score, for the comprehensive dataset (n = 3360).

Table 25. Distribution details for the generated response variables, Intensity score and Structure score, for the comprehensive dataset (n = 3360).

Intensity Score		**Structure Score**	
Mean	8.8810	Mean	5.1055
Std Dev	1.1721	Std Dev	1.3952
Std Error Mean	0.0202	Std Error Mean	0.0241
Mean Upper 95 %	8.9207	Mean Upper 95 %	5.1527
Mean Lower 95 %	8.8414	Mean Lower 95 %	5.0583
N (observations)	3360	N (observations)	3360
Maximum	15.51	Maximum	9.54
Minimum	7.32	Minimum	1.46
Median	8.77	Median	4.9
75% quartile	9.43	75% quartile	5.72
25% quartile	7.95	25% quartile	4.54

2.3.4 Populations of Spectra – Achieving Desired Detection Thresholds

While not necessarily demonstrating the *dependence* of desired uranyl detection on predictor variables, examining the populations of spectra achieving selected detection thresholds can be highly insightful. Figures 36 through 41 display the number of spectra with structure scores < 3.23 and intensity scores > 10.43 (n = 169), based on the predictor variables: [U] ppm, Over SG, Initial % MC, Read Time, Soil text. class., % Sand, % Clay, % Silt, % OM, Total CEC, Soil pH, Iron content (Mehlich III) and Total Iron.

Examining this subset of the full dataset allows for certain trends to be observed. It is clear from Figure 36 that higher concentrations of U, as well as the use of silica gel, are associated with improved detection. Similarly, Figure 37 shows that higher initial % moisture content is associated with improved detection *if* it is categorized as the low or high level selected for different soils; recall 2.5% and 5% were selected as 'low' values, while 10%, 25% and 35% were selected as 'high' values (see Table 22). Figure 38 indicates a weak trend of improved detection with time, however this is observed regardless of whether the reading was taken over silica gel or bare soil, implying that the loss of moisture with evaporation may be a reasonable explanation.

It is clear from Figure 39 that soil samples that are predominantly sand yielded improved detection. However, it is important to note that for this dataset, soil texture class 'clay' was represented by only the KGa-1b 'clay standard'. This soil sample was among the best for yielding uranyl detection, and was characterized by a high water-holding capacity. However, this 'soil sample' was not representative of environmental clay-soils, and was characterized by relatively low CEC, % OM and iron values (see Table 23). Therefore, this needs to be taken into

consideration when using predictor variables: % Sand, % Clay and soil text. class., in that the KGa-1b samples represented 0% sand and 100% clay.

Figure 40 seems to indicate that lower values for: % Silt, % OM and Total CEC may be associated with improved detection. It is noteworthy that the three soil samples characterized by the highest levels of % OM and % Silt (loams) did not produce any spectra achieving the desired detection thresholds. Similarly, Figure 41 shows evidence suggesting lower iron content (total and by Meh. III) may also be associated with improved detection, while Soil pH surprisingly displayed no observable trend.

It is intuitive that many of these soil parameters are related to each other, and overlap to varying degrees. Careful examination of the predictor (X) variables is required, therefore, in order to avoid multicollinearity issues as well as develop a parsimonious statistical model for the entire dataset.

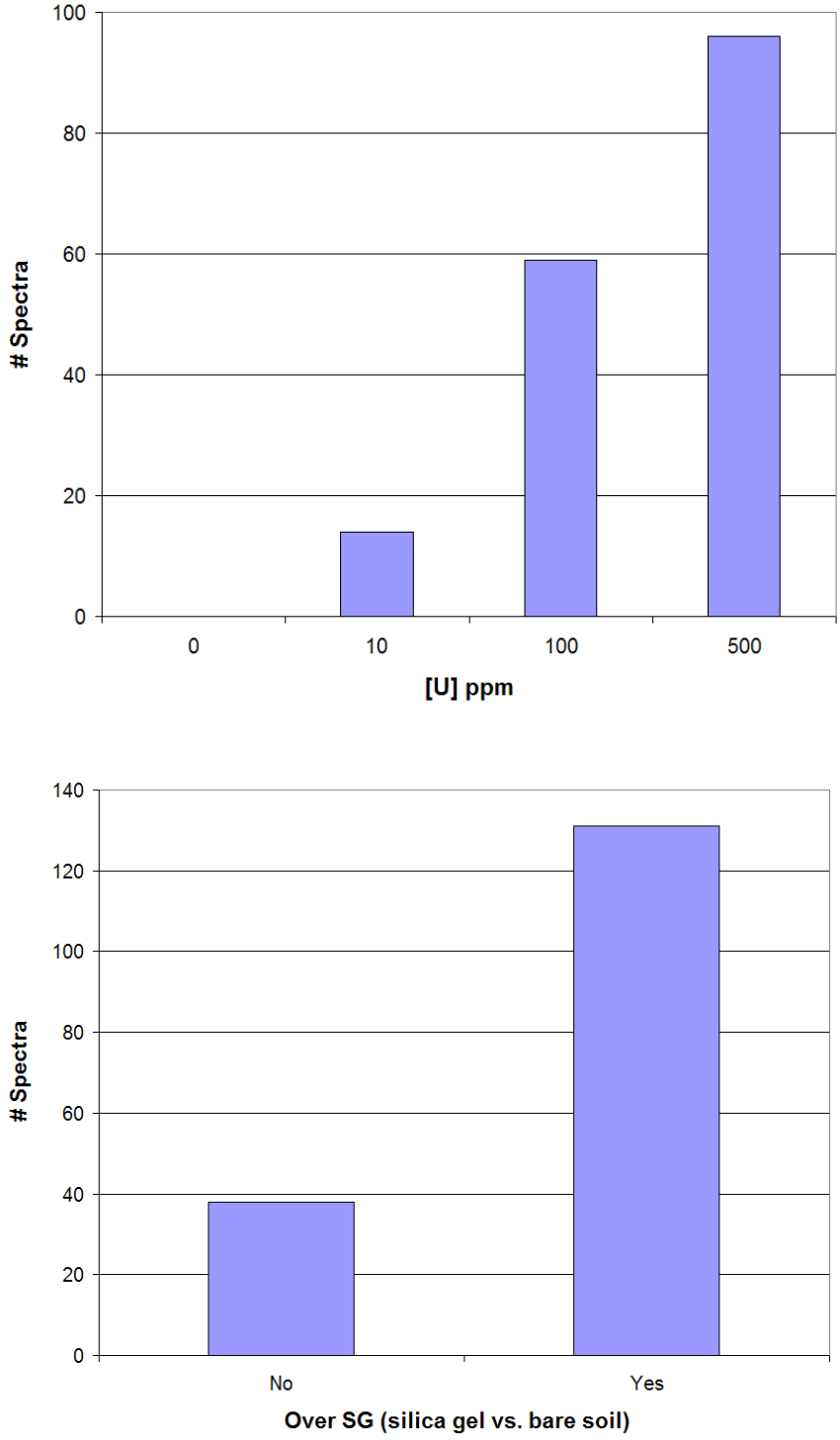

Figure 36. Number of spectra achieving selected detection thresholds (structure scores < 3.23, intensity scores > 10.43, n = 169), based on uranium concentration and whether readings were collected over silica gel versus bare soil.

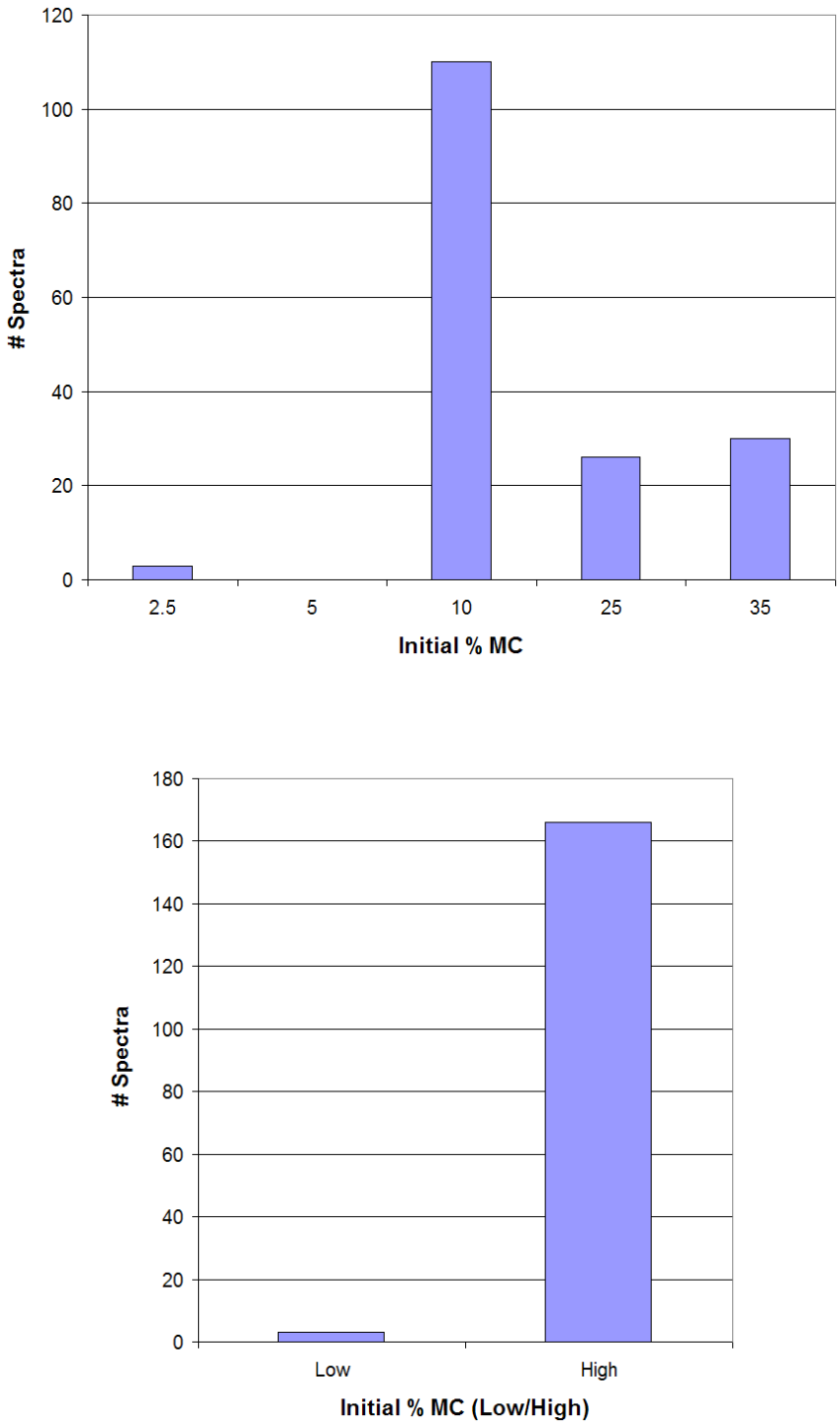

Figure 37. Number of spectra achieving selected detection thresholds (structure scores < 3.23, intensity scores > 10.43, n = 169), based on initial percent moisture content and further categorized as the low or high level selected for soils (see Table 22).

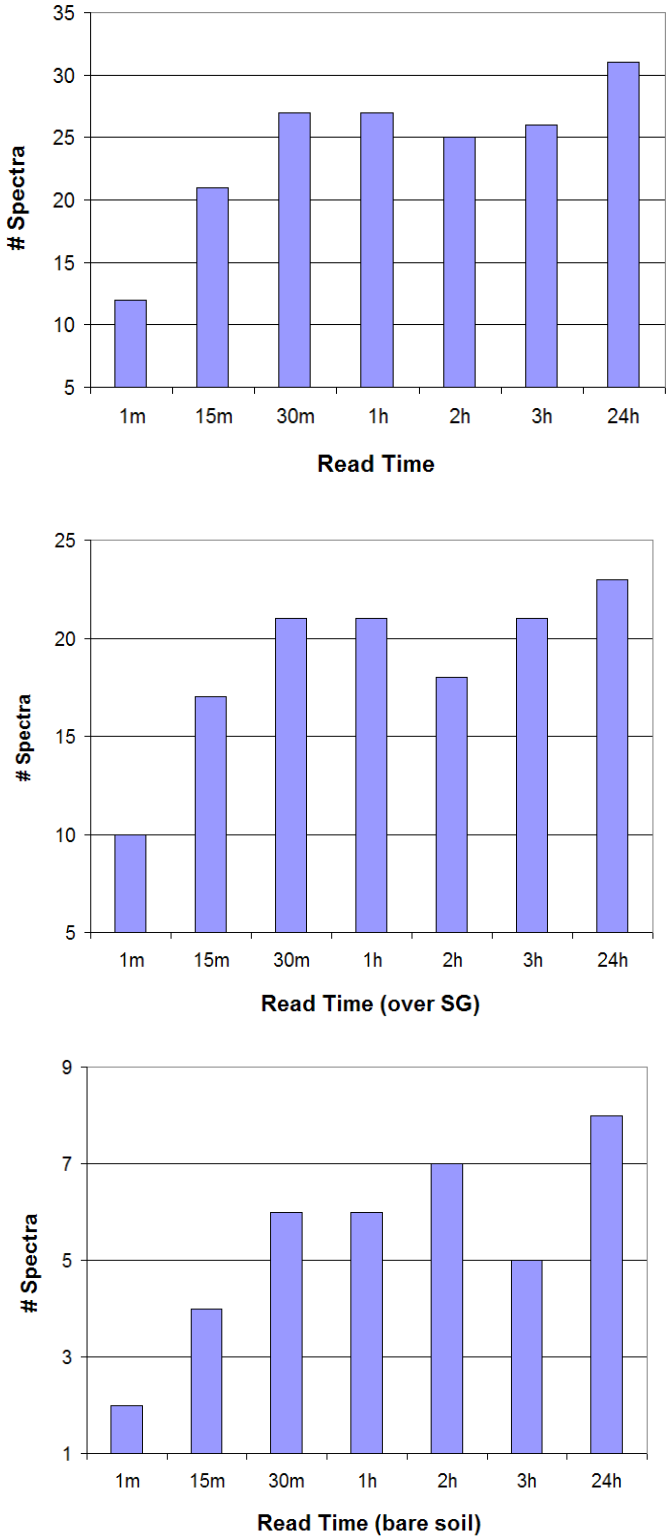

Figure 38. Number of spectra achieving selected detection thresholds (structure scores < 3.23, intensity scores > 10.43, n = 169), based on time of analysis and further distinguishing between readings collected over silica gel versus bare soil.

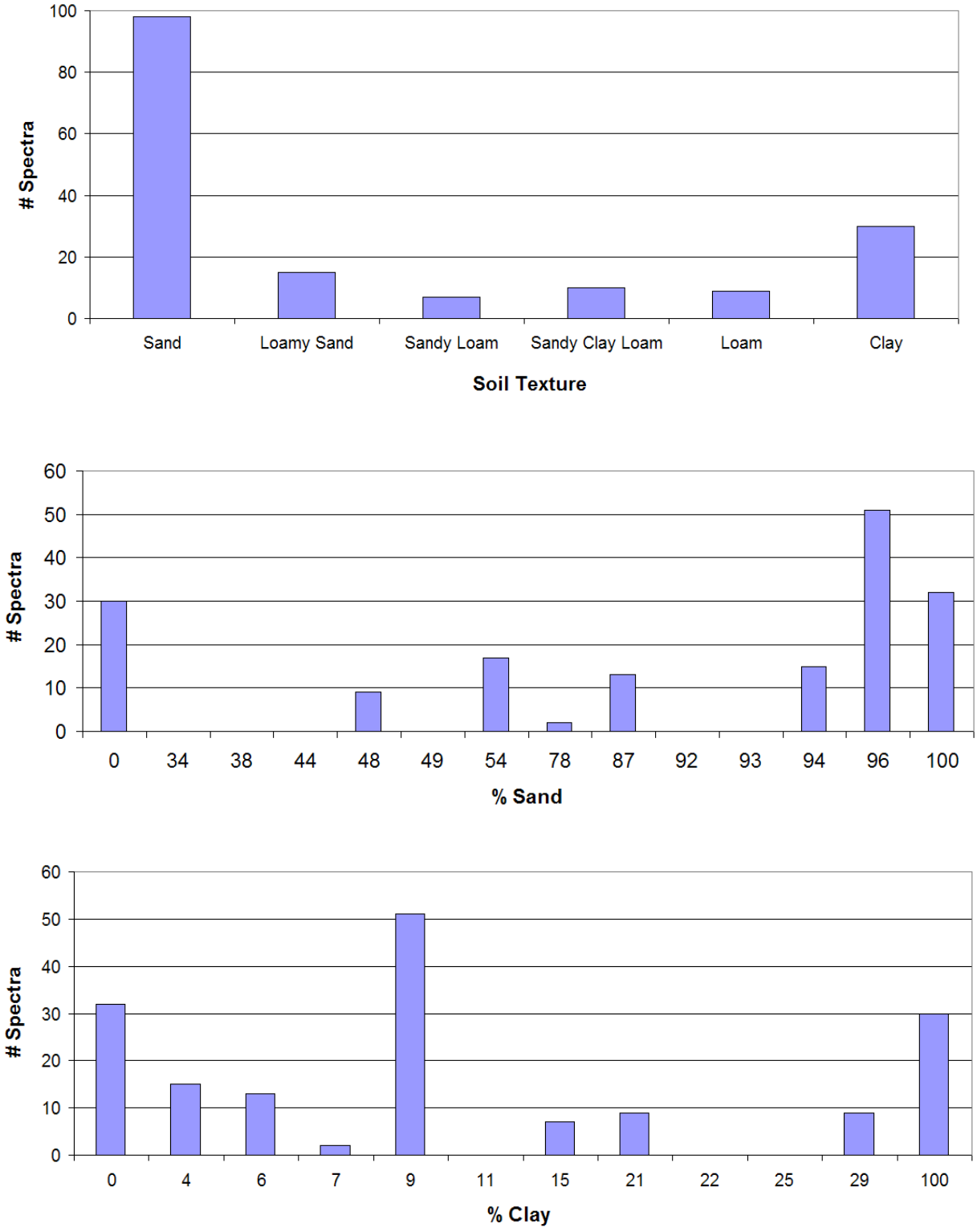

Figure 39. Number of spectra achieving selected detection thresholds (structure scores < 3.23, intensity scores > 10.43, *n* = 169), based on soil features: Soil texture, % Sand and % Clay.

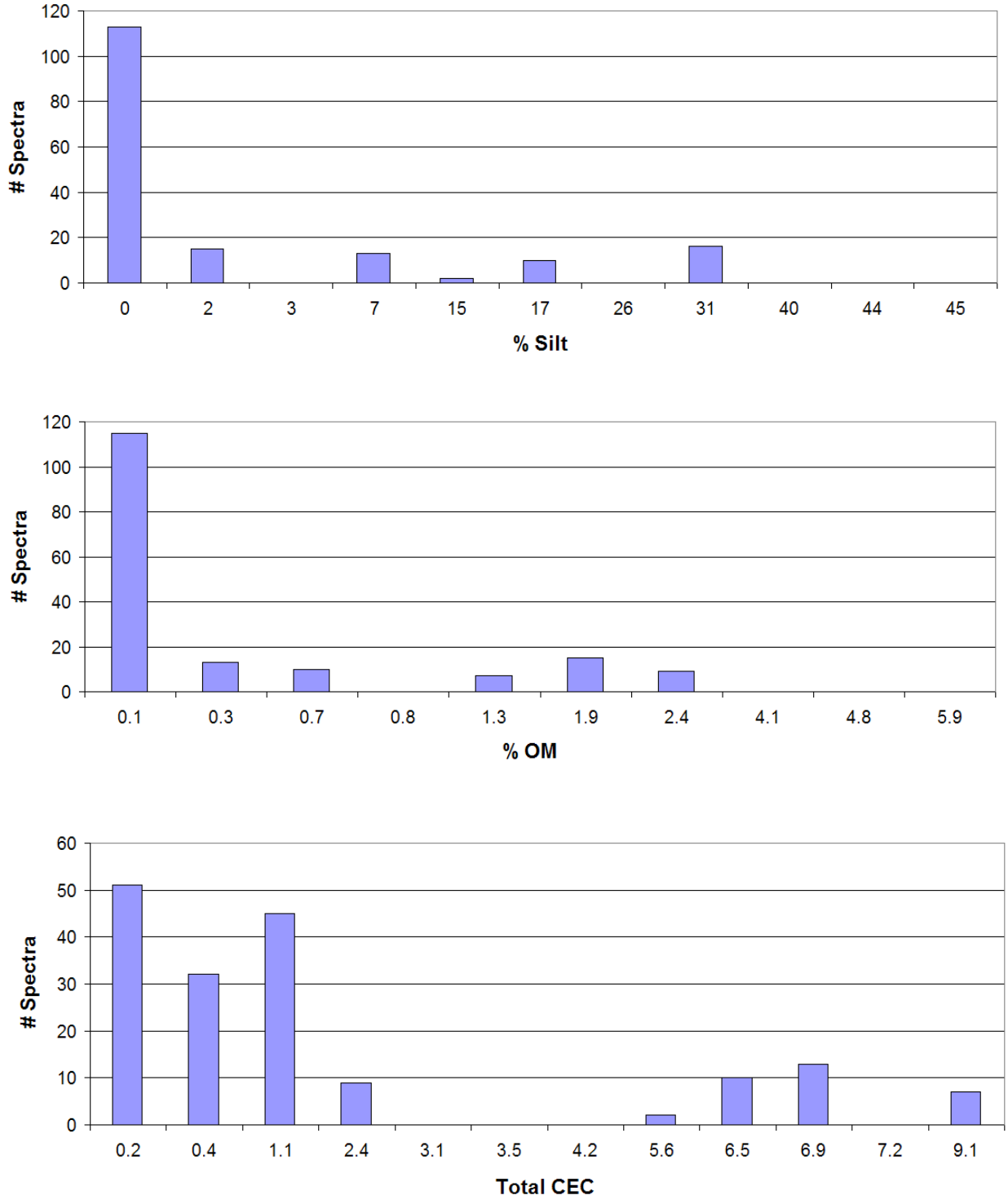

Figure 40. Number of spectra achieving selected detection thresholds (structure scores < 3.23, intensity scores > 10.43, *n* = 169), based on soil features: % Silt, % OM and Total CEC.

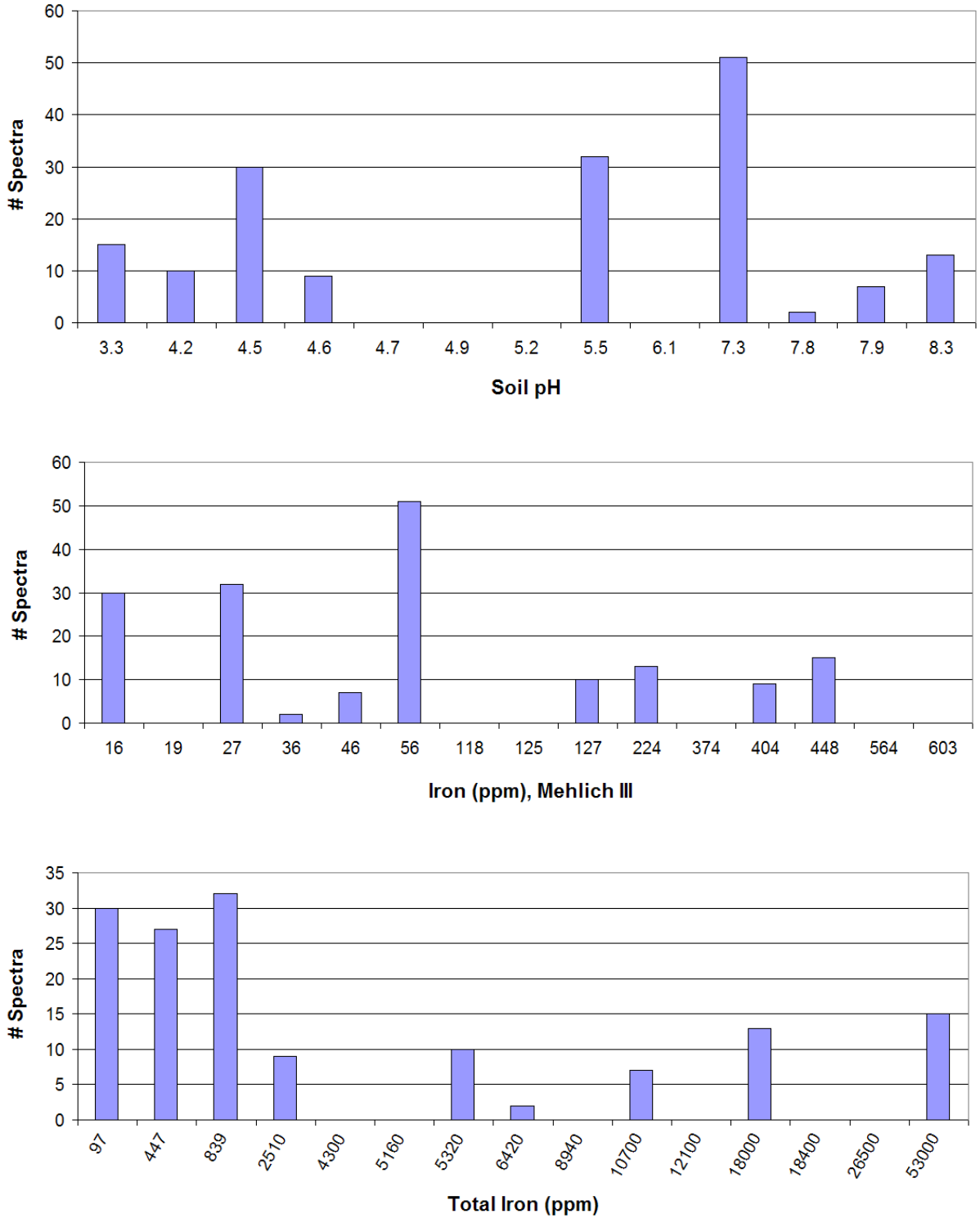

Figure 41. Number of spectra achieving selected detection thresholds (structure scores < 3.23, intensity scores > 10.43, n = 169), based on soil features: Soil pH, Iron content (Mehlich III) and Total Iron.

2.3.5 Predictor (X) Variables – Relationships

Multicollinearity issues associated with multiple regression models indicate that two or more predictor variables are highly correlated, and somewhat redundant of each other. While multicollinearity will not reduce the predictive capabilities of the model overall, it can affect the validity of the coefficient estimates for individual predictors. In order to avoid multicollinearity issues in the subsequent multiple regression models, the variance inflation factors (VIF) should be examined. High VIF values (> 10) indicate multicollinearity issues, with VIF values < 5 being desirable. Note that VIF = $(1-R_k^2)$ where R_k^2 is the coefficient of determination when the k^{th} regressor is regressed on the remaining X variables. If high VIF values are observed, efforts should be made to reduce the number of X variables included the models, specifically avoiding the simultaneous use of strongly related regressors. Therefore, all possible predictor variable pairs were examined for possible correlations. Table 26 lists pairs of continuous predictor variables resulting in correlation values greater than 0.4. Recall, a positive correlation indicates a tendency for one variable to increase as the other increases, while a negative correlation indicates a tendency for one variable to decrease as the other increases, and the absolute value of the correlation is reflective of the strength of the relationship.

Table 26. Correlation values generated by the multivariate routine (JMP v8) for pairs of continuous predictor variables.

Predictor Variables Compared		Correlation value [a]
Initial % MC	Est. % MC	+ 0.85
% Clay	% Sand	– 0.81
% Silt	% OM	+ 0.80
Iron (Meh. III)	Total Iron	+ 0.59
% Silt	% Sand	– 0.57
% Silt	Total CEC	+ 0.52
Total CEC	Soil pH	+ 0.50
Initial % MC	% Sand	– 0.47
Est. % MC	% Sand	– 0.43
% Sand	% OM	– 0.41

[a] Only correlations with absolute values greater than or equal to 0.4 shown.

Principal components analysis (PCA) is a form of factor analysis that can be used to assist in the decision making process of reducing the number of continuous predictor variables, by detecting relationships between them. Essentially, PCA extracts principal components, reducing highly correlated X variables into arbitrary factors, and attempts to maximize the *variation* represented by those factors. Each principal component represents a linear combination of the X variables. The generated eigenvalues are reflective of the variation of the new factors, with consecutive factors accounting for progressively less variability. Table 27 displays the output of the PCA routine (JMP, v8), and lists the continuous predictor variables examined, extracted factors and their corresponding percentages of total variation and eigenvalues. Based on the Kaiser criterion, factors with eigenvalues of ≈ 1 or greater should be retained, which included only five of the eleven extracted factors. Therefore, these PCA results provide further evidence supporting the need to reduce the number of predictor variables included in subsequent models, in order to avoid the simultaneous use of highly correlated regressors.

Table 27. Results of the principal components analysis routine (PCA, JMP v8), displaying the continuous predictor variables examined, the arbitrary extracted factors, their corresponding eigenvalues and the estimated percent of total variation and cumulative variation they represent.

Variables	Factor	Eigenvalue	Percent	Cum. Percent
[U] (ppm)	1	3.32 [a]	30.17	30.17
Initial % MC	2	2.18 [a]	19.86	50.03
Est. % MC	3	1.72 [a]	15.66	65.69
% Sand	4	1.06 [a]	9.60	75.29
% Silt	5	1.00 [a]	9.09	84.38
% Clay	6	0.86	7.83	92.21
Soil pH	7	0.43	3.88	96.09
Total CEC	8	0.22	2.03	98.11
% OM	9	0.15	1.35	99.46
Iron (Meh. III)	10	0.06	0.53	100.00
Total Iron	11	0.00	0.00	100.00

[a] Eigenvalue ≈ 1 or greater: factor should be retained according to the Kaiser criterion.

2.3.6 Predictor (X) and Response (Y) Variables – Bivariate Relationships

Prior to developing predictive models for the individual response variables based on multiple regressors (X's), examinations should first be made of the relationships between individual predictor variables and the response variables, for the entire dataset. A series of bivariate plots are displayed in Figures 42 through 51, which show the means for the different levels of the predictor variables (calculated by least squares), and their associated 95% confidence intervals. It is important to keep in mind that this dataset is predominantly characterized by intensity and structure scores *not* reflective of 'desired detection levels'. That being said, some trends similar to those previously seen for the sub-dataset (desired detection) are implied here as well for the entire dataset, for individual response variables. For example, it is clear from Figure 42 that higher concentrations of U, use of silica gel, and higher initial % moisture content (when categorized as high/low) are associated with higher intensity scores and lower structure scores. More specifically, higher initial % moisture content is typically

associated with higher intensity scores and lower structure scores when examined by soil texture (ST) classification (see Figures 43 and 44), with structure scores for the ST classes loam and clay being the exception. Regarding time of analysis, Figure 45 seems to weakly indicate that the 1 min time point tended to have lower intensity scores and higher structure scores.

With regards to soil sample features, Figure 46 shows the diversity of intensity and structure scores displayed by the different soil samples. ST classes: loamy sand, sand and clay tended to have higher intensity scores, with classes loamy sand and clay having lower structure scores as well. Contrary, ST classes: loam and sandy-clay loam tended to have lower intensity scores and higher structure scores (see Figure 47). Figures 48 through 51 give slight indication that very high levels of % sand, and very low levels of % silt, total CEC and total iron, may be associated with higher intensity scores. In contrast, means of structure scores did not give any indication of observable trends for these parameters.

The means comparison routine (JMP v8) was used to clarify which means for the different levels of predictor variables (treated as categorical) are significantly different from each other, based on the Tukey-Kramer HSD method. Table 28 displays these results, relative to the response variables, with means of levels not connected by the same letter being significantly different ($\alpha = 0.05$). For X variables 'Over SG' (yes/no) and 'Initial % MC' (high/low), the means of the different levels were significantly different, as would be expected. With regards to U concentration, for both intensity and structure score, the means for levels 0 ppm and 10 ppm were *not* found to be significantly different from each other, while the means for levels 100 ppm and 500 ppm were significantly different. For intensity scores relative to ST class, the following level means were *not* found to be significantly different from each other: clay and sand, sand and sandy loam, and loam and sandy-clay loam. For structure scores relative to ST class, the means

of levels sand and loamy sand were *not* significantly different from each other. With regards to time of analysis, for intensity scores, the means of all the time points were not significantly different from each other. For structure scores, the means of time points 1 min through 3 hrs were not significantly different from each other, while the means of time points 15 min through 24 hrs were not significantly different from each other, indicating that the 1 min and 24 hr time points were different from each other. Further examining the time point means, for readings collected over silica gel, the means of all the time points were not significantly different from each other, for both intensity and structure scores. For readings collected over bare soil, where Y is intensity score, the means of time points 15 min through 24 hrs were not significantly different from each other, while the means of time points 1 min, 15 min, 30 min and 24 hrs were not significantly different from each other. For readings collected over bare soil, where Y is structure score, the means of time points 1 min through 3 hrs were not significantly different from each other, while the means of time points 15 min through 24 hrs were not significantly different from each other, again indicating that the 1 min and 24 hr time points were different from each other.

These means comparison results give the initial impression that time of analysis will *not* serve as a good predictor of intensity and structure scores, while variables: 'Over SG', 'Initial % MC', '[U] ppm' and 'ST class.' are more promising candidate predictors.

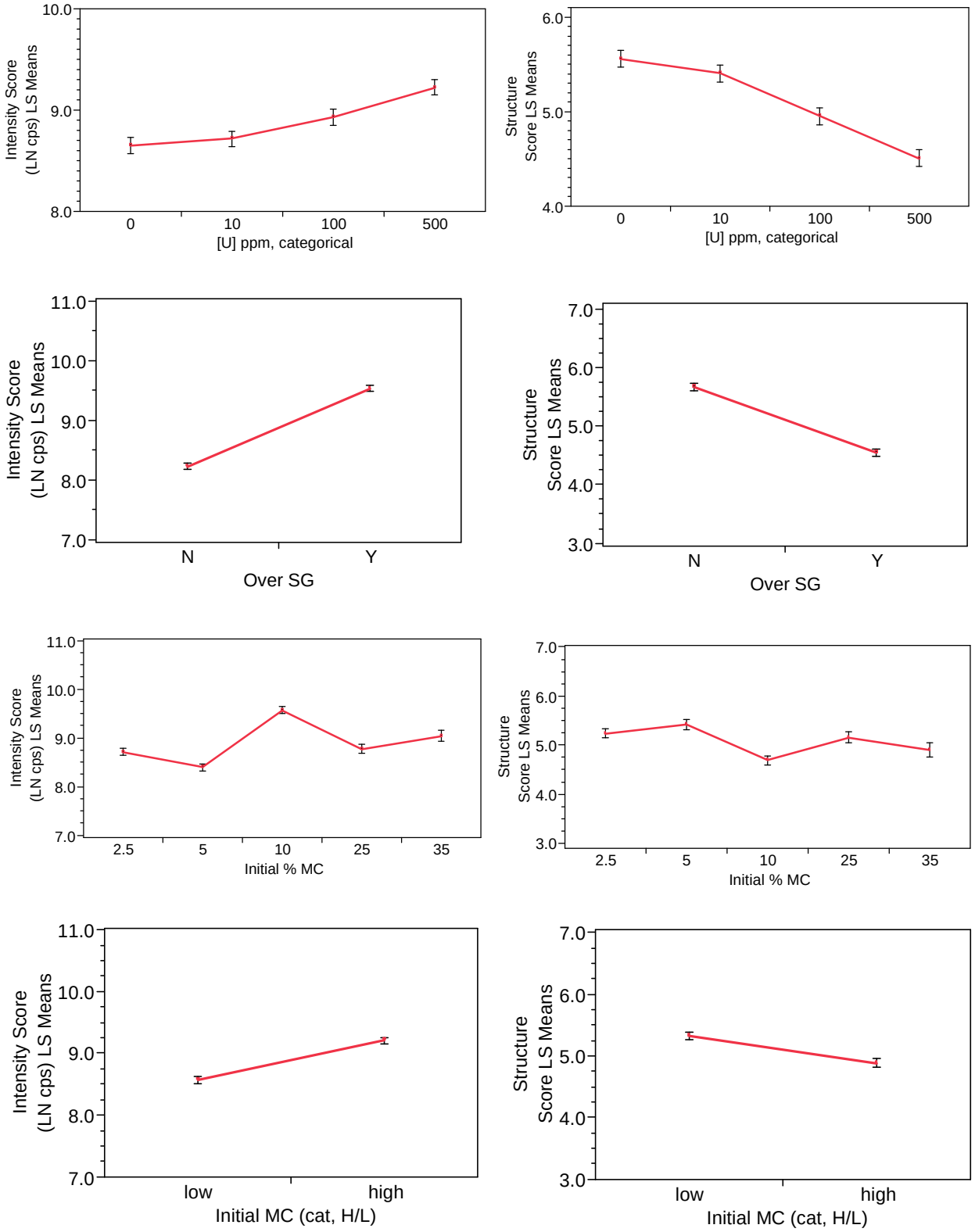

Figure 42. Least squares means plots relating intensity scores (left) or structure scores (right) to uranium concentration, whether readings were collected over silica gel versus bare soil, initial percent moisture content and further categorized as the low or high level selected for soils.

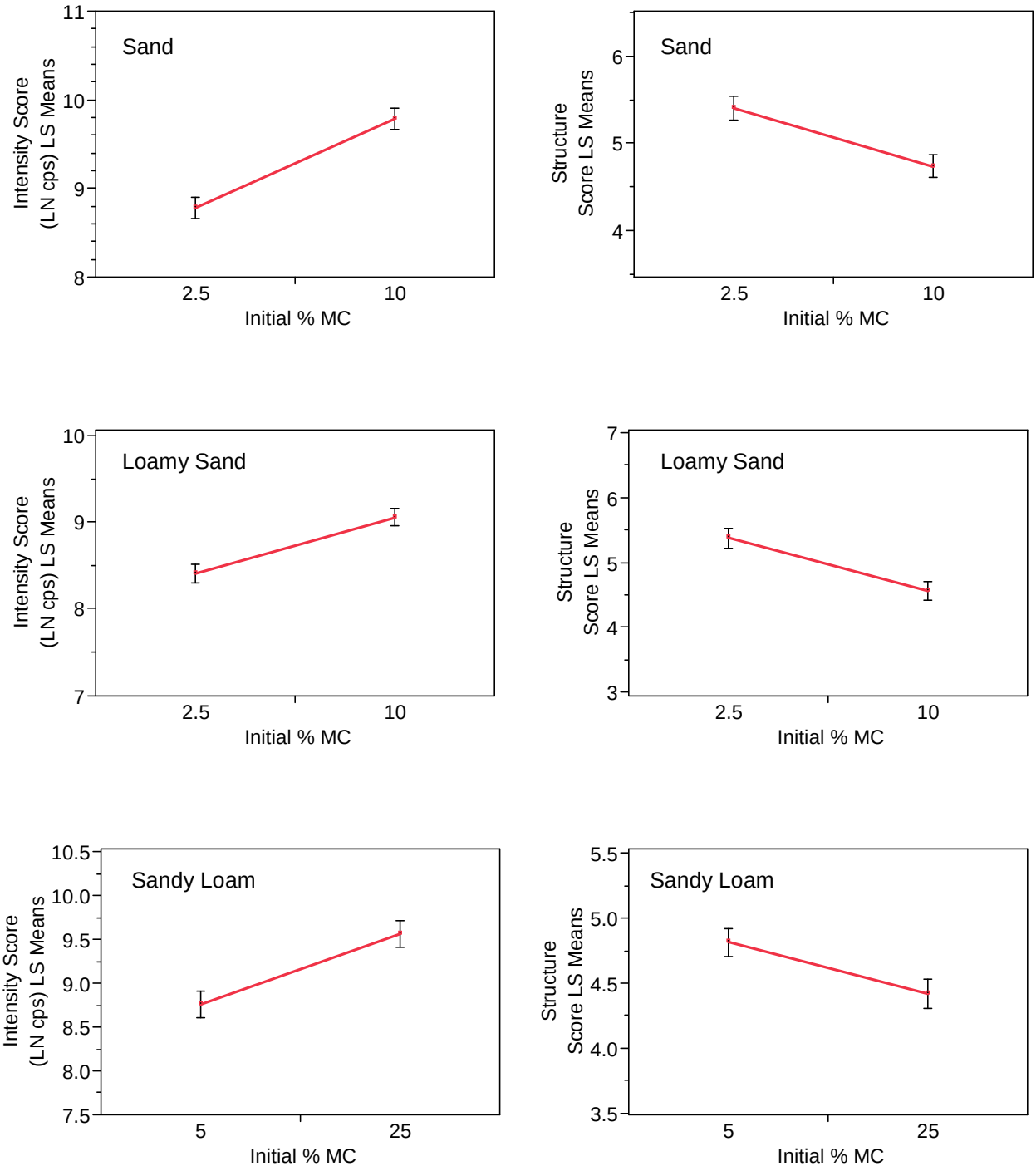

Figure 43. Least squares means plots relating intensity scores (left) or structure scores (right) to initial percent moisture content for soil texture groups: Sand, Loamy Sand and Sandy Loam.

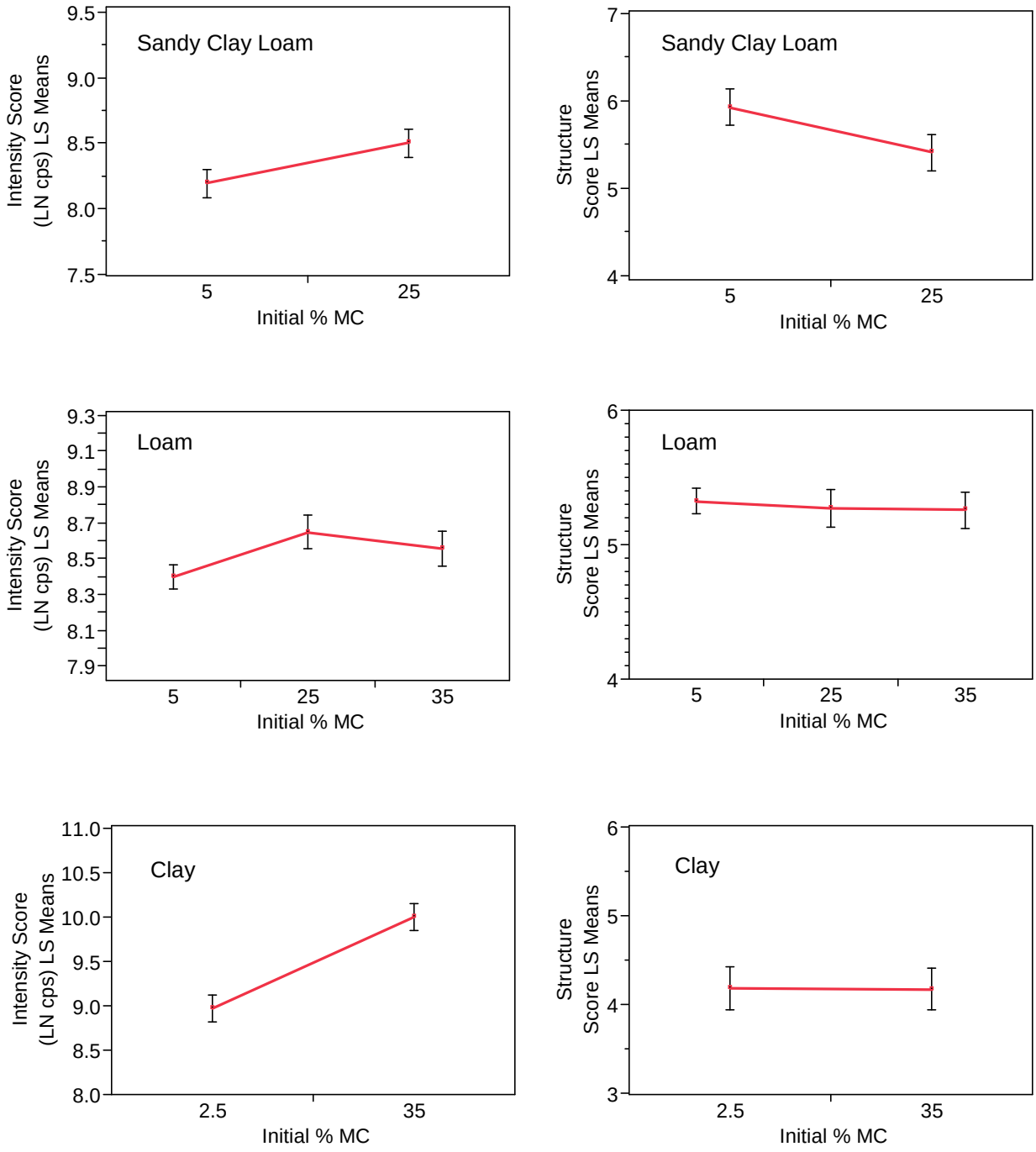

Figure 44. Least squares means plots relating intensity scores (left) or structure scores (right) to initial percent moisture content for soil texture groups: Sandy Clay Loam, Loam and Clay.

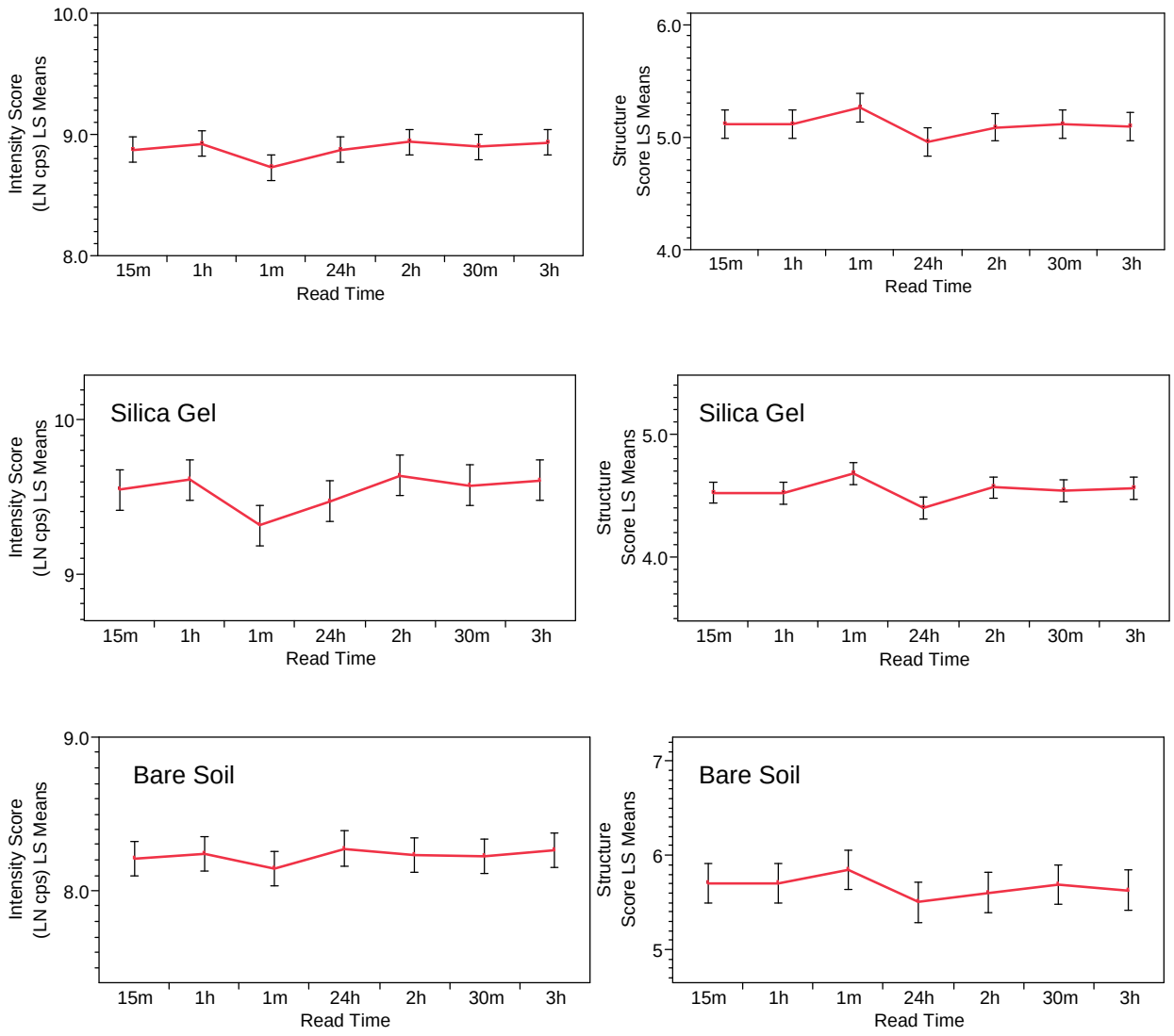

Figure 45. Least squares means plots relating intensity scores (left) or structure scores (right) to time of analysis and further distinguishing between readings collected over silica gel versus bare soil.

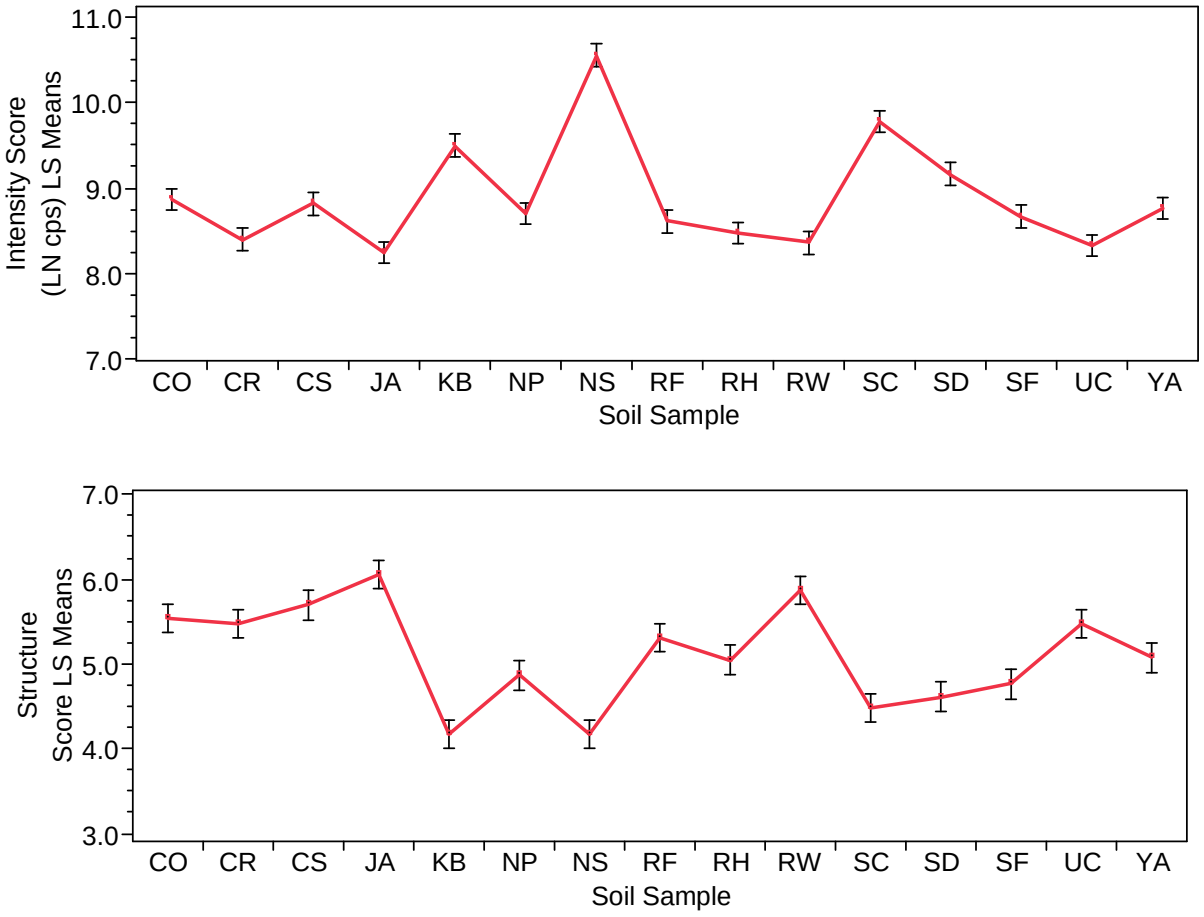

Figure 46. Least squares means plots relating intensity scores (top) or structure scores (bottom) to soil sample identity.

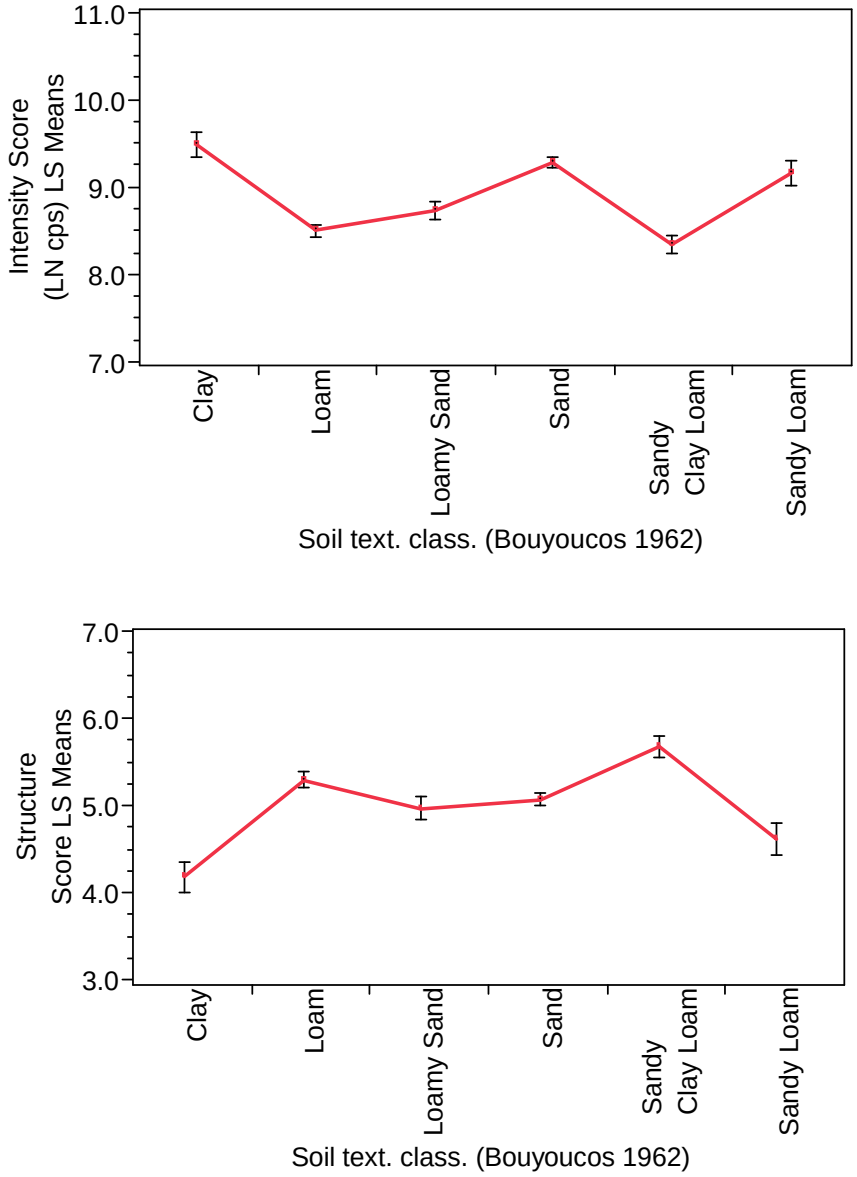

Figure 47. Least squares means plots relating intensity scores (top) or structure scores (bottom) to soil texture classification.

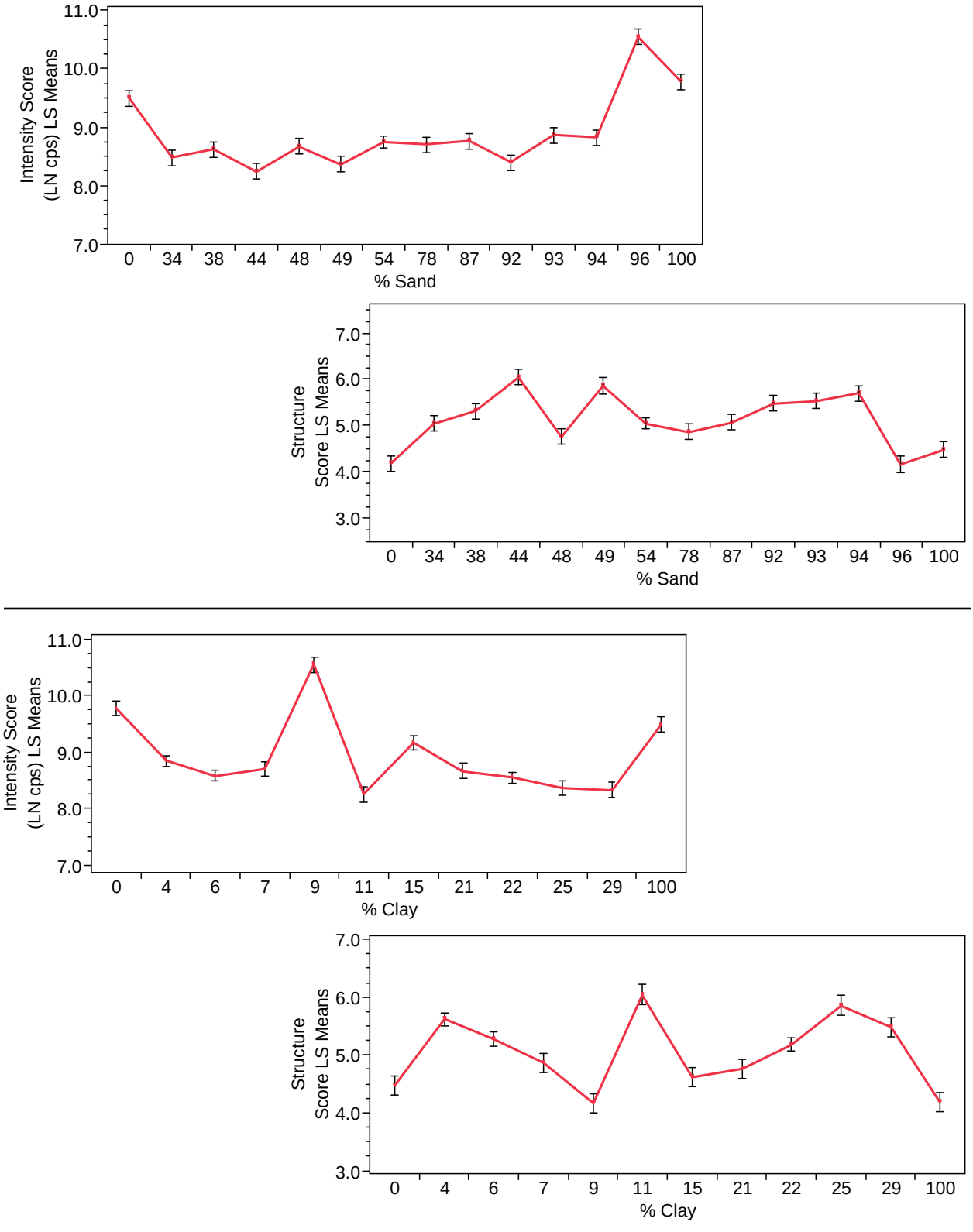

Figure 48. Least squares means plots relating intensity scores (left) or structure scores (right) to % Sand (top) and % Clay (bottom).

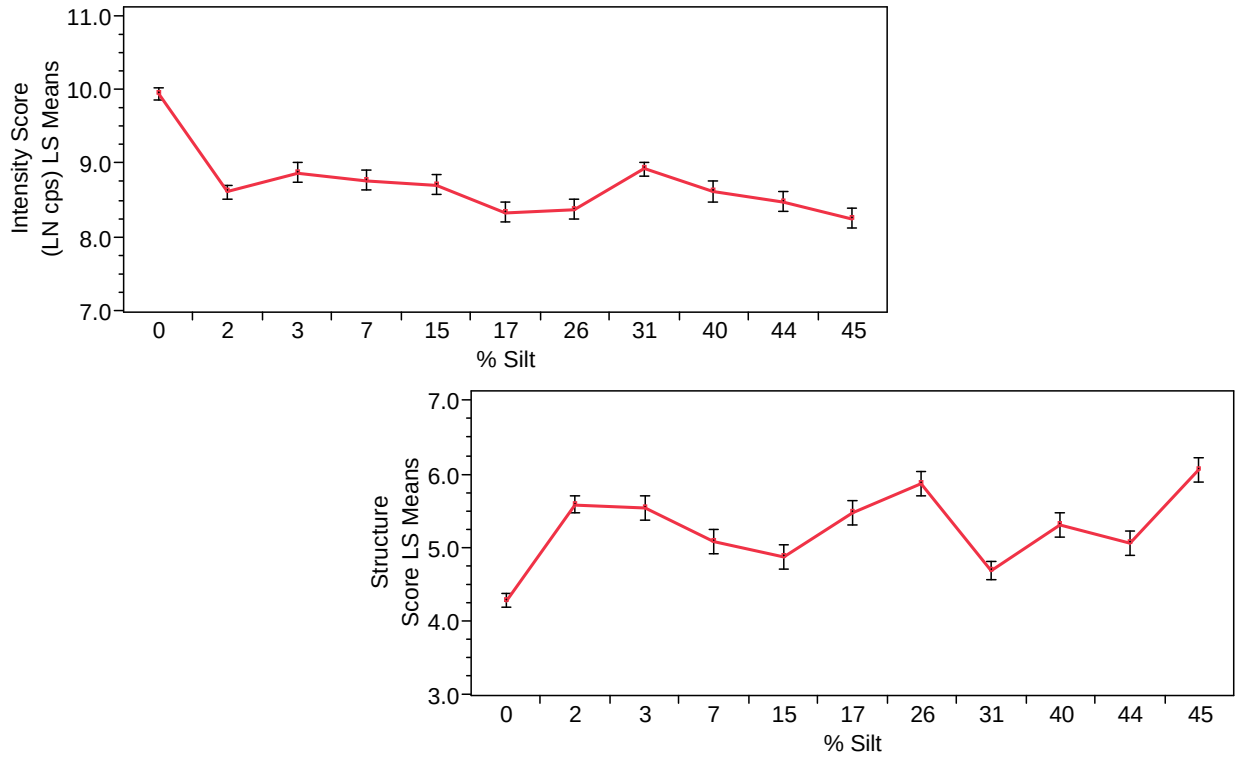

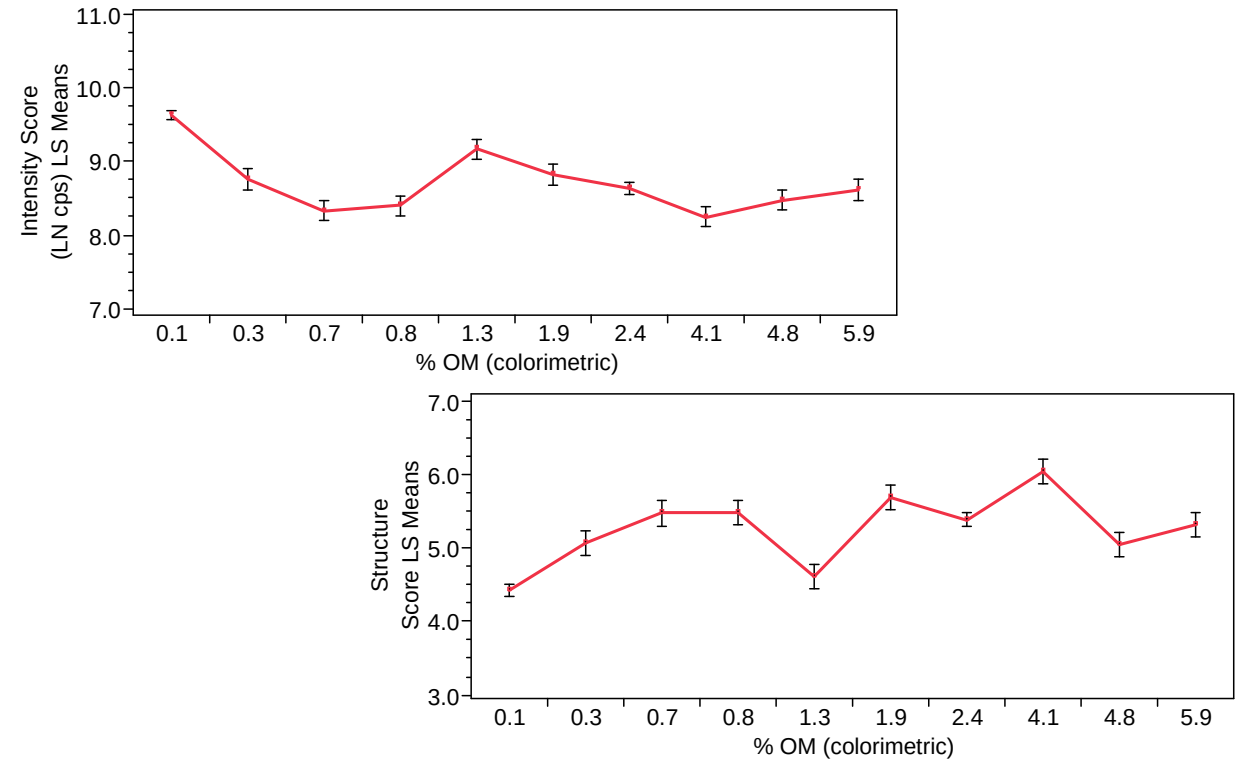

Figure 49. Least squares means plots relating intensity scores (left) or structure scores (right) to % Silt (top) and % OM (bottom).

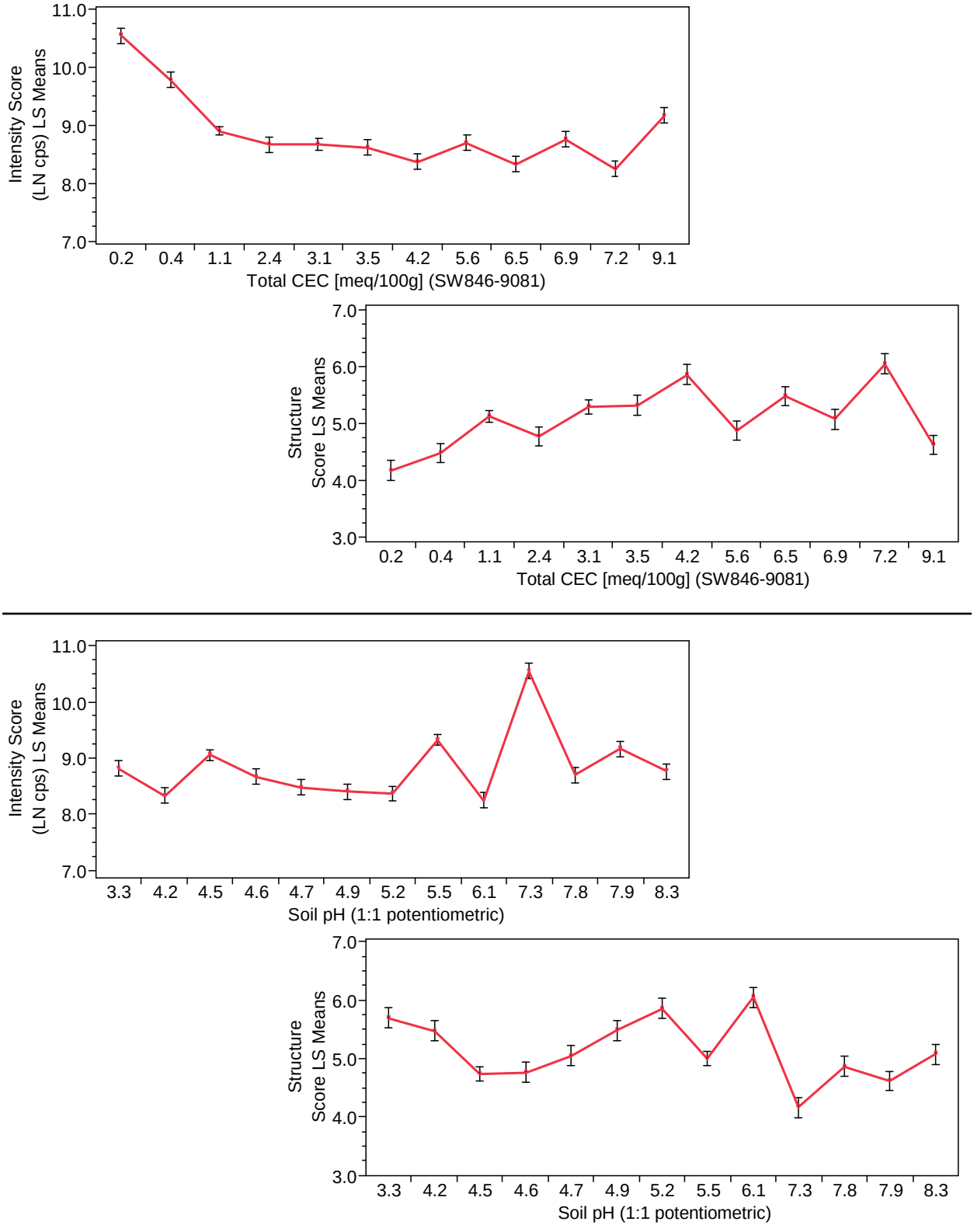

Figure 50. Least squares means plots relating intensity scores (left) or structure scores (right) to Total CEC (top) and Soil pH (bottom).

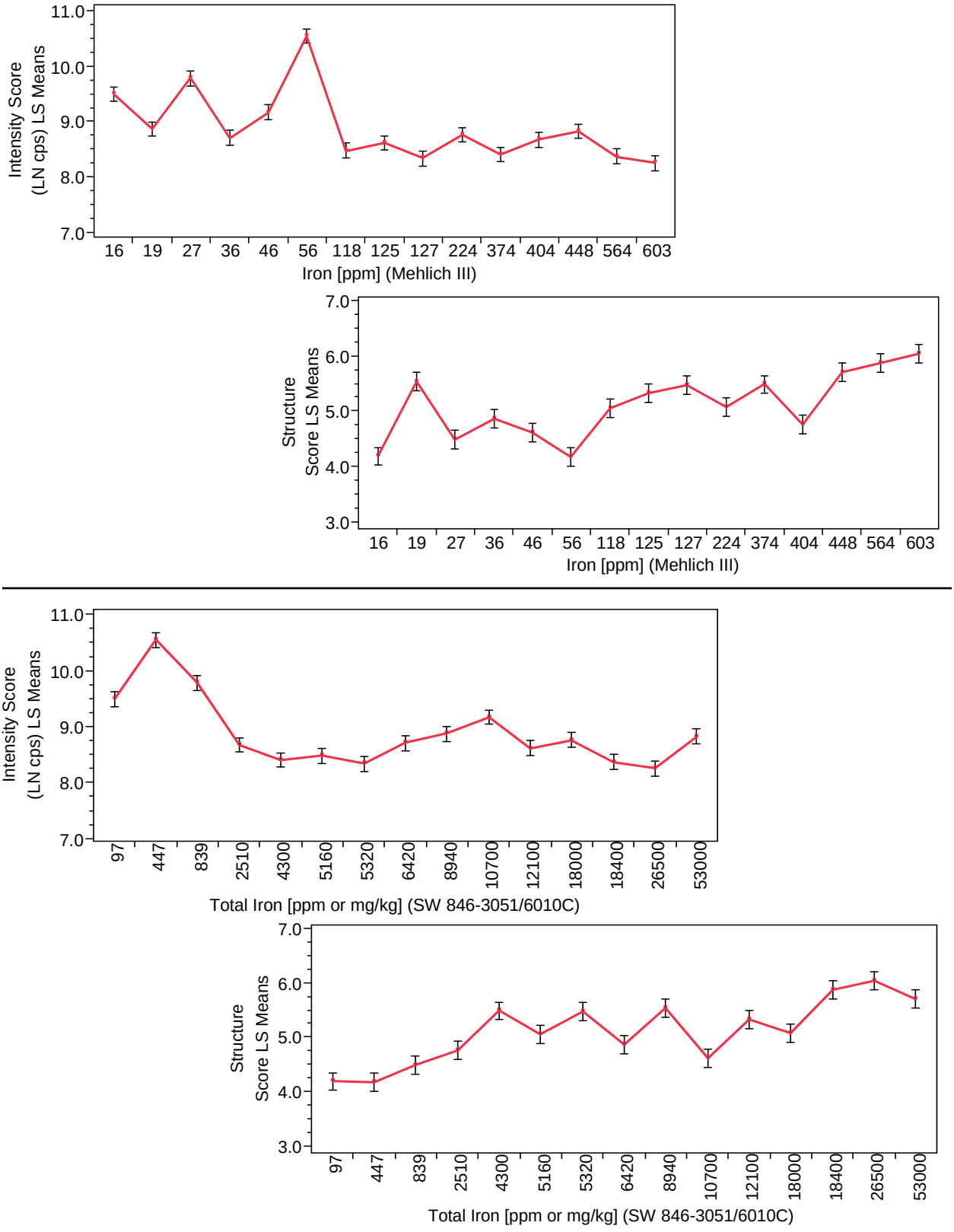

Figure 51. Least squares means plots relating intensity scores (left) or structure scores (right) to Iron content by Mehlich III (top) and Total Iron (bottom).

Table 28. Means comparison results (JMP v8) showing the means of different levels of X variables that are significantly different from each other, relative to the response variables.

Y variable	***Intensity Score***			***Structure Score***		
X variable	**Level**	**Groups** [a]	**Mean**	**Level**	**Groups** [a]	**Mean**
Over SG	Yes	A	9.5367	Yes	A	4.5416
	No	B	8.2254	No	B	5.6693
Initial % MC	Low	A	8.5621	Low	A	5.3258
	High	B	9.1999	High	B	4.8852
[U] ppm	0	A	8.6524	0	A	5.5578
	10	A	8.7160	10	A	5.4045
	100	B	8.9316	100	B	4.9535
	500	C	9.2241	500	C	4.5060
Soil text. class.	Clay	A	9.4900	S.C. Loam	A	5.6665
	Sand	A B	9.2811	Loam	B	5.2921
	S. Loam	B	9.1642	Sand	C	5.0705
	L. Sand	C	8.7306	L. Sand	C	4.9676
	Loam	D	8.5000	S. Loam	D	4.6150
	S.C. Loam	D	8.3474	Clay	E	4.1777
Read Time	2h	A	8.9372	1m	A	5.2628
	3h	A	8.9337	30m	A B	5.1165
	1h	A	8.9244	15m	A B	5.1153
	30m	A	8.8976	1h	A B	5.1110
	15m	A	8.8748	3h	A B	5.0941
	24h	A	8.8725	2h	A B	5.0856
	1m	A	8.7270	24h	B	4.9530
Read Time (Over SG = N)	24h	A	8.2757	1m	A	5.8470
	3h	A	8.2608	15m	A	5.7057
	1h	A	8.2375	1h	A	5.7009
	2h	A	8.2348	30m	A	5.6941
	30m	A	8.2222	3h	A	5.6292
	15m	A	8.2052	2h	A	5.6053
	1m	A	8.1417	24h	A	5.5032
Read Time (Over SG = Y)	2h	A	9.6397	1m	A	4.6785
	1h	A	9.6114	2h	A B	4.5659
	3h	A	9.6066	3h	A B	4.5590
	30m	A B	9.5730	30m	A B	4.5390
	15m	A B	9.5444	15m	A B	4.5249
	24h	A B	9.4693	1h	A B	4.5210
	1m	B	9.3124	24h	B	4.4029

[a] Means of levels not connected by the same letter are significantly different ($\alpha = 0.05$), based on the Tukey-Kramer HSD method.

Simple linear regression models (1 X, 1 Y) can be used to determine if promising *dependencies* exist for the response variables (intensity and structure scores) on individual predictor variables. Table 29 displays the results of the least squares fitting routine (JMP v8) in testing for the significance of single continuous X variable models (linear fits), in predicting the response variables individually. For single X regression models, the significance level is simultaneously reflective of model analysis of variance and individual effects (Prob > F), as well as parameter estimates (Prob > $|t|$). Highly significant test results (*) indicate that the predictor variable successfully explains *variation* observed in the specified response variable. The calculated parameter estimates (coefficients, β's), define the role of their corresponding X's in the individual models, and are reflective of both the direction (+/–) of the linear relationship, as well as the effect on Y of a single unit increase in that X variable. For example, the parameter estimate for Soil pH is + 0.1230 (approx. scale: 3 – 9), while the parameter estimate for U concentration is + 0.0010 (approx. scale: 0 – 500).

Table 29. Results of the least squares fitting routine (JMP v8) in testing for the significance of single continuous X variable models (linear fits), in predicting each of the response variables.

Y variable	***Intensity Score***			***Structure Score***		
X variable	**R^2**	**Sig. level [a]**	**Parameter Estimate**	**R^2**	**Sig. level [a]**	**Parameter Estimate**
[U] ppm	0.0334	< 0.0001 *	+ 0.0010	0.0748	< 0.0001 *	– 0.0017
Initial % MC	0.0067	< 0.0001 *	+ 0.0088	0.0048	< 0.0001 *	– 0.0089
Est. % MC	0.0008	0.1081	+ 0.0035	0.0003	0.3266	– 0.0025
Soil pH	0.0240	< 0.0001 *	+ 0.1230	0.0176	< 0.0001 *	– 0.1254
Total CEC	0.0597	< 0.0001 *	– 0.1061	0.0151	< 0.0001 *	+ 0.0635
Iron (Meh. III)	0.0815	< 0.0001 *	– 0.0017	0.0815	< 0.0001 *	+ 0.0020
Total Iron	0.0284	< 0.0001 *	– 0.0000	0.0639	< 0.0001 *	+ 0.0000
% Sand	0.0199	< 0.0001 *	+ 0.0058	0.0007	0.1208	+ 0.0013
% Silt	0.0801	< 0.0001 *	– 0.0200	0.0187	< 0.0001 *	+ 0.0115
% Clay	0.0023	0.0054	+ 0.0024	0.0195	< 0.0001 *	– 0.0083
% OM	0.0671	< 0.0001 *	– 0.1689	0.0406	< 0.0001 *	+ 0.1565

[a] Significance level simultaneously reflective of model analysis of variance and individual effects (Prob > F), as well as parameter estimates (Prob > $|t|$) for single X models.

The coefficient of determination (R^2) is reflective of the quality of prediction and the % of total variation in Y accounted for by the X. For Y = Intensity score, and R^2 values ordered from highest to lowest correspond to X variables: Iron (Meh. III), % Silt, % OM, Total CEC, [U] ppm, Total Iron, Soil pH and % Sand, while % Clay and Est. % MC were not highly significant. For Y = Structure score, and R^2 values ordered from highest to lowest correspond to X variables: Iron (Meh. III), [U] ppm, Total Iron, % OM, % Clay, % Silt, Soil pH and Total CEC, while % Sand and Est. % MC were not highly significant.

While these results are useful in gauging which predictor variables seem most important for explaining variations observed in the response variables, it is important to recall that several of these X variables are related to each other, and their corresponding effects in these single regressor models may be highly influenced by or reflective these relationships.

An overall tendency observed here in these single regressor models, as well as in subsequent multiple regressor models, is that most predictor variables examined are found to be highly significant for explaining variation in the Y's, and yet they do not appear to explain high percentages of the total variation in the Y's. This tendency is explained in part by the high degree of variability inherent to many of the variables examined, as well as the large sample size.

The results displayed in Table 29 for continuous predictor variables are based on linear (X^1) fit models. It is important to note that higher order models (X^2, X^3, X^4, etc.) were investigated. For the following predictor variables, the linear (X^1) fits proved most promising and intuitively made the most sense to use: [U] ppm, % OM, % Silt, Total CEC, Iron (Meh. III) and Total Iron. These models then represent the tendencies for the intensity or structure scores to increase or decrease as the values of the X variables increase or decrease (depending on the variable). For the predictors: % Sand and % Clay, the second-order (X^2) fit models actually

provided significantly improved fits, however this was due to the fact that 0% sand and 100% clay were represented by the KGa-1b 'clay standard' which was not representative of environmental soils. Therefore, the linear (X^1) fit models were still used for these X variables since it was intuitive to do so.

Decisions regarding which order-fit models to utilize for the X variables: Initial % MC and Soil pH were more challenging. As previously indicated, trends for Initial % MC were reflective of soil texture, and therefore the intuitive linear (X^1) fit model for this predictor should only be utilized if the interaction between Initial % MC and soil texture is accounted for (through the use of an interaction term for example, as seen in the subsequent multiple regression models). The use of a linear (X^1) fit model is not necessarily intuitive for Soil pH, though a tendency for intensity scores to increase and structure scores to decrease as pH values increase (3.3 to 8.3, acidic towards alkaline) could be reflective of: 1) increased concentrations of more fluorescent uranyl-hydroxo complexes, or 2) increased levels of uranyl-silica gel interactions. While the second-order (X^2) fit models did not provide improved fits for this predictor, the third-order (X^3) models did provide significantly improved fits, but only for when reading were collected over silica gel. However, since the goal was to develop models representative of the entire dataset, the decision was made again to utilize the linear (X^1) fit model for this predictor.

Similar to the results described above for continuous X variable single regressor models, the least squares fitting routine (JMP, v8) was also utilized to examine single categorical X variable models (see Table 30). For these categorical models, the Prob > F significance level is simultaneously reflective of model analysis of variance and overall effects, while the Prob > $|t|$ significance level is reflective of individual parameter estimates. While simple continuous regressors have only one degree of freedom, categorical models with complex classification

effects have parameters estimates reflective of the multiple levels of the X variables. Dummy indicator variables are constructed for these nominal effects, with the names of the levels shown in brackets. The baselines selected by the JMP software for categorical dummy variable comparisons were: Y (yes) for 'Over SG', Sandy Loam for 'Soil text. Class.', and 3h for 'Read Time'. Therefore, interpretations of the individual parameter estimates have to be made *relative* to these baseline reference levels.

For both intensity and structure scores, the R^2 values were highest for the 'Over SG' X variable, followed by 'ST class', with both predictors overall being highly significant, and with higher R^2 values for intensity score compared to structure score. However, 'Read Time' was not found to be significant overall. More specifically, the parameter estimates for the majority of levels of 'Read Time' were not significant, with the 1 min and 24 hr time points again weakly appearing to be the exception (compared to 3 hr). The majority of the parameter estimates for different levels of 'ST class' were found to be significant (compared to sandy loam), with loamy sand and sand for structure scores being the exception.

These in-depth investigations of individual X variables, relative to the response variables, have given the preliminary impression predictors: [U] ppm, Over SG, Initial % MC and ST class are strong candidates for subsequent multiple regression models. The X variables: Iron (Meh. III), Total Iron, % Silt, % OM, Total CEC and Soil pH also seem promising, while % Sand and % Clay may not be wise to use. Finally, repeated evidence indicated that Est. % MC and Read Time would most likely *not* serve as good predictors of intensity and structure scores.

Table 30. Results of the least squares fitting routine (JMP v8) in testing for the significance of single categorical X variable models, in predicting the response variables individually.

Y variable	***Intensity Score***		***Structure Score***	
X variable	**R^2**	**Prob > F** [a]	**R^2**	**Prob > F** [a]
Over SG	0.313	< 0.0001 *	0.1634	< 0.0001 *
Individual Terms	**Parameter Est.**	**Prob > |t|** [b]	**Parameter Est.**	**Prob > |t|** [b]
Over SG [N] [c]	– 0.6556	< 0.0001 *	0.5639	< 0.0001 *
X variable	**R^2**	**Prob > F** [a]	**R^2**	**Prob > F** [a]
Soil text. class.	0.1188	< 0.0001 *	0.0656	< 0.0001 *
Individual Terms	**Parameter Est.**	**Prob > |t|** [b]	**Parameter Est.**	**Prob > |t|** [b]
Soil text. class. [Clay] [d]	0.5711	< 0.0001 *	-0.7872	< 0.0001 *
Soil text. class. [Loam] [d]	-0.4189	< 0.0001 *	0.3272	< 0.0001 *
Soil text. class. [Loamy Sand] [d]	-0.1883	< 0.0001 *	0.0027	0.9632
Soil text. class. [Sand] [d]	0.3623	< 0.0001 *	0.1056	0.0145
Soil text. class. [Sandy Clay Loam] [d]	-0.5715	< 0.0001 *	0.7015	< 0.0001 *
X variable	**R^2**	**Prob > F** [a]	**R^2**	**Prob > F** [a]
Read Time	0.0033	0.0837	0.0036	0.0613
Individual Terms	**Parameter Est.**	**Prob > |t|** [b]	**Parameter Est.**	**Prob > |t|** [b]
Read Time [15m] [e]	-0.0063	0.8993	0.0098	0.8676
Read Time [1h] [e]	0.0434	0.3808	0.0055	0.9258
Read Time [1m] [e]	-0.1540	0.0019 *	0.1573	0.0076 *
Read Time [24h] [e]	-0.0085	0.8634	-0.1524	0.0097 *
Read Time [2h] [e]	0.0562	0.2563	-0.0199	0.7359
Read Time [30m] [e]	0.0165	0.7381	0.0111	0.8512

[a] Significance level simultaneously reflective of model analysis of variance and overall effects.
[b] Significance level reflective of individual parameter estimates.
Baselines for categorical dummy variable comparisons: [c] Y (yes) for 'Over SG', [d] Sandy Loam for 'Soil text. Class.', and [e] 3h for 'Read Time'.

2.3.7 Development of Predictive Models for the Comprehensive Dataset

The development of predictive models for the individual response variables, based on multiple regressors (X's), involved testing a vast number of trial models. In summary, these trial models utilized both: standard least squares and stepwise (mixed) variable selection routines, allowing for the examination of: main effects, interaction terms, and variance inflation factors

(VIF). Recall, high VIF values (> 10) indicate multicollinearity issues, with VIF values < 5 being desirable. Note that VIF = $(1-R_k^2)$ where R_k^2 is the coefficient of determination when the k^{th} regressor is regressed on the remaining X variables. Stepwise variable selection routines progressively add and delete predictors in the regression model based on defined significance levels, and are useful in guiding the selection of X variables (effects) to include in an optimal model. It is important to recall that the best multiple regressor model is the *simplest* model (fewest terms) that provides the highest significant level of explanation. For example, while overall model R^2 values are reflective of the % of total variation in Y accounted for by the X's, R^2 values will always increase as more X's are added to the model, regardless of whether they are truly meaningful, with higher R^2 values not necessarily representing improved quality of prediction. Contrary, adjusted R^2 values enable the comparison of different models characterized by varying numbers of predictor variables or parameters. As regressors are progressively added to the model, significant increases in R^2 are desirable, and if useless X variables are included in the model, the adjusted R^2 value will drop below the R^2 value.

Comprehensive observations associated with the trial models included: 1) whole model analysis of variance was always highly significant (indicating at least one X was useful in predicting Y), 2) parameters useful for explaining variation in intensity score typically were also useful for explaining variation in structure score, and 3) models for intensity score always provided higher levels of explanation compared to models for structure score (~ 20% higher). This third listed observation can be explained in part by the fact that uranyl fluorescence intensities are more vulnerable to change and only require the extraction of electrons and subsequent loss of energy. In contrast, changes in the band structure of the uranyl spectra are reflective of changes in the coordination environment in the equatorial plane of the uranyl ion.

Multiple regression models (assuming linear fits) were first examined including all potential main effects. All fourteen X variables listed in Table 21 were included in these preliminary models, which produced R^2 values of 0.66 (intensity) and 0.42 (structure), implying that this group of predictors explains approximately 66% and 42% of the variability observed in intensity and structure scores respectively. For intensity scores: Soil pH, Total Iron and % OM were *not* found to be significant, while % Sand, % Silt and % Clay were weakly significant. For structure scores: Soil pH, Total Iron, % Sand, % Silt, % Clay and Read Time were *not* found to be significant, while Est. % MC and % OM were weakly significant. That being said, examination of the VIF values, as expected, revealed high levels of multicollinearity. Specifically, VIF values > 10 were observed for: Soil pH, Total CEC, Iron (Meh. III), Total Iron, % Sand, % Silt, % Clay, % OM as well as all levels of ST class. Therefore, decisions had to be made regarding reducing the number of X variables included in the models, while maximizing the cumulative level of explanation they provide.

Based on previously discussed relationships between pairs of X variables, as well as individual X – Y variable relationships, the decisions were made to remove the following predictors: Est. % MC, Read Time, % Sand, % Silt, % Clay and Total Iron. The new reduced models included eight main effects, and produced R^2 values of 0.61 (intensity) and 0.41 (structure). For both intensity and structure scores, all eight effects were highly significant, were characterized by VIF values of ~ 5 or less, and the majority of the individual parameter estimates were highly significant as well. The decisions to remove the above listed predictors were further supported by multiple trial models where pairs of correlated or strongly related predictors (such as: Initial and Est. % MC, % Sand and ST class, % Silt and % OM, iron content estimations, etc.) were interchanged. These decisions were also based on which predictors seemed most useful for

predicting *both* intensity and structure scores. Inclusion of the X variable Read Time only added ~ 1% to the models, and was typically not significant at several levels (time points).

As previously indicated, the interaction between Initial % MC and soil texture should be accounted for, through the use of an interaction term (Initial % MC * ST class) for example. The stepwise variable selection routine repeatedly indicated that this interaction term was important, as did the models based on standard least squares. The addition of the 'Initial % MC * ST class' interaction term resulted in models with R^2 values of 0.67 (intensity) and 0.44 (structure). For both intensity and structure scores, all nine effects were highly significant, were characterized by VIF values of ~ 5 or less, and the majority of the individual parameter estimates were highly significant, including those for the new interaction term. It is important to note that all other possible interaction terms were also explored. However, no others seemed to provide significant improvement to the models.

The promising multiple regression models described above (nine effects) were examined further to determine if additional X variables should be removed, to further simplify the models. In summary, it was determined while Soil pH seemed important to the model for intensity scores, it provided no significant improvement to the model for structure scores and was therefore removed from the structure score regression model. It was then determined that while % OM and Iron (Meh. III) seemed important to the model for structure scores, they provided no significant improvement to the model for intensity scores and were therefore removed from the intensity score regression model. Table 31 and 32 list details for these selected multiple linear regression models for intensity score and structure score respectively. For both models, all effects were highly significant, were characterized by VIF values of ~ 5 or less, and all the

individual parameter estimates were highly significant, with the exception of ST class = clay for intensity.

Following the selection of these predictive models for intensity score and structure score (see Tables 31 and 32), an examination of the residuals was performed in order to check regression model assumptions, including the assumption of homoscedasticity or constant variance. Figures 52 and 53 display scatter plots of the residuals (by the predicted values), as well as distribution plots of the residuals, for the selected intensity score and structure score models respectively. For the structure score model, Figure 53 indicates normality of the residuals and no clear departures from the assumption of homoscedasticity, while Figure 52 reveals only minor departures from the assumptions for the intensity score model.

Table 31. Selected multiple linear regression model: Results of the least squares fitting routine (JMP v8) in testing for the significance of the whole model, parameter estimates and individual effects in predicting the response variable – *Intensity* Score.

Summary of Fit	R^2	Adj. R^2	RMS Error	Response Mean	Observations (*n*)
Whole model	0.6546	0.6530	0.6904	8.8810	3360

Parameter Estimates

Term	Estimate	Std Error	t Ratio	Prob > |t|	VIF
Intercept	6.9227	0.0938	73.81	0.0000 *	.
Initial % MC	0.0524	0.0020	25.76	< 0.0001 *	3.43
[U] ppm	0.0010	0.0001	17.97	< 0.0001 *	1.00
Over SG [N] [a]	-0.6556	0.0119	-55.05	0.0000 *	1.00
Soil text. class. [Clay] [b]	0.1005	0.0577	1.74	0.0816	3.13
Soil text. class. [Loam] [b]	-0.3294	0.0301	-10.93	< 0.0001 *	1.88
Soil text. class. [Loamy Sand] [b]	-0.3059	0.0607	-5.04	< 0.0001 *	5.07
Soil text. class. [Sand] [b]	0.5750	0.0479	12.00	< 0.0001 *	5.33
Soil text. class. [Sandy Clay Loam] [b]	-0.1463	0.0389	-3.77	0.0002 *	2.08
(Initial % MC-11.8333) * Soil text. class. [Clay] [c,b]	-0.0204	0.0031	-6.60	< 0.0001 *	1.88
(Initial % MC-11.8333) * Soil text. class. [Loam] [c,b]	-0.0456	0.0025	-18.25	< 0.0001 *	2.61
(Initial % MC-11.8333) * Soil text. class. [Loamy Sand] [c,b]	0.0343	0.0074	4.64	< 0.0001 *	4.79
(Initial % MC-11.8333) * Soil text. class. [Sand] [c,b]	0.0808	0.0049	16.38	< 0.0001 *	3.11
(Initial % MC-11.8333) * Soil text. class. [Sandy Clay Loam] [c,b]	-0.0370	0.0034	-11.05	< 0.0001 *	1.74
Total CEC	-0.1875	0.0098	-19.08	< 0.0001 *	4.96
Soil pH	0.3714	0.0144	25.87	< 0.0001 *	3.17

Effects Tests

Source	Nparm	DF	Sum of Squares	F Ratio	Prob > F
Initial % MC	1	1	316.25	663.43	< 0.0001 *
[U] ppm	1	1	153.90	322.84	< 0.0001 *
Over SG	1	1	1444.35	3029.97	0.0000 *
Soil text. class.	5	5	174.89	73.37	< 0.0001 *
Initial % MC * Soil text. class.	5	5	270.43	113.46	< 0.0001 *
Total CEC	1	1	173.56	364.10	< 0.0001 *
Soil pH	1	1	318.93	669.05	< 0.0001 *

Baselines for categorical dummy variable comparisons: [a] Y (yes) for 'Over SG', [b] Sandy Loam for 'Soil text. Class.', and [c] 11.8333 for 'Initial % MC'.

Table 32. Selected multiple linear regression model: Results of the least squares fitting routine (JMP v8) in testing for the significance of the whole model, parameter estimates and individual effects in predicting the response variable – *Structure* Score.

Summary of Fit	R^2	Adj. R^2	RMS Error	Response Mean	Observations (*n*)
Whole model	0.4315	0.4287	1.0545	5.1055	3360

Parameter Estimates

Term	Estimate	Std Error	t Ratio	Prob > |t|	VIF
Intercept	4.2553	0.0801	53.13	0.0000 *	.
Initial % MC	-0.0404	0.0031	-12.99	< 0.0001 *	3.43
[U] ppm	-0.0019	0.0001	-20.97	< 0.0001 *	1.00
Over SG [N] [a]	0.5639	0.0182	31.00	< 0.0001 *	1.00
Soil text. class. [Clay] [b]	0.4613	0.0868	5.31	< 0.0001 *	3.04
Soil text. class. [Loam] [b]	-0.3360	0.0754	-4.46	< 0.0001 *	5.03
Soil text. class. [Loamy Sand] [b]	-0.3639	0.0882	-4.13	< 0.0001 *	4.60
Soil text. class. [Sand] [b]	0.3809	0.0737	5.17	< 0.0001 *	5.40
Soil text. class. [Sandy Clay Loam] [b]	0.5405	0.0545	9.91	< 0.0001 *	1.76
(Initial % MC-11.8333) * Soil text. class. [Clay] [c,b]	0.0401	0.0047	8.51	< 0.0001 *	1.88
(Initial % MC-11.8333) * Soil text. class. [Loam] [c,b]	0.0399	0.0038	10.39	< 0.0001 *	2.63
(Initial % MC-11.8333) * Soil text. class. [Loamy Sand] [c,b]	-0.0665	0.0113	-5.89	< 0.0001 *	4.79
(Initial % MC-11.8333) * Soil text. class. [Sand] [c,b]	-0.0486	0.0075	-6.46	< 0.0001 *	3.11
(Initial % MC-11.8333) * Soil text. class. [Sandy Clay Loam] [c,b]	0.0146	0.0051	2.84	0.0045 *	1.74
Total CEC	0.1632	0.0155	10.56	< 0.0001 *	5.26
% OM	0.2470	0.0207	11.93	< 0.0001 *	4.19
Iron (Mehlich III)	0.0013	0.0001	12.41	< 0.0001 *	1.41

Effects Tests

Source	Nparm	DF	Sum of Squares	F Ratio	Prob > F
Initial % MC	1	1	187.51	168.63	< 0.0001 *
[U] ppm	1	1	489.15	439.90	< 0.0001 *
Over SG	1	1	1068.26	960.70	< 0.0001 *
Soil text. class.	5	5	252.58	45.43	< 0.0001 *
Initial % MC * Soil text. class.	5	5	187.23	33.68	< 0.0001 *
Total CEC	1	1	123.97	111.49	< 0.0001 *
% OM	1	1	158.13	142.21	< 0.0001 *
Iron (Mehlich III)	1	1	171.29	154.05	< 0.0001 *

Baselines for categorical dummy variable comparisons: [a] Y (yes) for 'Over SG', [b] Sandy Loam for 'Soil text. Class.', and [c] 11.8333 for 'Initial % MC'.

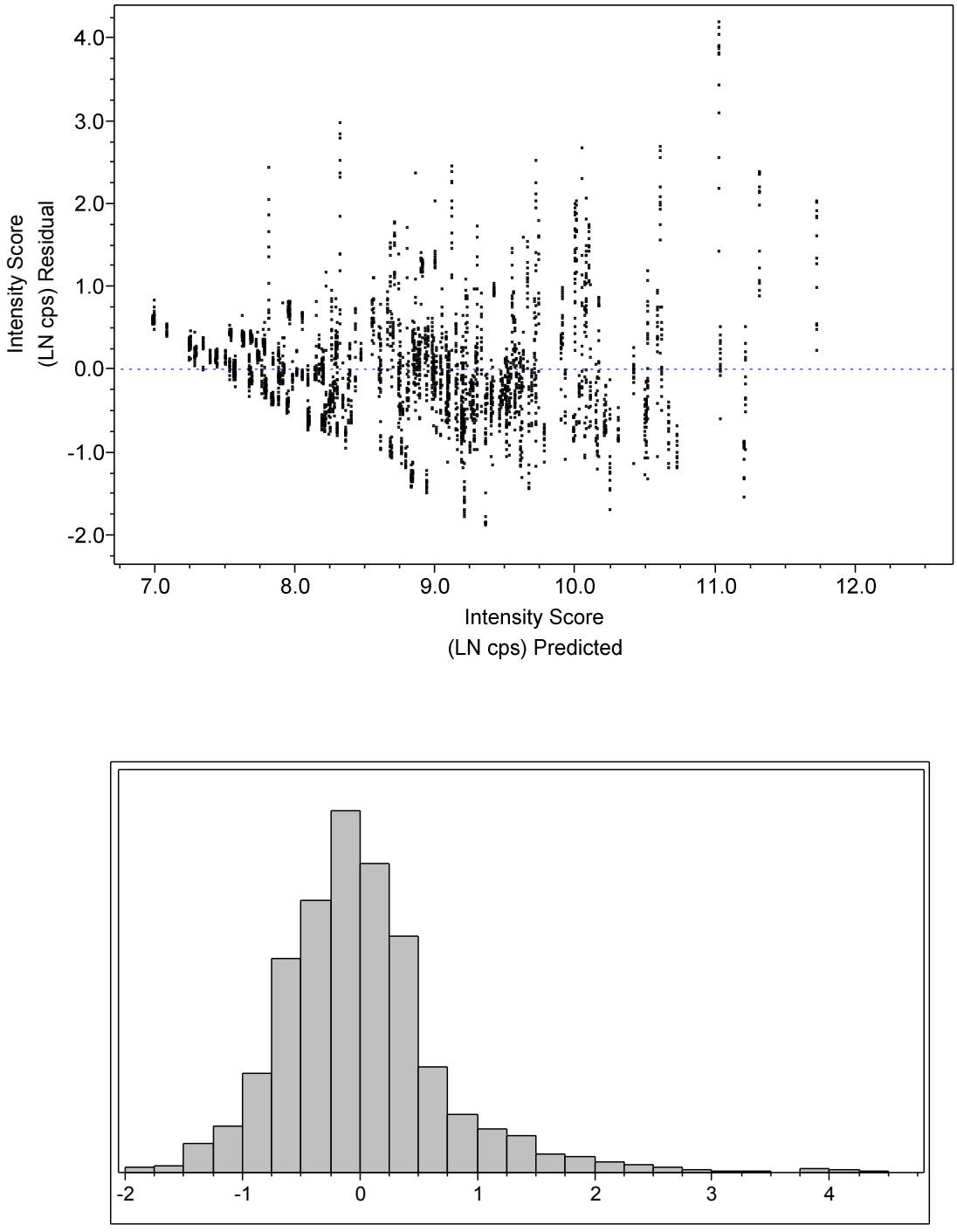

Figure 52. Scatter plot of the residuals by the predicted values (top), and distribution plot of the residuals (bottom) for the selected multiple linear regression model – *Intensity* Score.

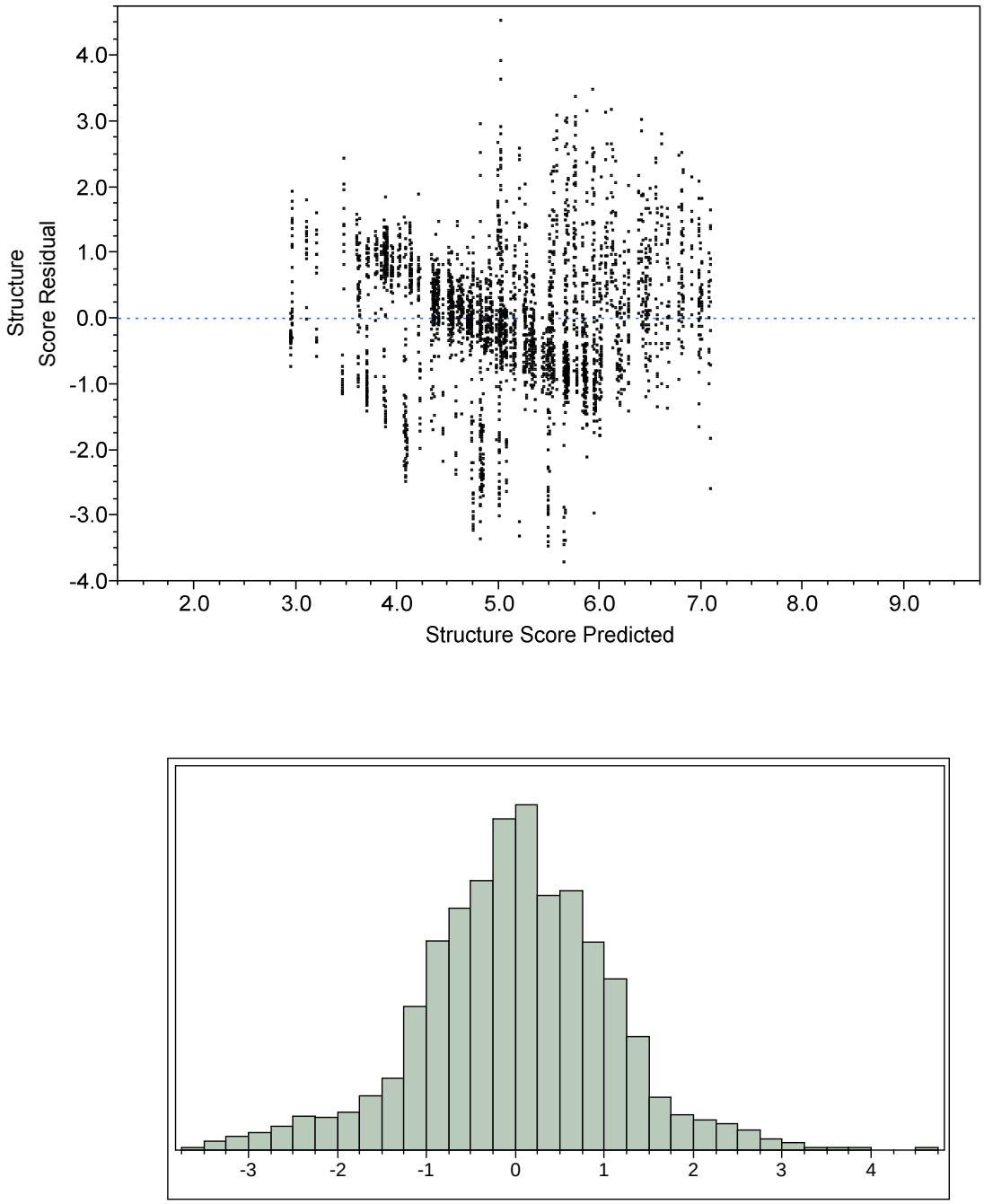

Figure 53. Scatter plot of the residuals by the predicted values (top), and distribution plot of the residuals (bottom) for the selected multiple linear regression model – *Structure* Score.

2.3.8 Multivariate Regression

Multivariate regression models address cases where more than one response variable is of interest. Construction of multivariate regression models allow one to test for the simultaneous dependence of multiple Y variables on multiple X variables. The previously described promising linear regression models (nine effects), useful for predicting both intensity and structure scores, were used as a reference. The MANOVA routine (JMP v8) tested for the significance of the whole model and individual effects in predicting *both* structure score and intensity score simultaneously. Table 33 lists the individual parameter estimates generated by the MANOVA routine, while Table 34 displays the model test results. As indicated in Table 34, the overall model, as well as all included predictor variables, were highly significant. It was concluded, therefore, that the following variables can significantly influence the intensity and structure of uranyl fluorescence spectra: Initial % MC, [U] ppm, Over SG, Total CEC, Iron (Meh. III), Soil pH, % OM, ST class, as well as the interaction between Initial % MC and ST class.

Table 33. Parameter estimates generated by the MANOVA routine (JMP v8) in developing a multivariate regression model for predicting both response variables: Structure and Intensity.

Parameter	**P.E. for Structure**	**P.E. for Intensity**
Intercept	5.0322	7.3010
Initial % MC	-0.0404	0.0523
[U] ppm	-0.0019	0.0010
Over SG [N] [a]	0.5639	-0.6556
Soil text. class. [Clay] [b]	0.2796	-0.0761
Soil text. class. [Loam] [b]	-0.3262	0.0038
Soil text. class. [Loamy Sand] [b]	-0.1619	-0.4057
Soil text. class. [Sand] [b]	0.3603	0.6496
Soil text. class. [Sandy Clay Loam] [b]	0.3790	-0.0912
(Initial % MC-11.8333) * Soil text. class. [Clay] [c,b]	0.0401	-0.0202
(Initial % MC-11.8333) * Soil text. class. [Loam] [c,b]	0.0397	-0.0462
(Initial % MC-11.8333) * Soil text. class. [Loamy Sand] [c,b]	-0.0664	0.0344
(Initial % MC-11.8333) * Soil text. class. [Sand] [c,b]	-0.0486	0.0809
(Initial % MC-11.8333) * Soil text. class. [Sandy Clay Loam] [c,b]	0.0146	-0.0369
Total CEC	0.1857	-0.1496
% OM	0.2082	-0.0862
Iron (Mehlich III)	0.0012	-0.0008
Soil pH	-0.1365	0.3224

Baselines for categorical dummy variable comparisons: [a] Y (yes) for 'Over SG', [b] Sandy Loam for 'Soil text. Class.', and [c] 11.8333 for 'Initial % MC'.

Table 34. Results of the MANOVA routine (JMP v8) in testing for the significance of the whole multivariate regression model and individual effects in predicting both response variables: Structure and Intensity.

Wilks' Lambda Test	**Value**	**Approx. F**	**Num DF**	**Den DF**	**Prob > F**
Whole Model	0.2750	178.22	34	6682	0.0000 *
Soil Text. Class.	0.8596	52.50	10	6682	< 0.0001 *
Initial % MC * Soil Text. Class.	0.8330	63.93	10	6682	< 0.0001 *
F Test	**Value**	**Exact F**	**Num DF**	**Den DF**	**Prob > F**
Intercept	3.3125	5533.54	2	3341	0.0000 *
Initial % MC	0.2070	345.73	2	3341	< 0.0001 *
[U] ppm	0.1616	269.88	2	3341	< 0.0001 *
Over SG	0.9589	1601.91	2	3341	0.0000 *
Total CEC	0.0738	123.30	2	3341	< 0.0001 *
% OM	0.0289	48.27	2	3341	< 0.0001 *
Iron (Mehlich III)	0.0529	88.45	2	3341	< 0.0001 *
Soil pH	0.1468	245.21	2	3341	< 0.0001 *

2.3.9 Final Discussion

Referring back to the comprehensive hypotheses, the data analyses described above sought to determine if the fluorescence detection of uranyl compounds is *dependent* upon: 1) key soil parameters, 2) the concentration of U contamination, and 3) time of analysis following the application of silica gel enhancing material.

In reference to the first hypothesis, and based on results previously discussed, it was confidently concluded that the uranyl fluorescence spectra, characterized by both intensity and structure, are significantly influenced by soil texture, moisture content, soil pH, organic matter, iron content and CEC. The dependency on soil texture was better demonstrated through the use of soil texture classification as opposed to percentages of sand, silt and clay. The dependency on iron content was better demonstrated through iron estimations by the Mehlich III soil extraction procedure, that are more representative of iron coatings on soils with which uranyl compounds readily interact.

Not surprisingly, U concentration (2^{cd} hypothesis) was clearly one of the strongest predictors of uranyl fluorescence responses. The concentration of U contamination greatly determines the dissolution, precipitation and diffusion behaviors of uranyl compounds in soils. This variable served as a strong predictor, in part, because it was unrelated to any of the other parameters investigated and represented a large percentage of the cumulative variation. For most soils, the higher selected U concentrations (100 ppm and 500 ppm), representative of contaminated areas, were distinguishable from very low levels, where as the 10 ppm level was typically not distinguishable from background levels.

Originally, it was anticipated that the fluorescence responses would be dependent upon time (3^{rd} hypothesis). Preliminary experiments using silica gel had demonstrated an initial, rapid

increase in positive detection as uranyl was absorbed by the silica gel along with water, with a slower subsequent improvement in signal likely due to: 1) gradually more uranyl being introduced to the silica gel via its migration through the aqueous phase, and/or 2) uranyl slowly forming more fluorescent complexes with the silica gel and being isolated in its protective pores. Typically in these preliminary experiments, however, the sand standard was used and initial moisture content levels were plenty adequate. Also, preliminary studies had shown improved detection for more challenging soil samples, but over much longer periods of time (days). For this dataset, however, time of analysis (1 min to 24 hr) did not prove to be a good predictor of variation in fluorescence responses. There was weak evidence supportive of the initial, rapid improvement in signal with the absorption of uranyl with the solution phase by the silica gel.

While the sorption of U to soils is a relatively fast process, the subsequent dissolution and mobilization of U is a much slower process (days), strongly dependent on U concentration, moisture levels, and soil features. In reflection, it is believed that had higher initial % moisture content levels been selected for the individual soils (~ 5 – 10% higher), a much greater percentage of promising detection results would have been observed. Recall, for this dataset, only 169 of 3360 spectra achieved desired detection thresholds. In addition, the resulting intensity and structure scores were *not* normally distributed (see Figure 35), with scores heavily weighted by background silica gel or bare soil signals. Had the response variables been more normally distributed throughout the score ranges, improved and more useful predictive models may have been developed. That being said, within the time frames utilized in these recent experiments ($\leq$ 24 hrs), the samples air dried relatively quickly, and it is believed that the combination of inadequate (or unmaintained) moisture levels along with reaction times greatly limited the detection of varying levels of U (depending on the soil).

In reference to the dataset and its analysis, a variety of different approaches could have proved highly useful. For example, given the previously described issues with using the KGa-1b 'clay standard' (not representative of environmental soils), and its undesirable influence on certain X variables (such as % Sand and % Clay), this sample could have been removed from the dataset. Detection of uranyl compounds utilizing distributed absorbing and enhancing materials is a scenario that differs greatly from detection through interrogation of bare soils. Therefore, segregating the dataset prior to analysis based on whether or not readings were collected over silica gel may have resulted in the development of more useful predictive models. With regards to generated structure scores and desired detection, a preliminary screening process could easily be employed such that only spectra characterized by some level of band structure are further investigated, then resulting in a subset of scores that do represent *progressive* improvements in band structure. For example, referring back to Table 24 (step 6), if the adjusted intensity value is higher in the 505:513 nm range compared to the adjusted intensity value at the 519 nm position (MATLAB 'if' statement), then this implies the absence of the diagnostic peaks and valleys.

The statistical models developed for this dataset confirmed the importance of the interaction between moisture content and soil texture, and that all three terms (Initial % MC, ST class, and Initial % MC * ST class) should be included in the models. That being said, recall that water potential (WP) is directly related to both % MC and soil texture, as well as affected by the chemical composition of the soil matrix, reflective of water movement tendencies. Therefore, WP could very well serve as a strong predictor of the fluorescence responses, and could *potentially* be used in place of these three terms, thereby further simplifying the models. Intuitively, other soil parameters could be utilized and investigated for improved prediction of uranyl detection. The regression models described above explained approximately 65%

(intensity) and 43% (structure) of the variability in the responses. However, soils are truly representative of complex systems with an over abundance of co-existing and interrelated effects. That being said, the inclusion of other soil-related metrics *could* prove useful, such as other known quenchers of uranyl fluorescence: salts (chlorides), other oxidizable metals, free carbonate (radicals), etc.

While the variety of statistical approaches described in detail above proved very useful, other more sophisticated approaches could be employed that are appropriate for this dataset. Analysis of covariance (ANCOVA), for example, can be used to determine the amount and significance of mean group differences while using a covariate to statistically correct for pre-existing differences between the groups, which can prove highly useful in quasi-experimental research designs.

LITERATURE CITED

LITERATURE CITED

Amayri, S., T. Reich, et al. (2005). "Spectroscopic characterization of alkaline earth uranyl carbonates." Journal of Solid State Chemistry **178**(2): 567-577.

Anderson, J. (1996). Spectral Measurements and Detection of Acid Mine Drainage Precipitates and Their Relationship to Water Quality Parameters at Contrary Creek, Mineral, Virginia. Environmental Science and Public Policy. Fairfax, George Mason University. **Doctor of Philosophy:** 177.

Arai, Y., M. McBeath, et al. (2006). "Uranyl adsorption and surface speciation at the imogolite-water interface: Self-consistent spectroscopic and surface complexation models." Geochimica et Cosmochimica Acta **70**(10): 2492-2509.

Bargar, J. R., R. Reitmeyer, et al. (1999). "Spectroscopic Confirmation of Uranium(VI)-Carbonato Adsorption Complexes on Hematite." Environ. Sci. Technol. **33**(14): 2481-2484.

Bargar, J. R., R. Reitmeyer, et al. (2000). "Characterization of U(VI)-carbonato ternary complexes on hematite: EXAFS and electrophoretic mobility measurements." Geochimica et Cosmochimica Acta **64**(16): 2737-2749.

Barnett, M. O., P. M. Jardine, et al. (2000). "Adsorption and transport of uranium(VI) in subsurface media." Soil Science Society of America Journal **64**(3): 908-917.

Bednar, A. J., V. F. Medina, et al. (2007). "Effects of organic matter on the distribution of uranium in soil and plant matrices." Chemosphere **70**(2): 237-247.

Beitz, J. V. and C. W. Williams (1997). "Uranyl fluoride luminescence in acidic aqueous solutions." Journal of Alloys and Compounds **250**(1-2): 375-379.

Benes, P., K. Kratzer, et al. (1998). "Adsorption of uranium on clay and the effect of humic substances." Radiochimica Acta **82**: 367-373.

Billard, I., E. Ansoborlo, et al. (2003). "Aqueous solutions of uranium(VI) as studied by time-resolved emission spectroscopy: A round-robin test." Applied Spectroscopy **57**(8): 1027-1038.

Blackburn, R. and M. S. Almasri (1994). "Determination of Uranium by Liquid Scintillation and Cerenkov Counting." Analyst **119**(3): 465-472.

Borggaard, O. K. (1982). "The influence of iron oxides on the surface area of soil." European Journal of Soil Science **33**(3): 443-449.

Bostick, B. C., S. Fendorf, et al. (2002). "Uranyl surface complexes formed on subsurface media from DOE facilities." Soil Science Society of America Journal **66**(1): 99-108.

Bourabee, F., Y. Bakir, et al. (1995). "Contribution of uranium to gross alpha-radioactivity in some environmental-samples in Kuwait." Environment International **21**(3): 293-298.

Brina, R. and A. G. Miller (1992). "Direct detection of trace levels of uranium by laser-induced kinetic phosphorimetry." Analytical Chemistry **64**(13): 1413-18.

Brina, R. and A. G. Miller (1993). "Determination of Uranium and Lanthanides in Real-World Samples by Kinetic Phosphorescence Analysis." Spectroscopy **8**(3): 25-31.

Buck, E. C., N. R. Brown, et al. (1996). "Contaminant uranium phases and leaching at the Fernald site in Ohio." Environmental science & technology **30**(1): 81-88.

Burrows, H. D., A. C. Cardoso, et al. (1985). "Photophysics of the excited uranyl ion in aqueous solutions. Part 4. Quenching by metal ions." Journal of the Chemical Society, Faraday Transactions 1: Physical Chemistry in Condensed Phases **81**(1): 49-60.

Catalano, J. G. and J. G. E. Brown (2005). "Uranyl adsorption onto montmorillonite: Evaluation of binding sites and carbonate complexation." Geochimica et Cosmochimica Acta **69**(12): 2995-3005.

Catalano, J. G., T. P. Trainor, et al. (2005). "CTR diffraction and grazing-incidence EXAFS study of U(VI) adsorption onto [alpha]-Al2O3 and [alpha]-Fe2O3 (11[combining macron]02) surfaces." Geochimica et Cosmochimica Acta **69**(14): 3555-3572.

Chang, H.-S., V. Korshin Gregory, et al. (2006). "Adsorption of uranyl on gibbsite: A time-resolved laser-induced fluorescence spectroscopy study." Environmental science & technology **40**(4): 1244-9.

Chen, J. P. and S. Yiacoumi (2002). "Modeling of depleted uranium transport in subsurface systems." Water Air and Soil Pollution **140**(1-4): 173-201.

Chimenti, R. J. L. (1981). Detection of uranium by light-induced luminescence. Application: CA CA, (Exxon Research and Engineering Co., USA). 32 pp.

Chisholm-Brause, C. J., J. M. Berg, et al. (2004). "Uranyl sorption by smectites: spectroscopic assessment of thermodynamic modeling." Journal of Colloid and Interface Science **277**(2): 366-382.

Chisholm-Brause, C. J., J. M. Berg, et al. (2001). "Uranium(VI) Sorption Complexes on Montmorillonite as a Function of Solution Chemistry." Journal of Colloid and Interface Science **233**(1): 38-49.

Clark, D. L., S. D. Conradson, et al. (1999). "Chemical Speciation of the Uranyl Ion under Highly Alkaline Conditions. Synthesis, Structures, and Oxo Ligand Exchange Dynamics." Inorganic Chemistry **38**(7): 1456-1466.

Cotton, S. (2006). Lanthanide and Actinide Chemistry. Chichester, England, John Wiley and Sons.

daSilva, J., A. Machado, et al. (1996). "Study of the interaction of a soil fulvic acid with UO22+ by self-modelling mixture analysis of synchronous molecular fluorescence spectra." Analyst **121**(10): 1373-1379.

Davis, J. A., D. E. Meece, et al. (2004). "Approaches to surface complexation modeling of Uranium(VI) adsorption on aquifer sediments." Geochimica et Cosmochimica Acta **68**(18): 3621-3641.

deNeufville, J. P., A. Kasdan, et al. (1981). "Selective detection of uranium by laser-induced fluorescence: a potential remote-sensing techinque. 1: Optical characteristics of uranyl geologic targets." Appl. Opt. ; Vol/Issue: 20:8: Pages: 1279-1296.

Denning, R. G. (1992). "Electronic-structure and bonding in actinyl ions." Structure and Bonding **79**: 215-276.

Denning, R. G., T. R. Snellgrove, et al. (1979). "The electronic structure of the uranyl ion." Molecular Physics **37**(4): 1109 - 1143.

Di Lella, L. A., F. Nannoni, et al. (2005). "Uranium contents and 235U/238U atom ratios in soil and earthworms in western Kosovo after the 1999 war." Science of The Total Environment **337**(1-3): 109-118.

DiBenedetto, J., R. Abbott, et al. (1996). Airborne and Ground Based Laser Induced Fluorescence Imaging (LIFI). Optical Remote Sensing for Environmental Process Monitoring, Bellingham, WA, SPIE.

Duff, M. C., J. U. Coughlin, et al. (2002). "Uranium co-precipitation with iron oxide minerals." Geochimica et Cosmochimica Acta **66**(20): 3533-3547.

Duff, M. C., D. E. Morris, et al. (2000). "Spectroscopic characterization of uranium in evaporation basin sediments." Geochimica et Cosmochimica Acta **64**(9): 1535-1550.

Eckert, D. and J. T. Sims (1995). Chapter 3: Recommended Soil pH and Lime Requirement Tests. Recommended Soil Testing Procedures for the Northeastern United States. Northeastern Regional Pub. No. 493 (2nd edition). J. T. Sims and A. M. Wolf. Newark, DE, Agricultural Experiment Station University of Delaware**:** 16-21.

Eliet, V., G. Bidoglio, et al. (1995). "Characterization of hydroxide complexes of uranium(VI) by time-resolved fluorescence spectroscopy." Journal of the Chemical Society-Faraday Transactions **91**(15): 2275-2285.

Formosinho Sebastiao, J., D. Burrows Hugh, et al. (2003). "Deactivation processes of the lowest excited state of $[UO_2(H_2O)_5]^{2+}$ in aqueous solution." Photochemical & photobiological sciences : Official journal of the European Photochemistry Association and the European Society for Photobiology **2**(5): 569-75.

Frimmel, F. H. (1998). "Characterization of natural organic matter as major constituents in aquatic systems." Journal of Contaminant Hydrology **35**(1-3): 201-216.

Gabriel, U., L. Charlet, et al. (2001). "Uranyl surface speciation on silica particles studied by time-resolved laser-induced fluorescence spectroscopy." Journal of Colloid and Interface Science **239**(2): 358-368.

Giammar, D. E. and J. G. Hering (2001). "Time scales for sorption-desorption and surface precipitation of uranyl on goethite." Environmental science & technology **35**(16): 3332-3337.

Greathouse, J. A. and R. T. Cygan (2005). "Molecular dynamics simulation of uranyl(vi) adsorption equilibria onto an external montmorillonite surface." Physical Chemistry Chemical Physics **7**(20): 3580-3586.

Greathouse, J. A. and R. T. Cygan (2006). "Water Structure and Aqueous Uranyl(VI) Adsorption Equilibria onto External Surfaces of Beidellite, Montmorillonite, and Pyrophyllite: Results from Molecular Simulations." Environ. Sci. Technol. **40**(12): 3865-3871.

Greathouse, J. A., R. J. O'Brien, et al. (2002). "Molecular Dynamics Study of Aqueous Uranyl Interactions with Quartz (010)." J. Phys. Chem. B **106**(7): 1646-1655.

Greathouse, J. A., H. R. Stellalevinsohn, et al. (2005). "Uranyl surface complexes in a mixed-charge montmorillonite: Monte Carlo computer simulation and polarized XAFS results." Clays and Clay Minerals **53**(3): 278-286.

Hennig, C., T. Reich, et al. (2002). "Structure of uranium sorption complexes at montmorillonite edge sites." Radiochimica Acta **90**(9-11): 653-657.

Hudson, E. A., L. J. Terminello, et al. (1999). "The structure of U6+ sorption complexes on vermiculite and hydrobiotite." Clays and Clay Minerals **47**(4): 439-457.

Hunter, D. B. and P. M. Bertsch (1998). "In situ examination of uranium contaminated soil particles by micro-x-ray absorption and micro-fluorescence spectroscopies." Journal of Radioanalytical and Nuclear Chemistry **234**(1-2): 237-242.

Johnson, W. H., B. J. Buck, et al. (2004). "Variations in depleted uranium sorption and solubility with depth in arid soils." Soil & Sediment Contamination **13**(6): 533-544.

Kaminski, R., F. J. Purcell, et al. (1981). "Uranyl phosphorescence at the parts-per-trillion level." Anal. Chem. **53**(7): 1093-1096.

Kasdan, A., R. J. L. Chimenti, et al. (1981). "Selective detection of uranium by laser-induced fluorescence: a potential remote-sensing technique. 2. Experimental assessment of the remote sensing of uranyl geologic targets." Applied Optics **20**(8): 1297-307.

Kelsh, D. J. and M. W. Parsons (1997). "Department of Energy sites suitable for electrokinetic remediation." Journal of Hazardous Materials **55**(1-3): 109-116.

Kirishima, A., T. Kimura, et al. (2004). "Speciation study on uranium(VI) hydrolysis at high temperatures and pressures." Journal of Alloys and Compounds **374**(1-2): 277-282.

Kowal-Fouchard, A., R. Drot, et al. (2004). "Use of spectroscopic techniques for uranium(VI)/montmorillonite interaction modeling." Environmental science & technology **38**(5): 1399-407.

Krepelova, A., V. Brendler, et al. (2007). "U(VI)-kaolinite surface complexation in absence and presence of humic acid studied by TRLFS." Environmental science & technology **41**(17): 6142-6147.

Krepelova, A., T. Reich, et al. (2008). "Structural characterization of U(VI) surface complexes on kaolinite in the presence of humic acid using EXAFS spectroscopy." Journal of Colloid and Interface Science **319**(1): 40-47.

Krepelova, A., S. Sachs, et al. (2006). "Uranium(VI) sorption onto kaolinite in the presence and absence of humic acid." Radiochimica Acta **94**(12): 825-833.

Kumke, M. U., C. Tiseanu, et al. (1998). "Fluorescence decay of natural organic matter (NOM)-influence of fractionation, oxidation, and metal ion complexation." Journal of Fluorescence **8**(4): 309-318.

Lee, S. Y. and J. D. Marsh, Jr. (1992). Characterization of uranium contaminated soils from DOE Fernald Environmental Management Project Site: Results of Phase 1 characterization**:** Size: Pages: (57 p).

Lenhart, J. J., S. E. Cabaniss, et al. (2000). "Uranium(VI) complexation with citric, humic and fulvic acids." Radiochimica Acta **88**(6): 345-353.

Lenhart, J. J. and B. D. Honeyman (1999). "Uranium(VI) sorption to hematite in the presence of humic acid." Geochimica et Cosmochimica Acta **63**(19-20): 2891-2901.

Liu, C., J. M. Zachara, et al. (2004). "Dissolution of uranyl microprecipitates in subsurface sediments at Hanford Site, USA." Geochimica et Cosmochimica Acta **68**(22): 4519-4537.

Lopez, M. and D. J. S. Birch (1996). "Uranyl photophysics on colloidal silica: an alternative luminescence-enhancing medium for uranyl assay." Analyst (Cambridge, United Kingdom) **121**(7): 905-908.

Lubal, P., D. Fetsch, et al. (2000). "Potentiometric and spectroscopic study of uranyl complexation with humic acids." Talanta **51**(5): 977-991.

Mason, C. F. V., W. Turney, et al. (1997). "Carbonate leaching of uranium from contaminated soils." Environmental science & technology **31**(10): 2707-2711.

Mehlich, A. (1984). "Mehlich-3 soil test extractant - A modification of Mehlich-2 extractant." Communications in Soil Science and Plant Analysis **15**(12): 1409-1416.

Meinrath, G. (1997). "Uranium(VI) speciation by spectroscopy." Journal of Radioanalytical and Nuclear Chemistry **224**(1-2): 119-126.

Mibus, J., S. Sachs, et al. (2007). "Migration of uranium(IV)/(VI) in the presence of humic acids in quartz sand: A laboratory column study." Journal of Contaminant Hydrology **89**(3-4): 199-217.

Moll, H., G. Geipel, et al. (1998). "Interaction of uranium(VI) with silicic acid in aqueous solutions studied by time-resolved laser-induced fluorescence spectroscopy (TRLFS)." Journal of Alloys and Compounds **271-273**: 765-768.

Monts, D., G. Wang, et al. (2009). Development of Fluorescence Spectral Imaging for Location of Uranium Deposited on Surfaces. Waste Management Symposium. Phoenix, AZ.

Moon, J. W., Y. Roh, et al. (2006). "Physicochemical and mineralogical characterization of soil-saprolite cores from a field research site, Tennessee." Journal of Environmental Quality **35**(5): 1731-1741.

Morawetz, H. and I. A. I. Taha (1971). "Catalysis of ionic reactions by polyelectrolytes. III. Quenching of uranyl ion fluorescence by iron(II) ions in poly(vinylsulfonic acid) solution." J. Am. Chem. Soc. **93**(4): 829-833.

Moriyasu, M., Y. Yokoyama, et al. (1977). "Quenching mechanisms of uranyl luminescence by metal ions." Journal of Inorganic and Nuclear Chemistry **39**(12): 2205-2209.

Moriyasu, M., Y. Yokoyama, et al. (1977). "Quenching of uranyl luminescence by water molecule." Journal of Inorganic and Nuclear Chemistry **39**(12): 2211-14.

Morris, D. E., P. G. Allen, et al. (1996). "Speciation of uranium in Fernald soils by molecular spectroscopic methods: Characterization of untreated soils." Environmental science & technology **30**(7): 2322-2331.

Morris, D. E., S. D. Conradson, et al. (1992). Uranium speciation in Fernald soils. Progress report, January 1--May 31, 1992**:** Size: 24 p.

Moulin, C., P. Decambox, et al. (1996). "Direct Uranium(VI) and Nitrate Determinations in Nuclear Reprocessing by Time-Resolved Laser-Induced Fluorescence." Analytical Chemistry **68**(18): 3204-3209.

Moulin, C., I. Laszak, et al. (1998). "Time-resolved laser-induced fluorescence as a unique tool for low-level uranium speciation." Applied Spectroscopy **52**(4): 528-535.

Moyes, L. N., R. H. Parkman, et al. (2000). "Uranium Uptake from Aqueous Solution by Interaction with Goethite, Lepidocrocite, Muscovite, and Mackinawite: An X-ray Absorption Spectroscopy Study." Environ. Sci. Technol. **34**(6): 1062-1068.

Murakami, T., T. Ohnuki, et al. (1997). "Mobility of uranium during weathering." American Mineralogist **82**(9-10): 888-899.

Ohnuki, T., H. Isobe, et al. (1997). "Change in sorption characteristics of uranium during crystallization of amorphous iron minerals." Journal of Nuclear Science and Technology **34**(12): 1153-1158.

Patsahan, T. and M. Holovko (2007). "Molecular dynamics study of aqueous uranyl in hydrophilic mesoporous confinement: the case of slit-like pore in amorphous silica." Condensed Matter Physics **10**(2): 143-150.

Payne, T. E., J. A. Davis, et al. (2004). "Surface complexation model of uranyl sorption on Georgia kaolinite." Applied Clay Science **26**(1-4): 151-162.

Payne, T. E., J. A. Davis, et al. (1994). "Uranium retention by weathered schists - the role of iron minerals." Radiochimica Acta **66-7**: 297-303.

Payne, T. E., J. A. Davis, et al. (1996). "Uranium adsorption on ferrihydrite - Effects of phosphate and humic acid." Radiochimica Acta **74**: 239-243.

Pestov, D., C.-C. Chen, et al. (2009). "Directed fluorescence sensor element for standoff detection of uranium in soil." Sensors and Actuators B: Chemical **138**(1): 134-137.

Rabinowitch, E. and R. L. Belford (1964). Spectroscopy and Photochemistry of Uranyl Compounds. New York, Pergamon Press Inc.

Radenkovic, M. B., S. A. Cupac, et al. (2008). "Depleted uranium mobility and fractionation in contaminated soil (Southern Serbia)." Environmental Science and Pollution Research **15**(1): 61-67.

Reeder, R. J., M. Nugent, et al. (2000). "Uranyl Incorporation into Calcite and Aragonite: XAFS and Luminescence Studies." Environ. Sci. Technol. **34**(4): 638-644.

Reich, T., H. Moll, et al. (1998). "An EXAFS study of uranium(VI) sorption onto silica gel and ferrihydrite." Journal of Electron Spectroscopy and Related Phenomena **96**(1-3): 237-243.

Sachs, S., V. Brendler, et al. (2007). "Uranium(VI) complexation by humic acid under neutral pH conditions studied by laser-induced fluorescence spectroscopy." Radiochimica Acta **95**(2): 103-110.

Saito, T., S. Nagasaki, et al. (2002). "Evaluation of the complexation behavior between humic acid and UO22+ with fluorescence spectroscopy and its mixture analysis." Radiochimica Acta **90**(1): 27-33.

Saito, T., S. Nagasaki, et al. (2002). "Molecular fluorescence spectroscopy and mixture analysis for the evaluation of the complexation between humic acid and UO22+." Radiochimica Acta **90**(9-11): 545-548.

Sansone, U., P. R. Danesi, et al. (2001). "Radioecological survey at selected sites hit by depleted uranium ammunitions during the 1999 Kosovo conflict." Science of The Total Environment **281**(1-3): 23-35.

Schreckenbach, G., P. J. Hay, et al. (1999). "Density functional calculations on actinide compounds: Survey of recent progress and application to [UO2X4](2-) (X = F, Cl, OH) and AnF(6) (An = U, Np, Pu)." Journal of Computational Chemistry **20**(1): 70-90.

Schulte, E. E. (1995). Chapter 8: Recommended Soil Organic Matter Tests. Recommended Soil Testing Procedures for the Northeastern United States. Northeastern Regional Pub. No. 493 (2nd edition). J. T. Sims and A. M. Wolf. Newark, DE, Agricultural Experiment Station University of Delaware**:** 52-60.

Singhal, R. K., A. Kumar, et al. (2005). "Association of uranium with colloids of natural organic matter in subsurface aquatic environment." Journal of Radioanalytical and Nuclear Chemistry **265**(3): 405-408.

Sowder, A. G., S. B. Clark, et al. (1998). "The effect of sample matrix quenching on the measurement of trace uranium concentrations in aqueous solutions using kinetic phosphorimetry." Journal of Radioanalytical and Nuclear Chemistry **234**(1-2): 257-260.

Stork, C. L., H. A. Smartt, et al. (2006). Systematic Evaluation of Satellite Remote Sensing for Identifying Uranium Mines and Mills. Albuquerque, NM, Sandia National Laboratories**:** 64.

Swift, R. S. (1996). Organic matter characterization. Methods of Soil Analysis, Part 3, Chemical Methods. D. L. Sparks. Madison, WI, American Society of Agronomy**:** 1011-1069.

Syt'ko, V. V. and D. S. Umreiko (1998). "Spectroscopic properties and electronic structure of uranyl complex compounds (review)." Journal of Applied Spectroscopy **65**(6): 857-870.

Sztajnkrycer, M. D. and J. O. Edward (2004). "Chemical and radiological toxicity of depleted uranium." Military Medicine **169**(3): 212-216.

Takumi, S., N. Shinya, et al. (2001). "Evaluation of complexation process between U(VI) and humic acid by fluorescence spectroscopy." Tokyo Daigaku Genshiryoku Kenkyu Sogo Senta Shinpojumu **9th**: 237-240.

Tokunaga, T. K., J. Wan, et al. (2008). "Real-Time X-ray Absorption Spectroscopy of Uranium, Iron, and Manganese in Contaminated Sediments During Bioreduction." Environ. Sci. Technol. **42**(8): 2839-2844.

Tokunaga, T. K., J. M. Wan, et al. (2004). "Hexavalent uranium diffusion into soils from concentrated acidic and alkaline solutions." Environmental science & technology **38**(11): 3056-3062.

Turner, G. D., J. M. Zachara, et al. (1996). "Surface-charge properties and UO22+ adsorption of a subsurface smectite." Geochimica et Cosmochimica Acta **60**(18): 3399-3414.

Um, W., R. J. Serne, et al. (2007). "U(VI) adsorption on aquifer sediments at the Hanford Site." Journal of Contaminant Hydrology **93**(1-4): 255-269.

USDOE (1999). Airborne Laser Induced Fluorescence Imaging, DOE/EM-0427, Office of Environmental Management, Office of Science and Technology**:** 21 pp.

Waite, T. D., J. A. Davis, et al. (2000). "Approaches to modelling uranium(VI) adsorption on natural mineral assemblages." Radiochimica Acta **88**(9-11): 687-693.

Waite, T. D., J. A. Davis, et al. (1994). "Uranium(VI) adsorption to ferrihydrite: Application of a surface complexation model." Geochimica et Cosmochimica Acta **58**(24): 5465-5478.

Walter, M., T. Arnold, et al. (2005). "An EXAFS and TRLFS investigation on uranium(VI) sorption to pristine and leached albite surfaces." Journal of Colloid and Interface Science **282**(2): 293-305.

Wang, G., Y. Su, et al. (2008). "Parametric Investigation of Laser-Induced Fluorescence of Solid-State Uranyl Compounds." The Journal of Physical Chemistry A **112**(42): 10502-10508.

Wang, Z., C. C. Ainsworth, et al. (2002). "A fluorescence study of uranyl sorption and speciation at clay mineral surface." Abstracts of Papers, 223rd ACS National Meeting, Orlando, FL, United States, April 7-11, 2002: NUCL-119.

Wang, Z., J. M. Zachara, et al. (2005). "Fluorescence spectroscopy of U(VI)-silicates and U(VI)-contaminated Hanford sediment." Geochimica et Cosmochimica Acta **69**(6): 1391-1403.

Wang, Z., M. Zachara John, et al. (2005). "Cryogenic laser induced U(VI) fluorescence studies of a U(VI) substituted natural calcite: implications to U(VI) speciation in contaminated Hanford sediments." Environmental science & technology **39**(8): 2651-9.

Wheeler, J. and J. K. Thomas (1984). "Photochemistry of the uranyl ion in colloidal silica solution." Journal of Physical Chemistry **88**(4): 750-754.

Williams, A. T. R. and J. N. Miller (1983). "The determination of uranium in aqueous samples by means of a pulsed-source fluorescence spectrometer." Analytica Chimica Acta **154**: 341-5.

Yokoyama, Y., M. Moriyasu, et al. (1976). "Electron transfer mechanism in quenching of uranyl luminescence by halide ions." Journal of Inorganic and Nuclear Chemistry **38**(7): 1329-33.

Zaidan, O. F., J. A. Greathouse, et al. (2003). "Monte Carlo and molecular dynamics simulation of uranyl adsorption on montmorillonite clay." Clays and Clay Minerals **51**(4): 372-381.

VITA

Jean (Renee) Dennis Nelson was born on January 17, 1977, in Silver Spring, Maryland, and is an American citizen. She graduated from Spotsylvania High School, Spotsylvania, Virginia in 1995. She received her Bachelor of Science in Biology from Radford University, Radford, Virginia in 1999 (Biology Department Dean Scholar). She received her Master of Science in Environmental Studies (Environmental Health focus) from Virginia Commonwealth University, Richmond, Virginia in 2001. From July 2003 until present, she has been employed as a Research Biologist by the Engineer Research and Development Center (ERDC) in Alexandria, Virginia. She received her Doctor of Philosophy in Integrative Life Sciences from Virginia Commonwealth University, Richmond, Virginia in 2009.